Skolkovo Institute of Science and Technology

ADVANCED SINGLE-WALLED CARBON NANOTUBE MEMBRANES FOR OPTOELECTROMECHANICAL APPLICATIONS.

Doctoral Thesis

by

JAVIER ANTONIO RAMIREZ BENAVIDES

DOCTORAL PROGRAM IN MATERIALS SCIENCE AND ENGINEERING

Supervisor

Dr. Sci. Tech, Professor R.A.S., Full Professor

Albert Galiyevich Nasibulin

Co-Supervisor

Ph. D. in Chemistry, Assistant Professor

Dmitry Viktorovich Krasnikov

Moscow – 2024

I hereby declare that the work presented in this thesis was carried out by myself at Skolkovo Institute of Science and Technology, in the city of Moscow, Russian Federation, except where due acknowledgement is made, and has not been submitted for any other degree.

Candidate (Javier Antonio Ramirez Benavides)

Supervisor (Prof. Albert G. Nasibulin)

Co- Supervisor (Prof. Dmitri V. Krasnikov)

Abstract

CNT membranes (*i.e.*, FSFs serving as protective, filtering, or separation units) represent a unique class of materials combining mechanical sturdiness and electrical conductivity with ultralow thickness and optical transparency. Ultrathin CNT films are exceptionally strong, chemically inert (*e.g.*, endure heating up to 400°C in the air), conductive, and transparent. The floating catalyst (aerosol) CVD method established on the Boudouard reaction on iron-based catalyst nanoparticles produces high-quality single-walled CNTs (SWCNTs). Due to the high surface area, cylindrical shape, and aerosol deposition pattern, SWCNTs form randomly oriented networks when collected downstream of the reactor on a filter. Remarkably, those networks can be put on a secondary substrate with an opening to form a free-standing membrane – a “macro material” with exceptional strength when normalized on thickness. This thesis aims to develop methods for modification of the membranes for specific applications. Firstly, a SWCNT renewable EUV (EUV) pellicle was designed to filter and further evaporate Sn particles (produced by an EUV light source) at a low pressure by the Joule heating of the membrane. Secondly, by applying the same low-pressure Joule heating, ethylene decomposes on the membrane surface due to the high-temperature pyrolysis. This allows "welding" of the nanotubes within the membrane, improving the mechanical properties and electrical conductivity. By engineering lateral carbon deposits and doping with $HAuCl_4$, we achieved one of the state-of-the-art performances for transparent conductors. This thesis opens new possibilities for CNTs to be applied for filtration in a harsh environment and for transparent electronics seeking to decrown indium tin oxide in consumer products using transparent electrodes.

Thesis Publications

1. **Javier A. Ramirez B.**, Dmitry V. Krasnikov, Vladimir V. Gubarev, Ilya V. Novikov, Vladislav A. Kondrashov, Andrei V. Starkov, Mikhail S. Krivokorytov, Vyacheslav V. Medvedev, Yuriy G. Gladush, Albert G. Nasibulin, Renewable single-walled CNT membranes for EUV pellicle applications, Carbon, Volume 198, **2022**, Pages 364-370, ISSN 0008-6223, https://doi.org/10.1016/j.carbon.2022.07.014.

   Author's contribution: methodology, synthesis and collection of CNTs, fabrication of holders, dry transfer to holders for freestanding membrane fabrication, reactor redesign, assembly preparation, testing and sample packaging, electrode fabrication, installation and alignment, aerosol production setup maintenance and operation, optimization of operating parameters for the supplied devices, aerosol investigation, data curation, writing, material characterization, original draft preparation, drawings, schemes, edition.

2. **Javier A. Ramirez B.**, Dmitry V. Krasnikov, Hassaan A. Butt, Veronika A. Dmitrieva, Vladislav A. Kondrashov, Anastasia E. Goldt, Dmitry V. Dzhurinskiy, Julia A. Baimova, and Albert G. Nasibulin, Rapid and efficient welding of single-walled CNT membranes with ethylene for transparent electrodes and mechanical stability (Submitted to Carbon).

Author's contribution: methodology, synthesis and collection of CNTs, fabrication of holders, dry transfer to holders for fabrication of freestanding membrane, reactor adaptation, testing and sample packaging, gas feed system fabrication, installation and alignment, investigation and optimization of operating parameters for the supplied devices, firmware and software for the cupping test device, data curation writing, material investigation, original draft preparation, drawings, schemes, edition.

3. V. Gubarev, M. Krivokorytov, **J.A. Ramirez Benavides**, V. Krivtsun, V. Ivanov, V. Medvedev, A. Pal, D. Krasnikov, and A. Nasibulin. InSn plasma penetration through protective single-walled CNT **-** based membranes. *Applied Physics Letters*, **2022**, 121, 14 AIP Publishing https://doi.org/10.1063/5.0097517.

Author's contribution: Synthesis and collection of CNTs, fabrication of holders, fabrication of holders, dry transfer to holders for fabrication of freestanding membranes, provision of operating parameters for the supplied devices, packaging and optoelectronic characterization of prepared devices, discussions.

Other related publications

1. Ramírez-Morales, M.A.; Goldt, A.E.; Kalachikova, P.M.; **Ramirez B., J.A.**; Suzuki, M.; Zhigach, A.N.; Ben Salah, A.; Shurygina, L.I.; Shandakov, S.D.; Zatsepin, T.; Krasnikov, D.V.; Maekawa, T.; Nikolaev, E.N.; Nasibulin, A.G. Albumin Stabilized Fe@C Core–Shell Nanoparticles as Candidates for Magnetic Hyperthermia Therapy. *Nanomaterials* **2022**, *12*, 2869. https://doi.org/10.3390/nano12162869.

2. Dmitry Mitin, Alexandr Vorobyev, Alexander Pavlov, Yury Berdnikov, Alexey Mozharov, Vladimir Mikhailovskii, **Javier A. Ramirez B.,** Dmitry V. Krasnikov, Daria S. Kopylova, Demid A. Kirilenko, Maxim Vinnichenko, Roman Polozkov, Albert G. Nasibulin, and Ivan Mukhin, Tuning the Optical Properties and Conductivity of Bundles in Networks of Single-Walled CNTs. *The Journal of Physical Chemistry Letters* **2022** *13* (37), 8775-8782 https://doi.org/10.1021/acs.jpclett.2c01931

3. Alisa R. Bogdanova, Dmitry V. Krasnikov, Eldar M. Khabushev, **Javier A. Ramirez B.**, Yakov E. Matyushkin, Albert G. Nasibulin, Role of Hydrogen in Ethylene-Based Synthesis of Single-Walled CNTs. *Nanomaterials*, **2022**, 13, 9, 1504. https://www.mdpi.com/2079-4991/13/9/1504.

4. Alisa R. Bogdanova, Dmitry V. Krasnikov, Eldar M. Khabushev, **Javier A. Ramirez B.**, Albert G. Nasibulin, Bithiophene as a Sulfur-Based Promotor for the Synthesis of CNTs and Carbon-Carbon Composites*, International Journal of Molecular Sciences*, **2023**, 24, 7, 6686. https://www.mdpi.com/1422-0067/24/7/6686.

Patent

Patent on the Russian Federation number 2786874, Method for Regeneration of Aerosol Filters and Protective Membranes (Способ Регенерации Аэрозольных Фильтров И Защитных Мембран). Krasnikov Dmitry Viktorovich, **Ramirez Benavides Javier Antonio**, Kondrashov Vladislav Andreevich, Gladush Yurii Genadievich, Nasibulin Albert Galievich. Request 2021137415, Priority date 17 December 2021, **assigned on 26 December 2022**.

Acknowledgements

I would like to thank for helping with this research project the following people: Prof. Albert Nasibulin and Prof. Dmitry Krasnikov, my tutors, who guided me so positively and who always made me feel confident in my abilities, Dr. Vladislav Kondrashov, Dr. Anastasia Goldt, Eng. Andrei Starkov, Dr. Vsevolod Yakovlev, Dr. Ignat Rakov, who contributed so thoroughly through their comments, designs, crafts, entertainment and valuable discussion.

Dedicated to my family: my mom Gladys, Dad Maximo (RIP), Aunt Lourdes (RIP), Uncle Marco Rubén (RIP) and Aunt Suni, Sister Fabiola, brother-in-law Roberto, Niece Fabiana, Niece Sarah, Cousin Natalia, Cousin Pedro, Uncle Isidro, Aunt Aura, Aunt Elvira, Cousin Daniela, Cousin Andres & family, Aunt Elisa, Cousin Andreina & family, and all members of my family; and colleagues that have supported me during this long journey in Moscow: Professor Alexei Buchachenko (RIP), Nikita Raginov, and Eldar Khabushev, René Cartaya, Christian Sierra, Cesar Molina, Yasmin Shakiba, Pierina Chamorro, Maria Parfyonova, Maria A. Ramirez, Maria Victoria Gasca, Jenani & Roberto Aguilar, Francisco de Asis Melazzini M., Anna Gorevaya, Nilson Rincon, Leonardo de Arantes B., Michelle Valsecchi, Margaret Erickson, Elizaveta Ricardo, Rizma Yoshi, Aleksandra Ushakova, Maria Movsesyan, Svetlana I. Marinicheva, Valeria Mikheeva, Victoria Valentina Carreño Bugrova, Valentina Morant, Juana Morant & familia, Jeanelle Greyling & Family My mentors from MIPT: Mikhail Vasiliev, Tatiana Vasilieva, Alexander Manohin; Gonzalo Ferrer, for his active support and patience. Thank you for being the best boss ever!

My friends: Lissete Hernandez & family, Sergio Medina, Leonardo Arriaga & family; Veronica Meléndez, Carlos Nieto, Luis Alejandro Díaz, Erdwing Nieto Sr., Ninoska Nieto, Alba Diaz, Luis Barroso, Belkis Dominguez, Nina Nikonova, Margarita Crespo y familia, My family from IVIC: Delmiro Pereira, Aristides Marcano, Lill Aranguren, Luis Gerardo Rodriguez, Humberto Cabrera, Leonardo Sigalotti, Carlos Jimenez Yenni Sánchez, Olgi Alcalá, Franklin Peña, Freddy Jimenez, Jose Luis Figuera, Jose Juan Suarez, Jesús Rodriguez, Pura Bolaños, Fabian Michelangelli, Jhoan Toro & Familia Rocío Ramos, that supported me actively on the adventure of me coming to Russia, thank you for the support, patience and encouragement.

The work was supported by Russian Science Foundation (Project Number 22-13-00436) and Council on grants (project for young scientists number МК-3000.2022.1.3).

Table of Contents

List of Symbols, Abbreviations, IUPAC names

AC	Alternating current
BNNT	Boron nitride nanotube
CNM	Carbon nanomaterial
CNT	Carbon nanotube
CVD	Chemical vapor deposition
CPC	Condensation particle counter
DC	Direct current
DIL	Dual in-line package
DMA	Dynamic mobility analyzer
EDS	Electron dispersion spectroscopy
EUV	Extreme ultraviolet
FSF	Free-standing film
HEPA	High efficiency particulate arresting filter
MWCNT	Multi-walled CNT
NaCl	Sodium Chloride
PECVD	Plasma enhanced CVD
PTFE	Polytetrafluoroethylene
RBM	Radial breathing mode
SCCM	Standard cubic centimeters per minute
SEM	Scanning electron microscope
SLPM	Standard liters per minute
STEM	Scanning transmission electron microscopy
SWCNT	Single-walled CNT

TEM	Transmission electron microscope
ITO	Indium tin oxide
TOF	Time of flight
UV	Ultraviolet
UV-Vis-NIR	Ultraviolet-visible-near infra-red
UTS	Ultimate tensile strength
XRD	X-ray diffraction

Introduction

Carbon nanomaterials, CNTs from now on, are a class of materials unifying tubular nanoparticles based on hexagonal (sp^2) carbon or, in other words, cylindrically shaped graphene derivatives. Similar to "myriads" of chemical compounds or accessible polymer chains, such a definition opens a box full of opportunities; for example, the angle of the graphene sheet wrapping determines the electrical characteristics of a nanotube [1]. Due to their high superficial area, they form bundles by van der Waals interactions between nanotubes. These bundles, in turn, form web-like networks with tailorable morphology and alignment. Thus, a CNT-based material can be tuned within a broad "space of parameters".

Since the landmark observations of CNTs (Carbon Nanotubes) [1,2] in the early 1990s, CNTs hold an ensemble of promising solutions for a wide variety of industries: electronics, construction, aerospace [3], *etc.* This is due to a unique integration of mechanical, electronic, and optical features.

Among the various assemblies of CNTs (powders, aerogels (Gel comprised of a microporous solid in which the dispersed phase is a gas [4] , yarns, buckypapers, individual objects, *etc.*), films (*i.e.*, free-standing or supported films serving as thin electrodes) membranes (*i.e.*, free-standing membranes serving as protective , filtering, or separation units) of SWCNTs hold special promise in filtrating [5], ultrasound-generating [6], heating, and shielding components [7]. Though various strategies have been developed during the last decades, the main avenue to obtain a membrane is a vacuum filtration of a nanotube dispersion. Nevertheless, as the formation of a stable dispersion usually comprises ultrasound treatment in a surfactant dispersion, the membranes are rather thick (microns in size), contain contaminations (surfactant), and have limited strength (due to the nanotube shredding during an ultrasound treatment [8–10]) . The aerosol CVD [10] method is an alternative route for FSFs (FSF) as it avoids most of the abovementioned drawbacks, being dry, almost contaminant-free (except minor catalyst impurities), and having the opportunity for long (tens of microns) nanotubes. Thus, aerosol CVD reaches even a few nm thick membranes, opening new opportunities [5] for air heating, aerosol filtration, transparent electrodes, *etc*. Since the membranes are also transparent and electrically conductive, exploring contemporary technological problems is necessary. Current microelectronics based on silicon follow Moor's law [11]. This law dictates that the size of the features is inversely proportional to the speed of operation and efficiency of the device. The state-of-the-art method to produce the nanometer-sized semiconductor features for integrated microelectronics is EUV lithography (Extreme ultraviolet) [12]. One of the three biggest challenges of EUV lithography is the protection of the mask from tin nanoparticles produced during the operation of the light source [13]. The element for this duty is called pellicle. Nevertheless, the utilization of aerosol CVD membranes in new applications, as well as the possibilities to improve their performance, has been unassessed.

The aim of the present thesis is to develop methods for modification of the SWCNT FSFs to specific applications: EUV (EUV) pellicles, aerosol filters, and transparent electrodes. For this, the CVD aerosol synthesis method is used to obtain high-quality

SWCNT-based FSFs, followed by the development of treatment methods, to achieve the evaporation of Sn particles deposited on the surface of SWCNTs restoring EUV transmittance, creating the first renewable EUV SWCNT based pellicle, and (ii) to achieve the enhancement of mechanical and electrical properties.

The following objectives can be formulated:

1. To assess the CNT membrane filtration efficiency on retention of In/Sn aerosol particles, study their lifetime, and develop technological building blocks for removal of model aerosols using Joule heating.
2. To assess the deposition of carbon on Joule heated single-walled nanotube film surface as a tuning agent for conductivity and mechanical strength.

The ultra-high performance transparent conductive and mechanically stable free-standing membranes can be used as transparent electrodes for transparent devices (like bolometers, supercapacitors, flexible electronics, aerosol protection, high-speed lasers, optical modulators, and solar cell electrodes).

The novelty of this work allowed the process of Joule heating tin indium aerosol regeneration to be patented because it is an industrially applicable new technology.

The process for the welding of the nanotube membranes/films is advantageous and faster than previously reported methods [14–18]. Low-pressure Joule heating has not been used before for the welding of films, though it is faster, energetically efficient, tailorable, and maintains the chemical composition of the membranes. As a side effect, a structural improvement of the crystalline quality of the nanotubes was observed.

Chapter 1: Literature review

1.1. CNT structure and properties

Benjamin Collins Brodie was aware of the tight laminated structure present in the graphite, on his work published in 1859 [19], he distinguished two different types of graphite, one more carbon lamellar (with a stacked flake morphology), and one more amorphous (glassy, vitreous). By carefully grinding the graphite in water, he managed to cleave it in a way that flakes were formed. By acid treatment [19], he managed to "dissolve" it. His careful work [19] yielded extremely thin and transparent flakes, that exhibited a degree of polarization while examined under the microscope. His observations [19] also shed light on the crystalline nature of a few different examined samples of graphite, highlighting their carbon content compared to other elements known at the time. He [19] also performed experiments where the crystals were evaporated while heated in the presence of air. Since the article was devoted to the atomic weight of graphite, it can be considered as one of the first steps for the long road leading to the structural resolution of the "graphite family" (Figure 1), which, in particular, contains the natural building block for CNTs.

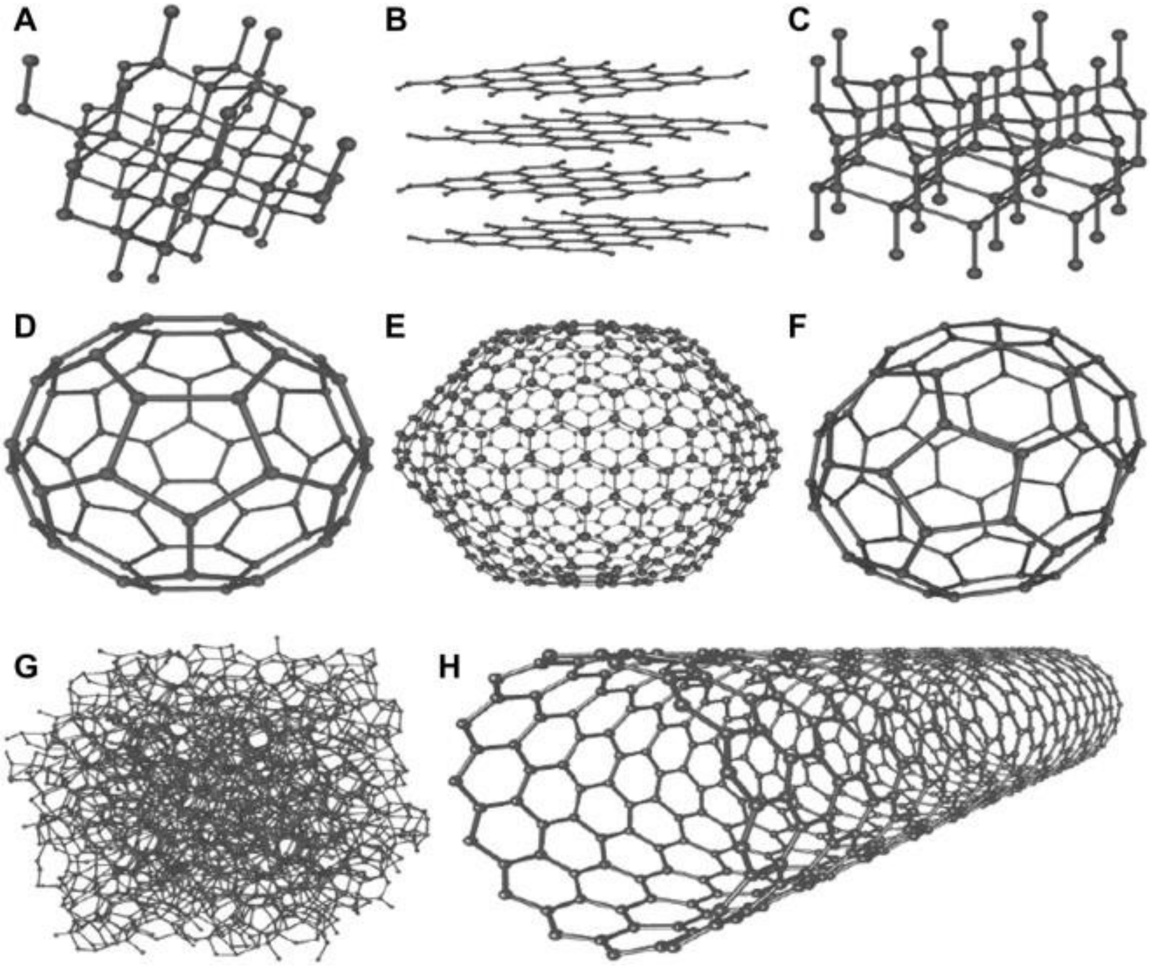

Figure 1: The structures of eight allotropes of carbon: A) Diamond [3D, network covalent structure], B) Graphite [2D, covalent plates] (graphene is a single atom thick layer of graphite), (C) Lonsdaleite, D) C60 [0D, molecules] (Buckminsterfullerene or bukyball), E) C540 Fullerene, F) C70 Fullerene, G) amorphous carbon H) zig-zag single walled CNT. Missing: Cyclocarbon, nanobuds, schwarzites, glassy carbon, and linear acetylenic carbon. reproduced from [20]

One of the first reports of CNTs (Figure 1H) belongs to Soviet scientists L.V. Radushkevich and V.M. Lukyanovich and dates back to 1952 [1]. This first study corresponds to electron microscopy and spectroscopic study of the objects within a soot (carbon black) obtained at 600°C during the decomposition of carbon monoxide.

The authors described the nanoparticles as worm-shaped, while providing microphotographs. They concluded the presence of a growth direction and filamentary crystals formed during a two-stage decomposition of CO in the presence of iron. It is important to highlight that the resolution power of the instruments by that time was insufficient to further elucidate the structure.

The drawings provided in this article are marked at a micrometer scale. Another work with a different route of synthesis was made by Oberlin *et al. [21]*. A thorough discussion of the credits for the first discovery of CNTs was elaborated by Monthioux & Kuznetsov [22].

A more detailed investigation involving DC arc synthesis in argon atmosphere method and a more detailed structural analysis was reported on the year 1991 by Sumio Iijima [2], where he successfully observed “needle-like” tubules of sp^2 carbon synthesized by using an apparatus of low-pressure DC arc discharge, similar to the one used to produce fullerenes (Figure 1D,1E,1F).

The nanotubes grew on the negative electrode of the machine at a $13x10^{-2}$ atm pressure of argon. This process yielded multi-walled nanotubes comprising from 2 up to 50 walls (from 4 to 30 nm in diameter). Thanks to the resolving power of the instrument other produced structures were identified showing that his process is not selective for a certain kind of particle to be produced.

The nanotubes produced by this process were examined by electron dispersion; the smallest specimen analyzed was 2.2 nm in diameter. The diameter was estimated at around 30 carbon hexagons, Iijima also recognized the approximated diameter reduction required between the size of coaxial (multi-walled) nanotubes to fit inside of one other. By following the Bragg law [23], the first approach to investigate the concept of what we now know as chirality was established, and the simplified concept of a folded graphene sheet, with their corresponding diffractograms.

This article spiked the curiosity about how the electrical and mechanical properties of these nanotubes could be. Since it was, they are single crystal, single molecule, inert, and stable structures, nanotubes are the candidates to replace metals to some extent. Some properties are shared with other graphitic and carbon-based materials including diamond. They are an atom-thick tube of hexagonal carbon (graphene).

In 1992, Hamada *et al.* [24] studied the electrical conductivity of the graphitic one-dimensional conductors. Here they confirmed electrical transport properties of a few nanometers diameter rolled graphitic sheet (SWCNT).

They found that the nanotubes exhibited different electric behaviors, from a semiconductor to a completely metallic behavior that depends on the angle of rolling. Through this, they defined the rules of chirality and derived a law to understand all the possible folding angles for CNTs. Their band structure calculation using the tight binding model became a standard in CNT research to understand the electronic behavior of the nanotubes.

Since the isolation of individual sheets of graphene by Geim and Novoselov (Figure 2) through scotch tape exfoliation [25], reported in 2004 [26]; the authors described the unique electronic behavior of one atom thick carbon films. It is important to highlight the field effect of this material, which compared to other single-atom layer matrixes, was stable at ambient conditions and was able to withstand high currents. No other one-atom naturally occurring thickness films have such a conductivity, or field effect, and the behavior is different from both multilayered graphene and bulk graphite. The information provided by this prior research holds some insights into the possible applications for CNTs, which are rolled graphene described in a simplified manner.

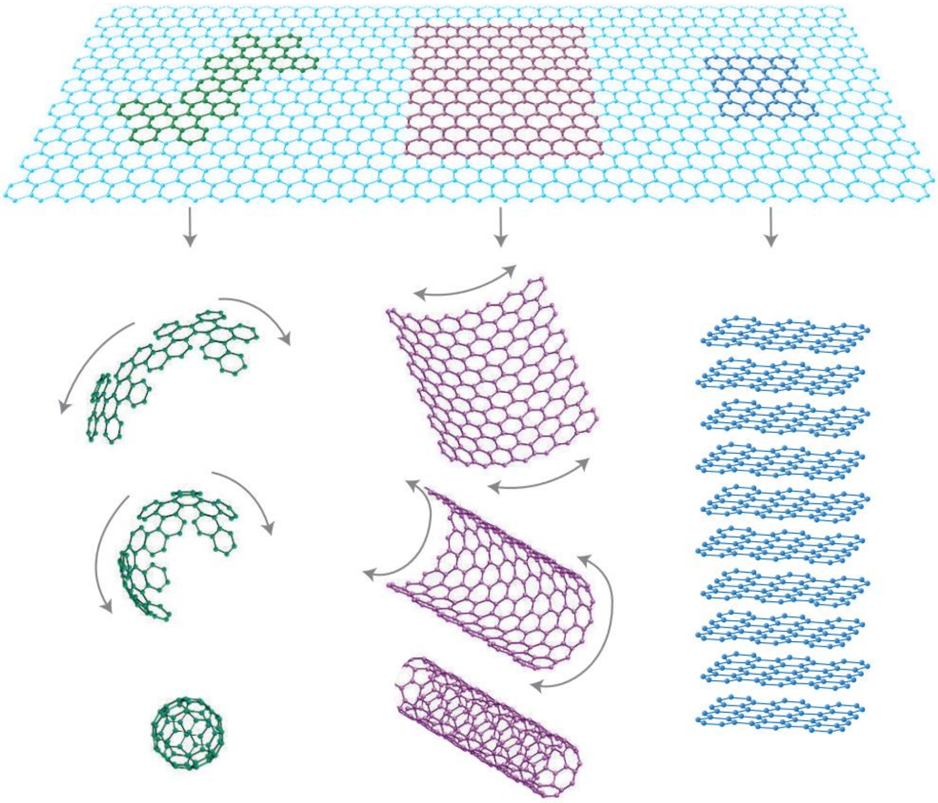

Figure 2: Mother of all graphitic forms. Graphene is a 2D building material for carbon materials of all other dimensionalities. It can be wrapped up into 0D buckyballs, rolled into 1D nanotubes or stacked into 3D graphite. Reproduced from [25].

Further studies confirmed the possibilities of high electric conductance and increased the industrial interest in consumer applications where the advantages over other materials justified the high cost of investment in the early years of the application of CNTs [27].

Some challenges remain to be solved, as the resulting materials are far in quality from the theoretical promises made for materials on ideal structure and conditions. Nevertheless, despite these limitations, the current status of CNTs allowed the humanity to take integrated electronics to the molecular level heading to outperform the physical limits of silicon microelectronics.

This is one of the most important CNT developments because it can allow further microelectronics miniaturization than currently possible with silicon-lithography, especially for the catalytic CVD method, which can be compatible with microelectronic construction and devices [28]. Diameters from 10 to 100 nm are possible; different diameter distributions favor different properties for creating 1D systems [29]; the extraordinary strength of the carbon-carbon bond (which is responsible for the strongest materials known by mankind) plus free π electrons in the graphitic configurations summarized remarkable electric and mechanical characteristics.

For electric conductance, the most promising features are the ballistic (scattering free) and spin-conserving transport of electrons along the tubes, with a current handling capability of ~10^{10} A/cm^2 and an elastic modulus of 1000 GPa [28].

Thus, the background of the properties and assemblies of CNTs presents a wide application chemically stable material that can endure harsh environments and high temperatures while still providing high mechanical resistance and transparency, which allows devices for advanced technology. These properties depend directly on many different structural parameters of the nanotubes; the control over their structure is paramount to target specific applications.

1.2. CNT Synthesis

CNTs were first observed in soot from CO catalyst mediated decomposition [1]. A systematic effort for synthesis was made dry by arc discharge in argon atmosphere by equilibrium DC plasma (arc discharge) synthesis by Ijima [2] as a variant of the method used by Kroto *et al.* to synthesize fullerenes [30].

Other successful synthesis routes have been investigated; they can be divided first between wet and dry methods. Rathinavel *et al.* [31] mentioned that the arc discharge method has a yield rate of this method is superior to 75% and the defect rate is good compared to other methods.

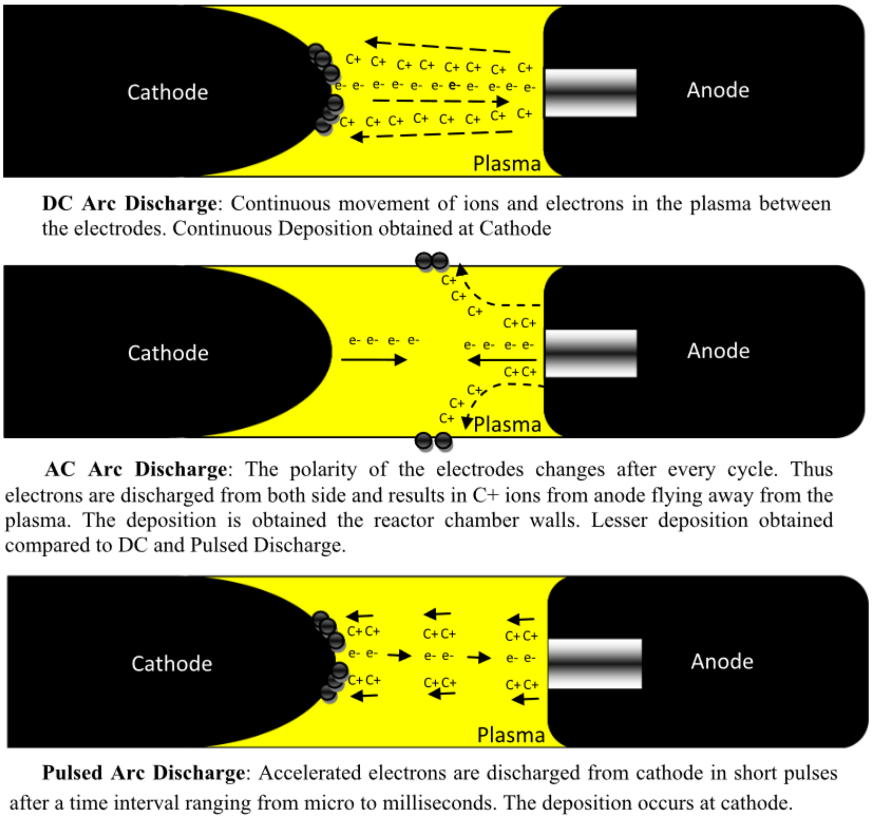

Figure 3: Schematic of the syntheses process for CNTs: DC Arc discharge, AC Arc discharge, Pulsed Arc discharge. Reproduced from [32].

Since the nanotubes grow on the negative electrode of the machine (Figure 3), this can be considered a supported catalyst method, as no airborne catalyst or vapor of it is being provided. The nanotubes obtained are from 4 to 30 nm diameter and up to 4 mm long. Commonly SWCNT synthesis uses catalyst precursors and anodes made of graphite or metal, that may contain carbon. MWCNTs can be synthesized without catalyst precursors, but the presence of metallic catalysis makes the nanotubes longer. The evolution of this method allowed it to be used to create a variety of nanotubes.

Another method is the laser ablation technique (Figure 4). First used by Tess *et al.* in 1996, the purity of the nanotubes by this method is higher, the yield is much lower than for the arc method (Figure 3) and due to the energy levels required and the composition of reactants involved, both methods can be directly compared.

Thermal synthesis is a group of the methods where non-plasma-based heating occurs, including the use of plasma to enhance CVD, called PECVD (PECVD); comprehends different methods that heat reactants to no more than 1200 °C. The resulting CNTs depend on the carbon feedstock and other numerous parameters. It is considered the most facile method to synthesize CNTs owing to the low investments, high scalability, and possibility of an advanced control over the properties (Figure 4).

The methods where plasma is the main source of heat to the reactants, are denominated depending on the specific type of plasma source used, like for example, microwave plasma [33], or inductively coupled plasma [34] laser ablation (Figure 4A), can produce plasma, but the specific heating mechanism is to be considered to accurately name the process plasma based or not, or plasma enhanced, when other heat sources + precursor treatment / injection are used together with a plasma generating setup.

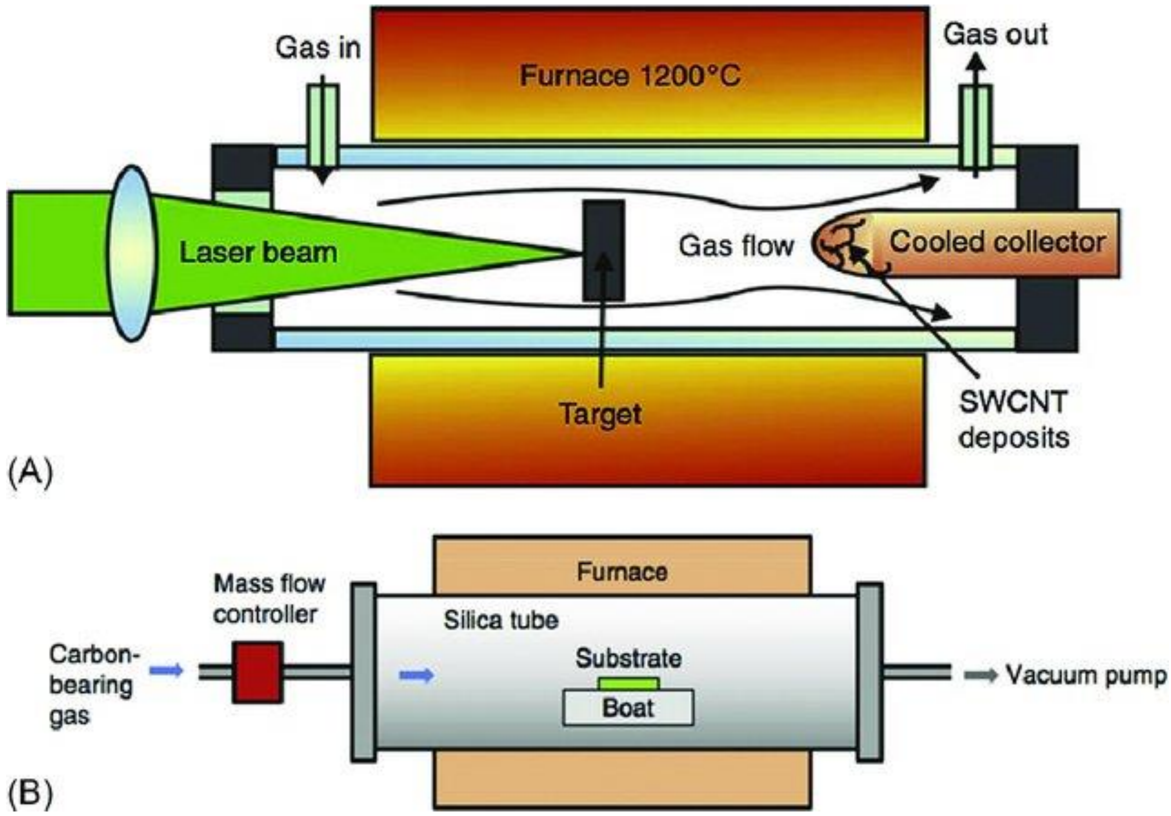

Figure 4: Schematic of the syntheses processes for CNTs: A) Laser Ablation, B) CVD supported catalyst aerogel like vertically aligned forest. Reproduced from [35].

Flame synthesis (Figure 5) provides both reactants and energy for the synthesis process simultaneously and forms many different kinds of nano-carbon [31]. Carbon source is normally supplied in the form of hydrocarbons in gas form, mixed with an oxidizer to produce a gaseous mixture of water vapor, carbon monoxide and dioxide among other minor components; to form nano-carbons a gaseous or vaporized reactant(s) with or without a catalyst is / are supplied [31]. It is an autothermal process, the reactants can be injected together with the fuel + oxidizer or aside of the flame [31]. The process is scalable and is industrially popular where the selectivity of the type of nanocarbon produced is not critical. Due to the similarity with CVD growth process (Figure 5), it was useful to assess the growth rate and structure of CNTs [31].

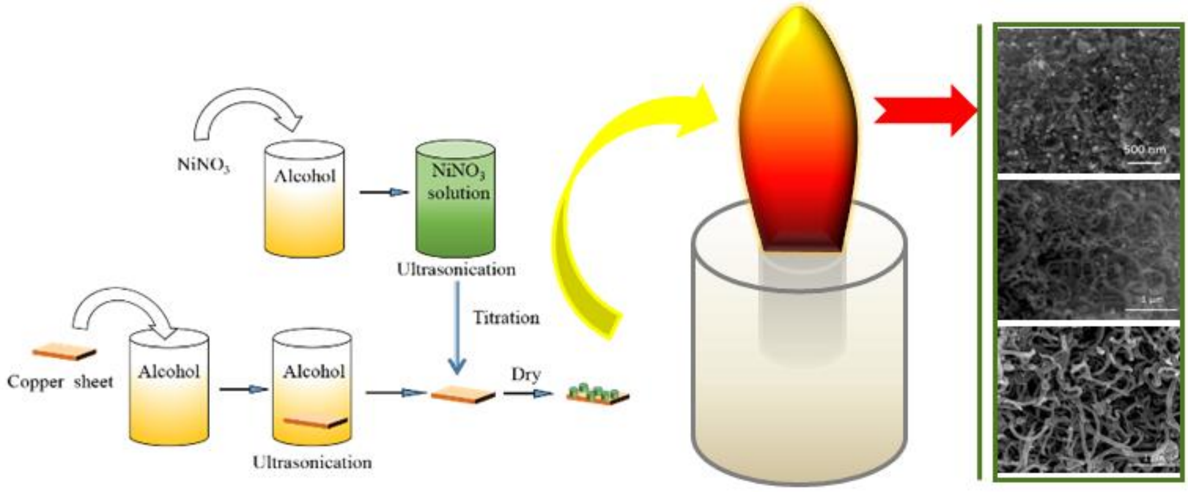

Figure 5: Process for single walled nanotube flame synthesis, reproduced from [36]

CVD process for SWCNT synthesis achieved to eliminate most of the purification stages required for the first methods of synthesis for CNTs, while additionally improving the yield in a significant manner [31], selectivity is also better. Since a catalyst is necessary, it can be floating or it can be placed in a substrate, heated up from 700 to 900°C.

The process of synthesis starts by gradually adding a carbon bearing gas, while regulating its concentration by the addition of an inert gas like argon or nitrogen. Yield is of around 90% and high purity [31]. It allows the growth of a well-organized structure [31].

One of the advanced CVD methods is the vapor phase growth or also called floating catalyst method. Catalytic particles or precursor is supplied in vapor phase and allows for the nanotubes to grow in the absence of a substrate [31]. From a viewpoint of applications, low cost, high-purity, high-yield, and large-scale production is important and thus, the vapor phase growth method has been studied intensively [37]. The method of iron pentacarbonyl bubbling with acetylene pyrolysis developed by [37] reported a large-scale synthesis of high purity CNTs with a maximum length of 2 mm, using a single furnace system without a water-cooled injector.

They used a horizontal quartz furnace with a heating zone of 200 mm. It is noteworthy that not only the deposits are found everywhere on the inner surface of the reactor, but the length and the diameter of those CNTs are homogeneous. High-purity MWCNTs without any trace of carbonaceous particles are produced [37].

The CVD selective synthesis for SWCNT thought iron pentacarbonyl route has been successful. While the catalyst precursor has applied for the synthesis of SWCNTs, it is worth reviewing the investigation of Nasibulin *et al.* [38], where single- and multi-walled CNTs were synthesized by a novel aerosol method using alcohols, namely ethanol and octanol, as carbon precursors.

Preformed iron and nickel aerosol nanoparticles, produced by evaporation from resistively heated metal wire, were used as catalysts. Multi-walled CNTs were initiated by 10 nm sized catalyst particles and produced in the presence of ethanol vapor with the partial pressure of 7072 Pa, while combination of 2.4 nm particles and decreased alcohol vapor pressure (123 Pa) resulted in the formation of mainly single-walled and a small fraction of double-walled CNTs. The effect of a promoter (thiophene) in the system was found to be very important for the synthesis of multi-walled CNTs, while only a 30% number concentration increase was found for the SWCNT production [38].

The work [39] provides an easy and affordable fast route for single- and double-walled CNT synthesis. Further work was done towards a high yield SWCNT synthesis; selectivity was complete with the work of Moisala *et al [39].* where a gas-phase process of SWCNT formation, based on thermal decomposition of iron pentacarbonyl or ferrocene in the presence of carbon monoxide (CO), was investigated in ambient pressure laminar flow reactors in the temperature range of 600–1300 °C.

Ferrocene was found by the authors [39] to be a more productive catalyst precursor compared to iron pentacarbonyl decomposes at lower temperatures resulting in the excessive growth of catalyst particles. In situ sampling carried out at 1000 °C showed that the SWCNT growth occurred from individual metal particles in the heating section of the furnace in the temperature range of 891–928 °C, in which the growth rate was estimated to exceed previous methods. FTIR measurements of gaseous products revealed that the majority of the CO disproportionation took place on the reactor walls. Raman measurements confirmed the results of TEM observations, namely, the formation of a very high purity SWCNT product [39].

The controlled catalyst production by a separate mechanism was investigated by Krasnikov and Nasibulin *et al.* [40,41], where two different approaches for production of iron catalyst were applied in the CVD process. The fine tuning of synthesis parameters was investigated by Krasnikov *et al.* [42], where development of multiparametric process of SWCNT synthesis took place. The authors examined the implementation of machine learning techniques and discussed features of the optimal dataset size and density for aerosol CVD method with a complex carbon source. They employed the dataset of 369 points, comprising synthesis parameters (catalyst amount, temperature, feed of carbon sources) and corresponding CNT characteristics (yield, quality, structure, optoelectrical Figure of merit).

Assessing the performance of six machine learning methods on the dataset, it was demonstrated that artificial neural network to be the most suitable approach to predict the outcome of synthesis processes [42]. Also, it is relevant to mention the work of Iakovlev *et al. [43]*, where the authors propose to use artificial neural networks to process the experimental data and to predict the performance of the aerosol CVD synthesis of SWCNTs based on the Boudouard reaction.

The authors employed five key input parameters of the growth (pressures of CO, CO_2 and ferrocene as well as the residence time and the growth temperature) to control the performance of produced nanotube films (yield, mean and standard deviation of the diameter distribution, and defectiveness). The prediction errors were found to be comparable with the corresponding experimental errors [43].

Further improvements of this method were developed by Novikov *et al.* [44], where aerosol (Figure 6) CVD method based on CO disproportionation (the Boudouard reaction), which is one of the most promising techniques for the synthesis of SWCNTs, especially in the form of thin transparent conductive films.

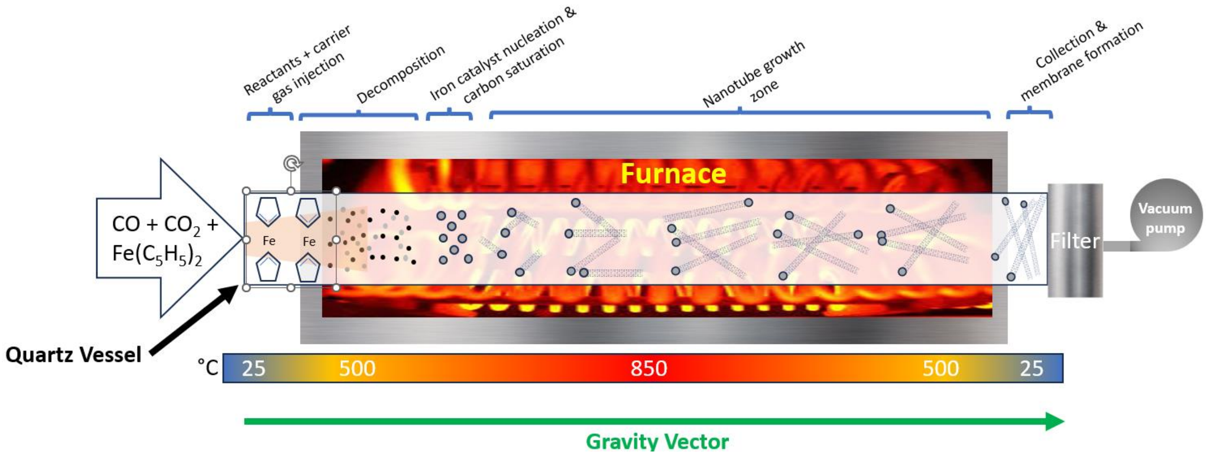

Figure 6: Schematic of the floating catalyst method [10] Nanotubes are aligned for depiction of the growth process. The direction of individual nanotube growth is random for this case. The reactor was operated in vertical position, with the collection unit pointing downwards. Gravity vector direction for reference.

However, despite its advantages (*i.e.*, high quality of nanotubes, absence of double- or multiwalled nanotubes, and high controllability of the process), synthesis based on CO disproportionation fails to provide high yield production required for industrial purposes. In this work, they examined the effect of hydrogen, admixed to the CO atmosphere as a growth promoter, on the synthesis and properties of SWCNTs. Using optical spectroscopy techniques, conductivity tests, and thermodynamic calculations, the authors revealed hydrogen to affect both catalyst activation and nanotube growth.

A positive H_2 effect was found in two different temperature regimes: the yield increase by a factor of ~ 15 at a low-temperature regime (880 °C), a 3-fold decrease in an equivalent sheet resistance (R_{90}) coupled with a noticeable increase in the yield at a high-temperature regime (1000 °C).

This knowledge was extended by Bogdanova *et al.* [45], where the effect of hydrogen on the growth of SWCNTs in the aerosol CVD process using ethylene as a carbon source and ferrocene as a catalyst precursor was studied.

With a comprehensive set of methods (UV-vis-NIR and Raman spectroscopies, transmission electron microscopy, scanning electron microscopy, differential mobility analysis, and four-probe sheet resistance measurements), the authors show hydrogen to inhibit ethylene pyrolysis extending the window of synthesis parameters. Moreover, the detailed study under different temperatures allows us to distinguish three different regimes for the hydrogen effect: pyrolysis suppression at low concentrations (I) followed by surface cleaning/activation promotion (II), and surface blockage/nanotube etching (III) at the highest concentrations.

Among the other synthesis techniques, the aerosol CVD method produces high purity high quality SWCNTs that are suitable for production of advanced membranes and their assemblies.

Thus, the methods for synthesis of SWCNTs have evolved sufficiently to allow the synthesis of high quality and high purity materials for the construction of, for example, advanced devices usable as filters for special aerosols, in space-like environments.

1.3. CNT Assemblies

The unique properties of CNTs and the applications developed for them created the need for their industrial production [46–48]. The features of the nanotubes dictate the possible applications for them [49–51].

The assemblies obtained are related to the synthesis method used, thus, affecting the integration possibilities [52]. We can enumerate different obtained arrangements that show different bulk characteristics: individual nanotubes, fibers/yarns, powder, aerogel [4], forests, and membranes (or buckypapers).

Different characteristics are due to changes in synthesis/postprocessing procedure. While the “powder” nanotube growth happens in a supported catalyst, the obtained CNTs grow in a state called forest [52], where vertically aligned CNTs grow over each catalytic seed deposited on the substrate.

Fibers of nanotubes can be produced [53–55] which have exceptionally high strength [56]. Aerogels [4] made of CNTs have found uses as well [57–59]. In order to assess the properties of the nanomaterial and their arrangements, it is necessary to use different characterization methods. An example of a bulk power, flake-aerogel like CNT composed material are presented in Figure 7.

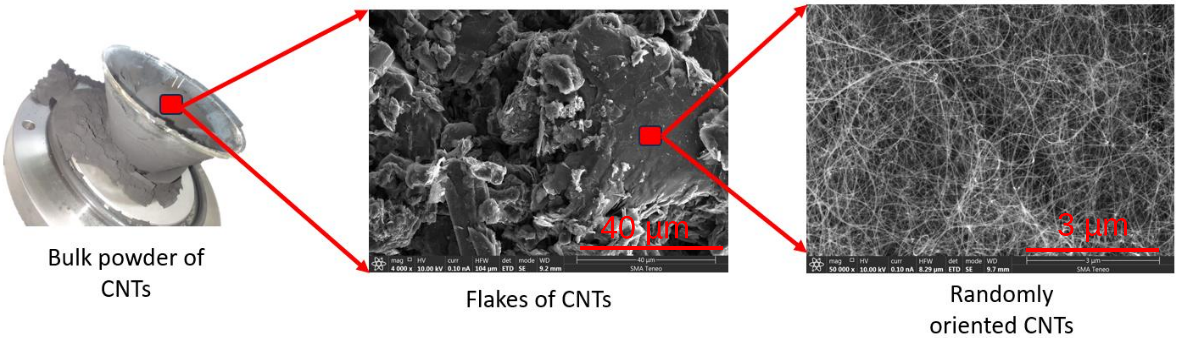

Figure 7: Example of CNT macro and micro arrangement: Powder of flakes composed by CNTs. Scale bar for flakes is 40 µm, for randomly oriented CNTs is 3 µm.

Among the first intents of elucidating the structure of different carbon allotropes, the work of Lipson and Stokes [60] by using X-ray diffraction, paved a way to use different methods of diffraction to understand and classify sp^2 and sp^3 hybridized bonds of carbon structures. Popova [61] summarizes a collection of knowledge towards a precise characterization of X-ray diffraction of graphite, *Li et al.* [62] provides details of microstructural variations for X-ray diffraction characterization of graphite and turbostatic carbon. Since the analyses applied here to bulk material share the same structural composition of CNTs [63] this knowledge proved angular to understand the single molecule monocrystalline nature of CNTs.

While these entirely different arrangements of CNTs exhibit many different bulk collective behavior, the type, size and quality of nanotubes allow predicting to some extent certain properties of the resulting bulk material. For this purpose, different physical and chemical analysis methods are applied.

Since all CNTs are electrically conductive, the preferred morphological method for the study of thick (>10 nm) specimens is scanning electron microscopy (SEM). The method is a de facto standard [64–66] even for composites that have other nonconductive components [67] because the nanotubes add a meaningful conductive component [68] even in low concentrations, including elastic nanocomposites [69]. Raman spectroscopy allows one to assess the quality of nanotubes [70]. Due to the hexagonal ring structure shared with the graphene [71] crystallinity metrics have been established from Raman spectroscopy measurements [72].

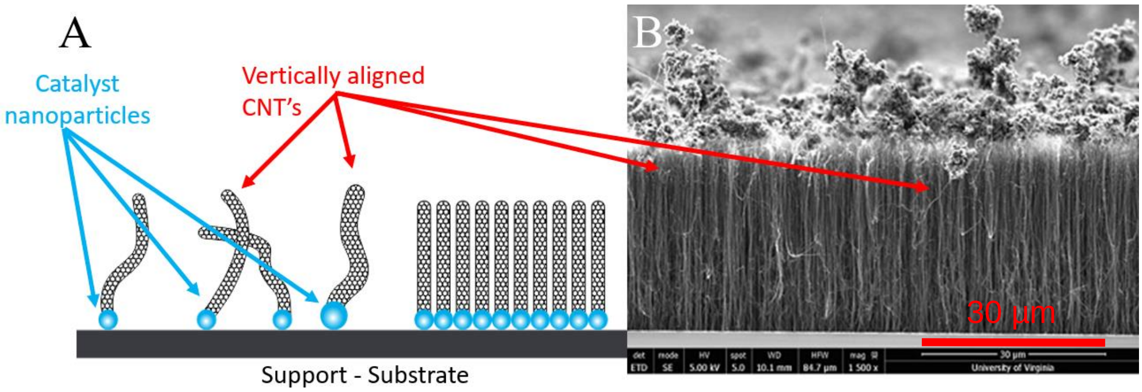

Figure 8: A) Illustration of nanotube distribution in a supported catalyst (forest like structure) reproduced from [73] and B) SEM photo of an aerogel like vertically aligned CNT forest [74].

Thin samples containing CNTs (< 10 nm) (Figure 7,8) can be successfully studied morphologically by means of transmission electron microscopy [75] and the complementary methods for the particular microscope. Relevant knowledge about the growth mechanism has been also obtained through this imaging method [76].

UV-vis-NIR spectroscopy of transparent specimens containing CNTs [77] established a set of metrics for assessing the Van der Waals interaction [78] between nanotubes, and their dispersions in liquids [79] allow for characterization of the presence and diameter [80] of CNTs by analysis of π plasmon peak. Other features can be assessed by this method as well and they will be discussed in further sections. It should be noted that assemblies might significantly vary with respect to bulk density (Figure 9).

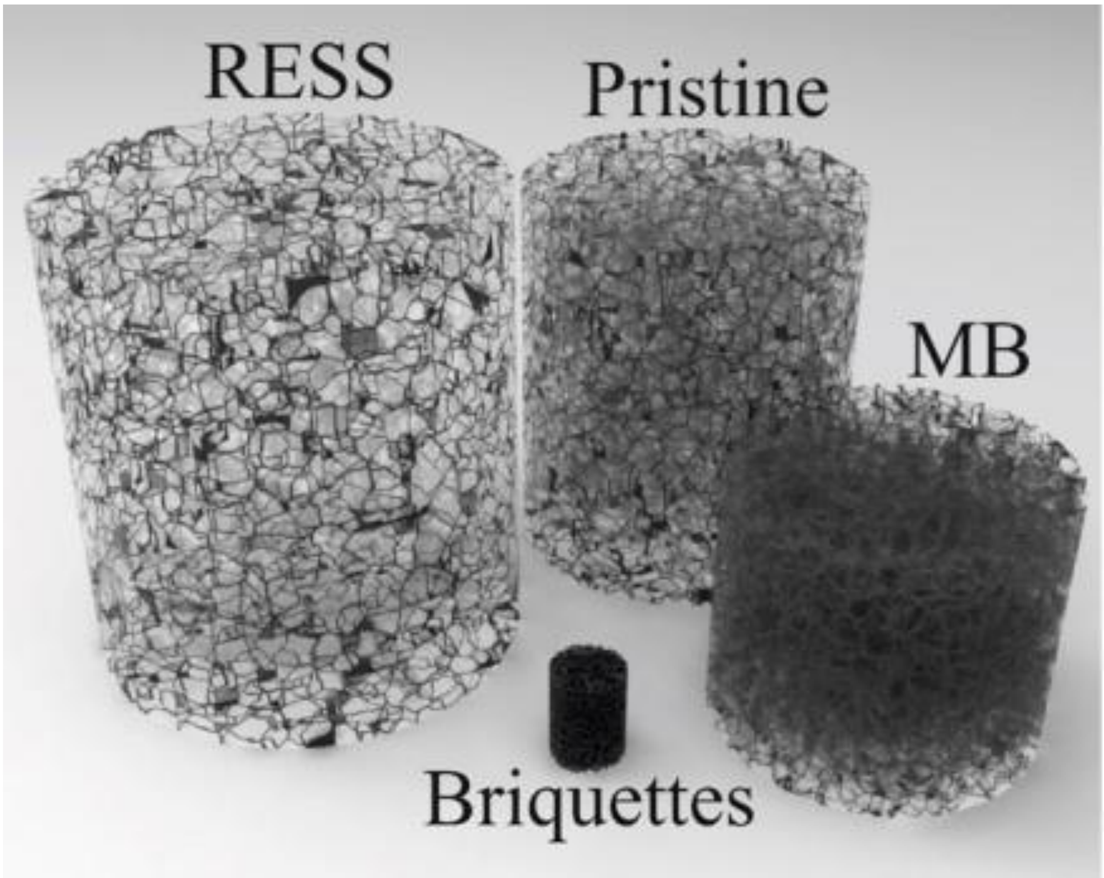

Figure 9: Illustrative representation of the bulk density difference between the four kinds of SWCNTs used, from the left: RESS (expanded), pristine, briquette (compressed), and commercial masterbatch (MB). The cylinders are of equal mass. Reproduced from [81]

Depending on the synthesis method for the nanotubes, forests (a supported aerogel of parallel standing vertically aligned nanotubes) (Figure 8) or free-standing membranes (Figure 10D) of the nanotubes can be obtained.

For the specific goal of obtaining thin membranes of stacked CNTs (Figure 10 A), the CVD floating catalyst method (Figure 6) produces membranes of tunable thickness collected by filtration.

These membranes are denoted as multifunctional by Nasibulin *et al. [5]*, where the authors explore a wide range of possibilities for SWCNT based membranes.

The authors report a simple and rapid method to prepare multifunctional free-standing SWCNT films or membranes with variable thicknesses ranging from a sub monolayer to a few micrometers having outstanding properties for a broad range of exceptionally performing devices.

Nasibulin *et al. [5]* have fabricated state-of-the-art key components from the same single component multifunctional SWCNT material for several high-impact application areas.

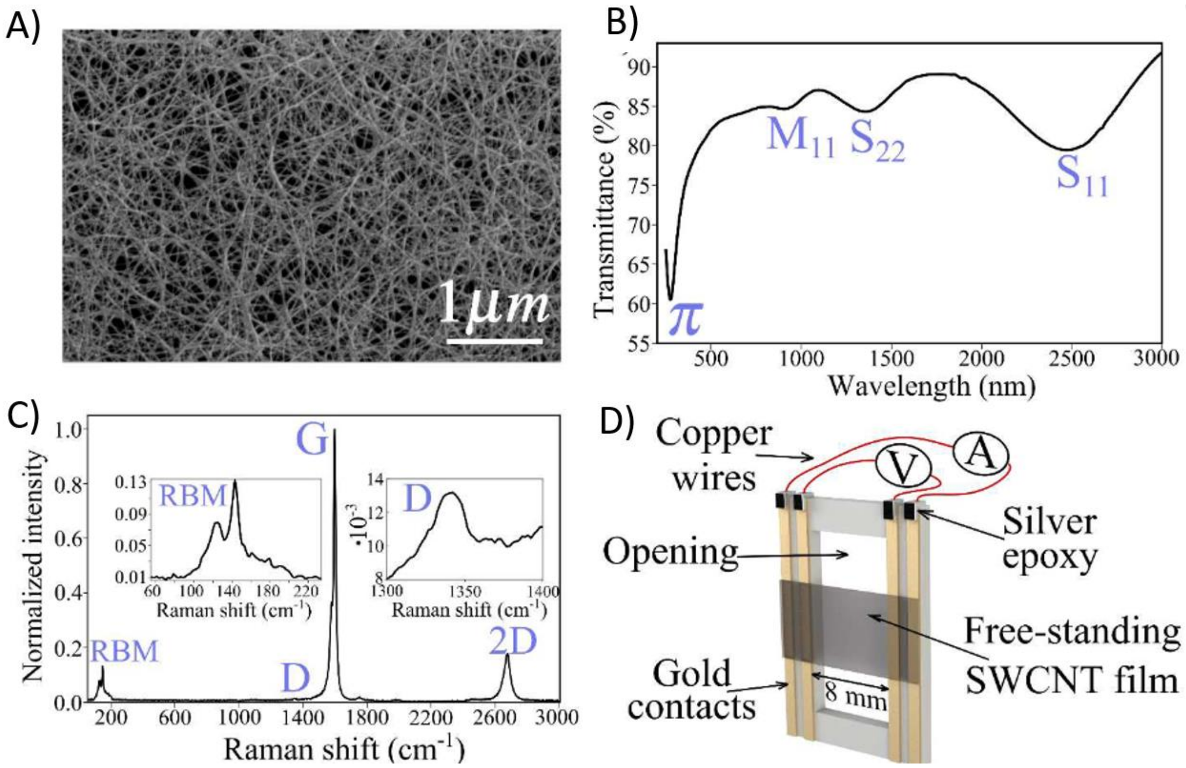

Figure 10: A) SEM micrography of a freestanding SWCNT membrane on holder, B) Typical UV-Vis-NIR spectra of SWCNT's C) Typical Raman spectra of low-defect SWCNT's, D) Original holder used previously for Joule heating research. Reproduced from [82].

The different methods to rearrange the CNTs [83,84] permit the manufacture of different elements suitable for various applications.

They let a wide exploitation of the unique properties exhibited by each different bulk material composed of CNTs, like for example: fibers, aerogel, membranes and briquettes for conductive polymer composites, just to mention a few.

The resulting arrangements can be further processed to tailor certain features or change their behavior using methods like functionalization.

1.4. CNT Functionalization

Due to the sp^2 hybridization of carbon in graphene / nanotube external structure and their high surface area, they can be easily tuned via functionalization, which is according to Dubey *et al.* “Functionalization is the generation of functional groups on the surfaces of CNTs” [85] .

Functionalized CNTs (Figure 11) have been successfully applied to environmental and biomedical sciences [85], for example they have promising applications in therapeutics and diagnostics [86].

Depending on the desired alterations for the nanotubes in questions, many different methods have been proposed [87].

Functionalization can be covalent or non-covalent. High quality composites can be made with functionalized CNTs. Functionalization can be inside of the nanotube or outside of it on the sidewall [88].

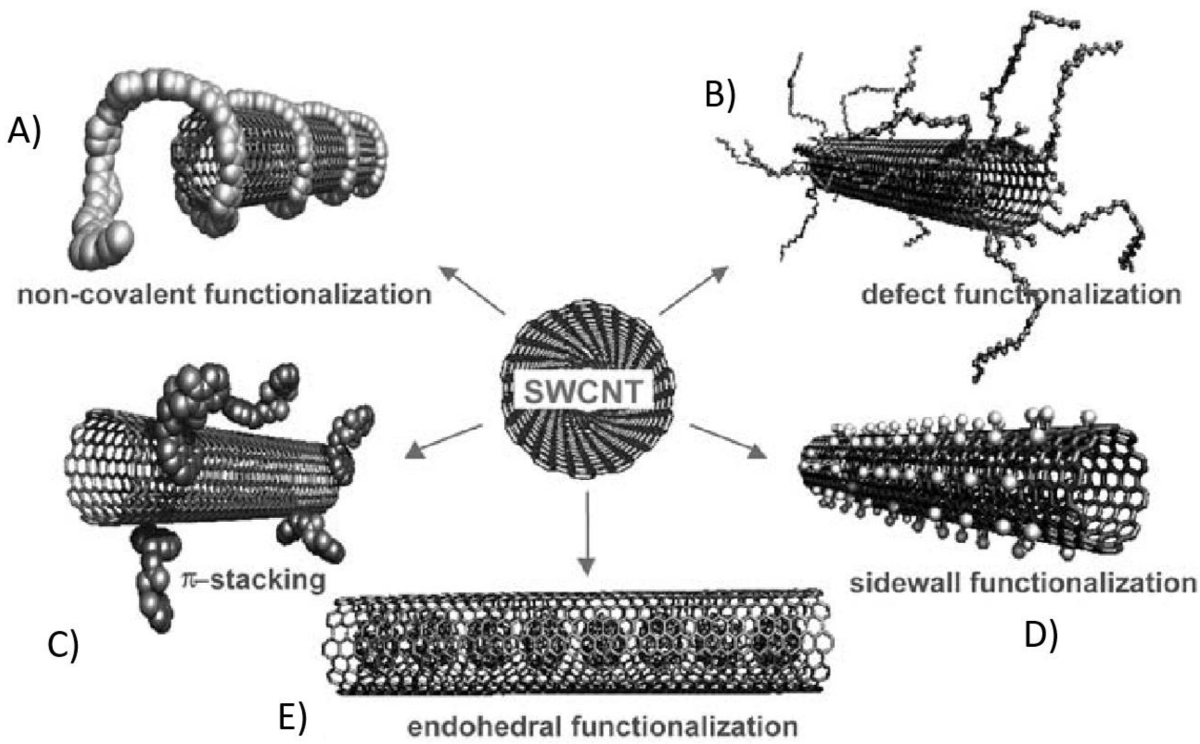

Figure 11: Different possibilities of functionalization of SWCNT's: A) Noncovalent exohedral functionalization with polymers. B) Defect-group functionalization. C) Noncovalent exohedral functionalization with molecules through p-stacking. D) Sidewall functionalization. E) Endohedral functionalization, in this case C 60 @SWCNT. Reproduced from [89].

Functionalization of CNTs has the ability to alter the properties of the nanotubes in a repeatable and predictable manner. Dubey *et al.* [85] highlights functionalization as a possible remedy for agglomeration and bundling.

Bundles can as well be tuned and functionalized, a detailed study was elaborated by Mitin *et al.* [90]. The degree of bundling proved to be meaningful for the effectiveness of doping / functionalization of the nanotubes and affects the mechanical and electrical properties of the resulting material.

The advantages of CNT functionalization, made it a preferred method to tailor the properties of CNTs [85]. Chemical functionalization, organic functional groups are generated/attached to the surfaces as well as the tip of CNTs which opens up the possibilities for tailoring the properties of nanotubes and extending their application areas.

Different research efforts have been devoted towards both covalent (electrons between atoms become electron pairs and become shared) and non-covalent (non-electron sharing electromagnetic interaction) functionalization for different applications. Functionalized CNTs have been used successfully for the development of high-quality nanocomposites, finding wide application as chemical and biological sensors, in optoelectronics and catalysis. Non-covalently functionalized (Figure 11A, 11C) CNTs have been used as a substrate for the immobilization of a large variety of biomolecules to impart specific recognition properties for the development of miniaturized biosensors as well as designing of novel bioactive nanomaterials.

Functionalized CNTs have also been demonstrated as one of the promising nanomaterials for the decontamination of water due to their high adsorption capacity and specificity for various contaminants. Specifically modified CNTs have been utilized for bone tissue engineering and as a novel and versatile drug delivery vehicle".

Functionalization of CNTs permits the enhancement of certain structural features of the nanotubes, changing the bulk material behavior, providing a material tuned for certain applications, depending on the required operating conditions.

1.5 Applications of SWCNT based membranes

Nasibulin *et al.* [5] "have fabricated state-of-the-art high efficiency nanoparticle filters with a Figure of merit of 147 Pa^{-1}, transparent and conductive electrodes with a sheet resistance of 84 Ω/□ and a transmittance of 90%, electrochemical sensors with extremely low detection limits below 100 nM, and polymer-free saturable absorbers for ultrafast femtosecond lasers". Furthermore, the films are demonstrated as the main components in gas flowmeters, gas heaters, and transparent thermoacoustic loudspeakers [91].

SWCNT electrodes have been manufactured and used [15,92–95] Owing to their unique properties such as high conductivity and surface area, electrochemical stability, low background currents, and electro catalytic properties in many electrochemical reactions, SWCNTs have been extensively used for electrochemical sensing. In [96], the authors show the excellent sensing properties of FSF electrodes for the electrochemical detection of dopamine, a neurotransmitter often taken as a benchmark analyte for investigating the sensing properties of electrode materials. Another important application for FSFs is a laser component, namely, a saturable absorber for ultrafast photonics.

A key element in the cavity of a mode locked fiber laser is the nonlinear element that initiates the pulsed operation. SWCNTs have been demonstrated to initiate short pulses in mode-locked fiber and solid-state lasers. The first thermoacoustic speaker based on CNMs was introduced by Xiao *et al.* [97] These authors fabricated loudspeaker elements from free standing sheets of aligned multiwall CNTs (MWCNTs) prepared by drawing from a substrate consisting of a CVD-grown MWCNT forest.

Xiao *et al.* [97] also claimed that SWCNT networks could be used as loud speakers, but that the fabrication of elements from SWCNT FSFs would be extremely tedious. The authors of [91], for the first time, have demonstrated thermoacoustic speakers using FSFs made from randomly oriented SWCNTs. Ultrahigh-performance transparent electrodes were made by Jiang [15] and a method for welding of CNTs through ultrafast Joule heating was demonstrated by [16].

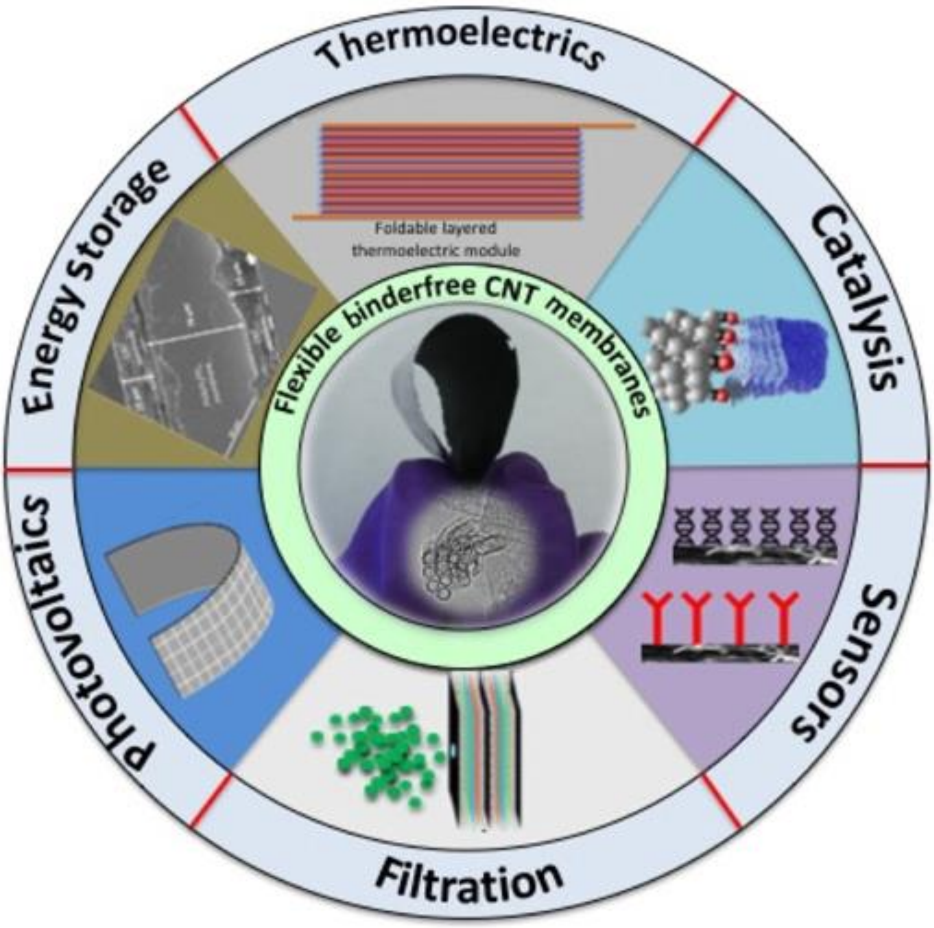

Figure 12: Some potential applications of CNT membranes reproduced from [98].

Many different applications of nanotube-based membranes (Figure 12) exposed to radiation have been demonstrated successfully. The metal droplet shielding has been demonstrated as well. The production of semiconductors is key for current technology and the life of humanity. The main technology for semiconductor production is EUV, which has a dire need for special aerosol protection in a space like environment, inside of an EUV lithograph.

1.6 EUV lithography and aerosol protection pellicles

Integrated microelectronics were thought in 1952 by Geoffrey Dummer [99] invented in 1958 by Kilby *et al. [100]* at Texas instruments incorporated, and later independently by Robert Noyce [101]. The first integrated circuits were drawn by hand, nevertheless, the preferred way to miniaturize the design as required was being done through the method of lithography [12,102,103].

Moore's law [11,104] tells that at twice smaller features the speed of operation and efficiency of the devices increases. The limiting factor to achieve smaller features becomes the wavelength of the light used to engrave the design into the wafer. State of the art method uses 13 nm light [105] (Figure 13). This method is named EUV Lithography [12]. This is the preferred method to achieve features in integrated microelectronics as small as $2x10^{-3}$ μm [106].

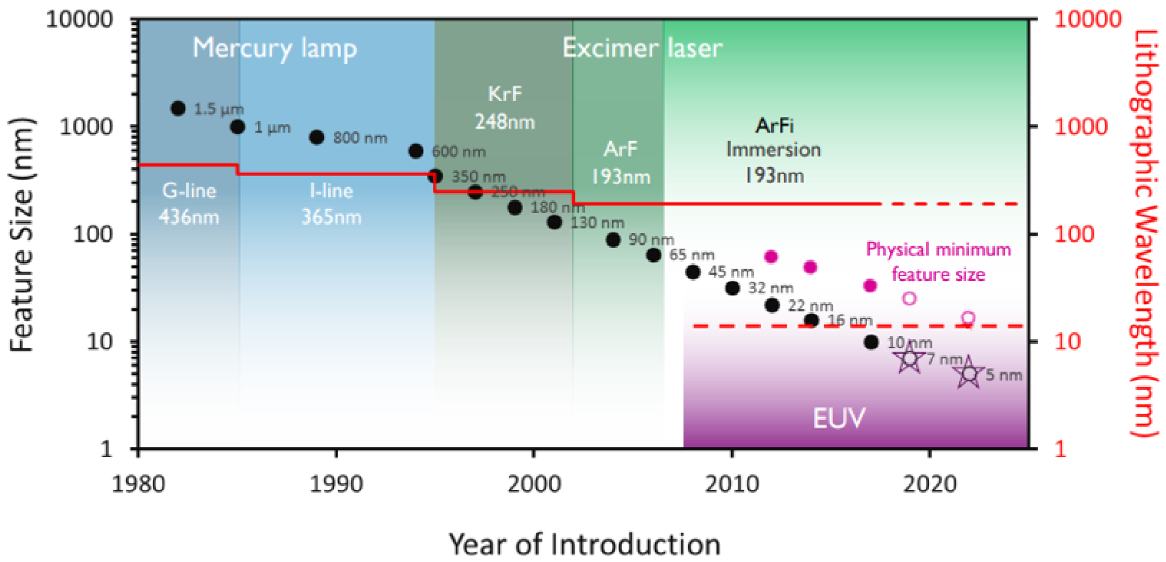

Figure 13: Evolution of lithography technologies, showing the feature size achievable with each light source & optics technology. Reproduced from [106]

The damages of the mask [106] caused by the tin aerosol particles has been extensively investigated as well. The authors [107] also suffers damage. Different pellicle technologies are worth mentioning [13,108–111], their cleaning methods [13,112–116], and the downtime of the EUV equipment has been assessed thoroughly [105].

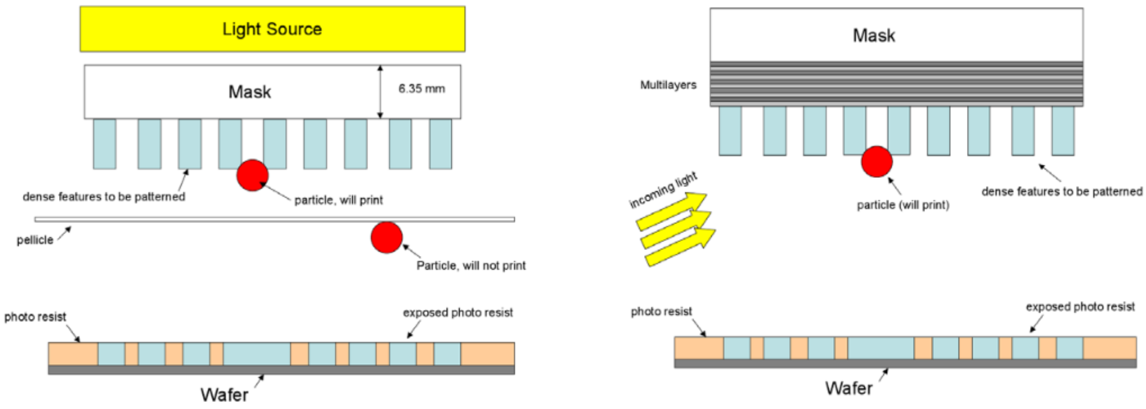

Figure 14: Example of characteristic wafer damage caused by presence of particles on the lithography reticle. Reproduced from [114].

Since extreme UV is de facto the state-of-the-art standard for the production of the fastest integrated microelectronics (2023) with the smallest features, it is industrially relevant worldwide. The industry requires to decrease equipment downtime and a pellicle material that can be cleaned ideally in-situ.

The damages caused by aerosol particles landing on the surface of the reticule are of concern (Figure 13) since they can remain undetected until the inspection phase (Figure 14), compromising the quality of a great number of devices.

SWCNT membranes have been evaluated as EUV pellicle material successfully. It is fundamental to understand their properties to assess the possibility of building the first renewable EUV pellicle based on SWCNTs. The ion penetration through SWCNT membranes is also relevant for the life extension of short-wave optical equipment that operates with metal-plasma light sources [7].

The criteria for renewability can be resumed in the following manner: “The ability of the pellicle to eliminate EUV shadowing material from its surface with minimal damage and with minimal intervention”. The abovementioned can be further improved by: “The pellicle not requiring removal from the EUV lithograph for its renewal”.

1.7 Conclusions of the literature review

Carbon materials are considered as the means of life to be possible on our planet; graphite has been an industrially meaningful form of carbon since centuries ago, the applications of this carbonaceous material range from fireplaces to the discovery of electricity and atomic energy.

The discovery of graphene as a stable isolated structure and the knowledge accumulated from it opened new technological possibilities. CNTs proved to be a valuable candidate for the technological future of mankind from space travel to stretching Moore's law, allowing for more efficient, smaller, and faster semiconductor-integrated devices, as well as biocompatible flexible and stretchable electronics.

The research on this versatile material is relevant to achieve technological progress beyond mainstream materials. The literature review shows a wide background about the possibilities of the application of CNTs to settle different technological challenges. The unique properties of SWCNT-FSFs, mechanically sturdy, chemically inert, and able to withstand temperatures up to 400°C in the air [5], and >1500°C in an inert atmosphere or vacuum [82], are used for the development of renewable pellicles [7], because they endure both vacuum and EUV radiation, thermophones [91], bolometers [117] and other technological applications like stretchable and flexible electronics [92,97,98,118–121]. Work in progress exists towards 1D van der Waals materials [77,78,122]. Moreover, the previously consulted research provides useful information for the development of devices to fulfill the future industrial needs for the EUV technology and in general present and future applications of SWCNT membranes.

A method of reinforcing mechanically an SWCNT membrane has the possibility to enhance present devices and develop new ones that have been impossible to develop previously due to mechanical constraints.

Moreover, the resonance of highly conductive and ultrahigh performance thin film electronics is enough to compete with metals and getting closer to match indium-tin oxide (ITO) technology from a practical point of view with stronger and more conductive SWCNT membranes by the application of welding and doping at low-pressure Joule heating.

Indium tin oxide (ITO) and single-walled carbon nanotube (SWCNT)-based transparent conductors, while both serving as transparent electrodes, exhibit fundamental differences in their material properties and fabrication processes, rendering direct comparison challenging and often misleading.

The literature review shows that the application of CNT membranes for EUV aerosol and plasma protection is feasible, moreover, renewal technology can be developed for these SWCNT pellicles, also the CNT welding technologies are a thriving opportunity to enhance the mechanical stability of the produced membranes towards new applications or lifetime extension of technological applications beyond the scope of relativistic and shortwave optic systems.

Thus, the aim of this thesis (namely, to develop methods for modification of the membranes to specific applications: EUV (EUV) pellicles, aerosol filters, and transparent electrodes) is relevant and the objectives represent novel and promising ideas:

(1)To assess the CNT membrane filtration efficiency on retention of In/Sn aerosol particles, study their lifetime, and develop technological building blocks for removal of model aerosols using Joule heating.

(2) To assess the deposition of carbon on Joule heated single-walled nanotube membrane surface as a tuning agent for conductivity and mechanical strength.

Chapter 2: Experimental Methods

2.1 Synthesis and collection of SWCNT

Due to the requirement of high-quality randomly oriented nanotubes as a building block for membranes, the method chosen for synthesis was floating catalyst (aerosol) CVD. The aerosol CVD was investigated and optimized previously [123].

An iron-based metallocene compound (ferrocene, Sigma Aldrich, 98%) was injected as vapor at room temperature to a tubular quartz reactor heated to 850 °C in CO/CO_2 atmosphere (99.99% CO – carbon source, 99.995% CO_2 – an etching agent; Figure15).

The Boudouard reaction ($2\ CO \leftrightarrow C + CO_2$) happens on formed iron particles and “creates” nanotubes of average diameter 1 – 2 nm, which can further be deposited SWCNT aerosol on nitrocellulose filters (HAWP, Merck Millipore, USA) as a randomly oriented network on which the transmittance tuning was done by changing the collection time [5].

It is worth noting that various nanotube parameters, namely length, diameter, defectiveness, and bundling degree, can be tuned during the synthesis, forming a possible window for fine-tuning. Though extremely interesting, such a study of the synthesis parameters is beyond the scope of the work and will focus on the development of FSFs.

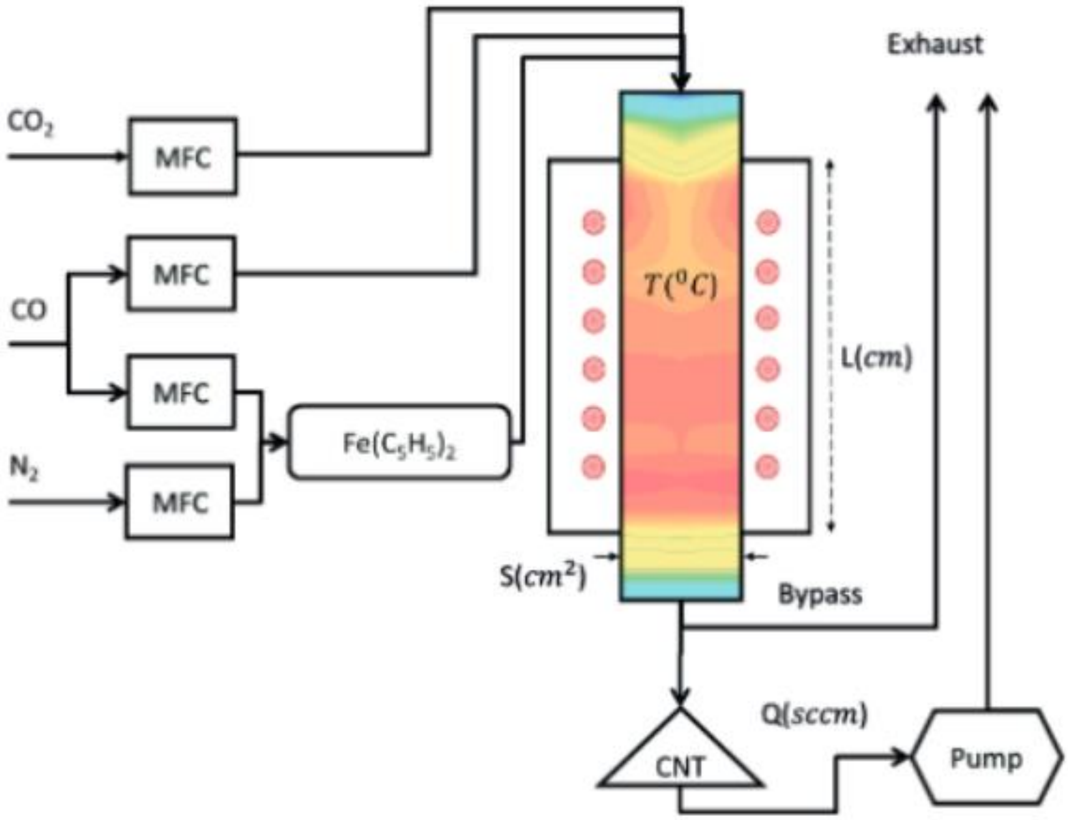

Figure 15: Schematic of the system & reactor used for synthesis of SWCNTs. Reproduced from [10].

The SWCNT thin films are formed by the gradual accumulation (deposition) of floating aerosol of nanotubes and bundles from the gas stream of the reactor on the surface of the nitrocellulose foam filter.

A vacuum pump (Figure 15) was used to ensure an exact flow through the filter, leaving behind a randomly stacked uniform CNT film layer. Despite their high affinity for any surface, the SWCNT adhesion for the nitrocellulose filters (HAWP, Merck Millipore, USA) used for their collection is poor, which means that any other material might work as a secondary substrate to hold the membrane after the dry transfer of the film from the filter.

A small amount of mechanical pressure helps to homogeneously attach the layer to a substrate different than the nitrocellulose filter. This dry transfer method [124] has different variants, depending on the features of the final substrate. Unlike the case of a continuous substrate (*e.g.*, glass, silicon, or a polymer) forming a film, if the dry transfer is performed onto an object with an opening, it would form an FSF.

Many different materials can be used as holders for the freestanding or supported membranes. For the specific cases of this thesis, surgical grade stainless steel, borosilicate glass, and UV fused silica grade quartz glass are used as final substrates during characterization and prototypes of the technological products.

2.2 Control of the film thickness via transmittance

The control of the film thickness through a direct relationship between the optical transmission and membrane thickness was established. Indeed, the Beer-Lambert law predicts the absorbance of a SWCNT film to be in direct relation to the thickness (if the same composition and morphology are preserved).

This approach was previously proven and applied [125] for the collection of SWCNT films with a given thickness.

Since the rate of deposition is linear with respect to time, any desired thickness or transmittance can be calculated by cross-multiplication after knowing three or more different collection times with the resulting membrane transmittance [125].

The collection was performed using a hermetic filter holder with a microperforated steel mesh and a copper mask underneath the cellulose sponge filter to shape the SWCNT membrane to the desired geometry (Figure 16).

Flow was regulated by means of a needle valve fixed to a position calibrated using a flowmeter and a membrane vacuum pump. The collection time was set using a timer and the collection ended by shutting off the vacuum pump.

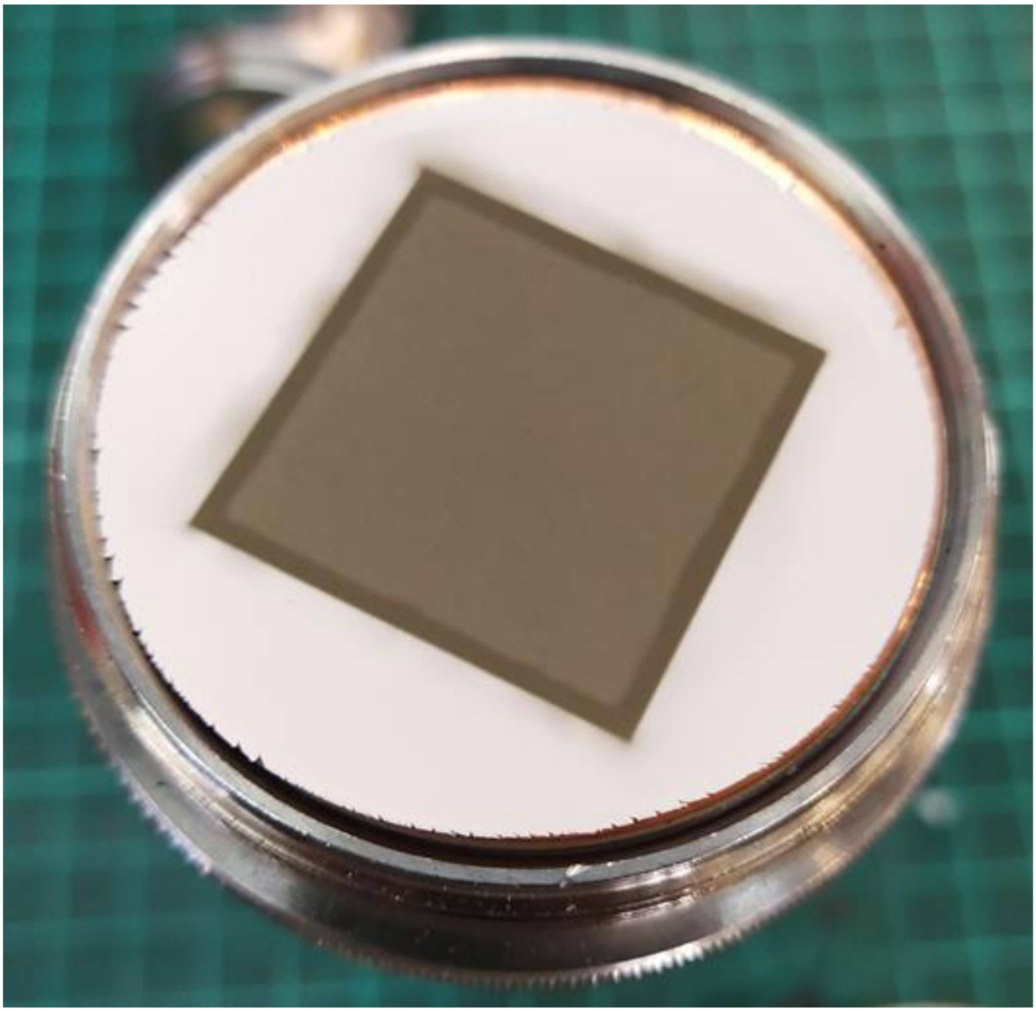

Figure 16: Photo of a SWCNT thin film with 80% transmittance (550 nm) on a filter, shaped as a square by means of a copper film laser cut mask underneath.

2.3 Dry transfer method for fabrication of SWCNT FSF

The dry transfer method described in [126] was modified to satisfy the constraints of the new low-pressure chamber and magnetic sample holder.

The SWCNT membrane border is to be lifted from the filter using a cylindrical stainless-steel electrode (304L stainless steel tube with a diameter of 0.8 mm) by using the adhesion of the SWCNTs to the polished surface of the stainless-steel electrode and wrapped around the electrode, held by a DIL socket by twisting it, or by pulling the membrane using a tool (tweezer or wire for example)

The other side of the membrane is to be picked up by the second electrode by slowly detaching the membrane from the filter (Figures 17 and 18) while detaching simultaneously the membrane from the filter by careful pulling.

Due to the geometry of the low-pressure chamber used for most of the experiments, a system for quick electric connection and a magnetic holder were also developed. A design similar to [97] was used: parallel metallic support rods supported by a refractory material (Figure 10D). As an electrode, we used surgical-grade stainless steel needles of 0.8 mm in diameter (Figure 17). A transfer method was adapted from the guidelines provided by [125].

These previous designs were sufficient to hold the film in freestanding state, but they lacked a multi mating capable connection system and their sturdiness from repeated manipulation within the different analysis was questionable; moreover, the need to transfer to another holder was deemed necessary to test and install the membranes on specialized frames to implement devices for further testing after the membranes were welded.

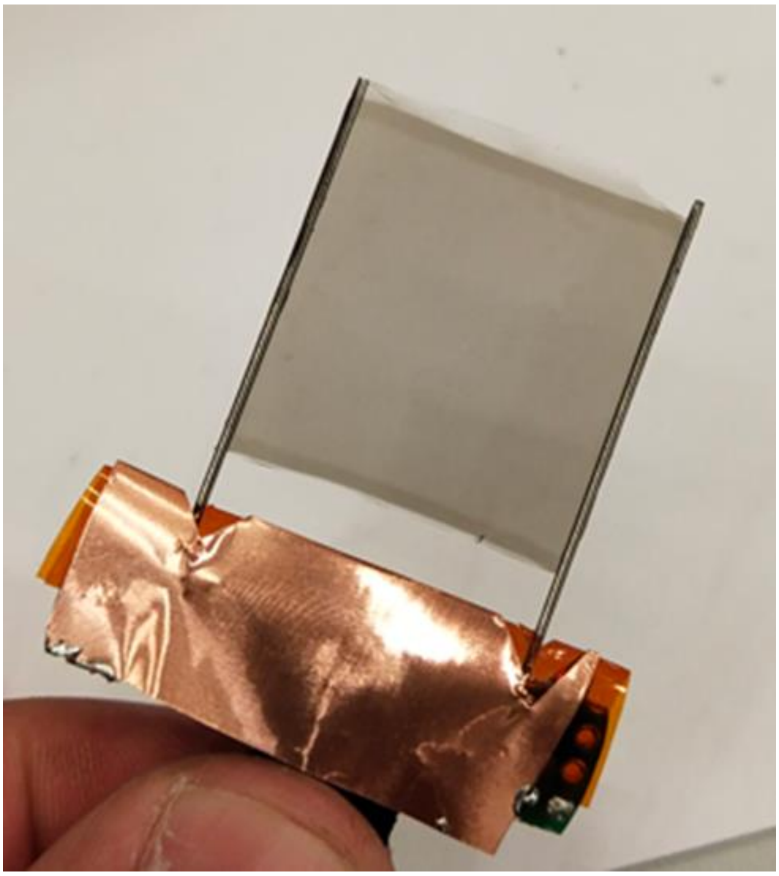

Figure 17: Photo of a SWCNT freestanding membrane on a special heat shielded stainless steel rod holder.

The electrical connection between the film and the rods of the frame had to be good and mechanically sturdy (Figure 17).

Thanks to the high surface area of the CNTs, the adhesion between the membrane and the stainless-steel rod was sufficient to hold the film in place.

To maximize the conductance area of the film in contact with the metallic rod, the film was purposely wrapped around it, covering as much as 70% of the circumference of the membrane.

2.4 Low pressure Joule heating

The welding treatment is to be applied in the same vacuum chamber of the Joule heating (Figure 18,19; P ≤ 2.89×10^{-5} atm), using Pfeiffer hi-cube 80 vacuum station (Germany) with two vacuum gauges (Pfeiffer MPT100, Germany cold cathode and Pirani, Thyracont Vacuum instruments GmBH, Pirani) discussed in detail previously [82].)

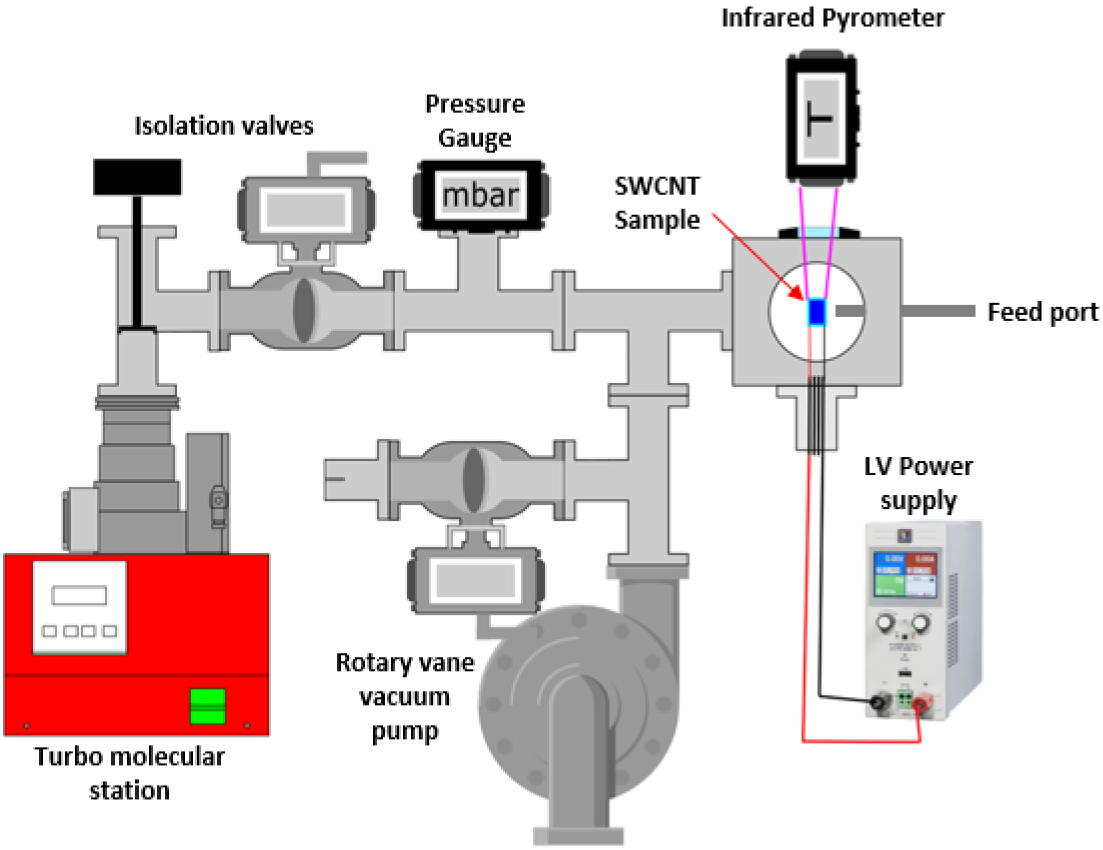

Figure 18: Schematic of the low-pressure Joule heating device.

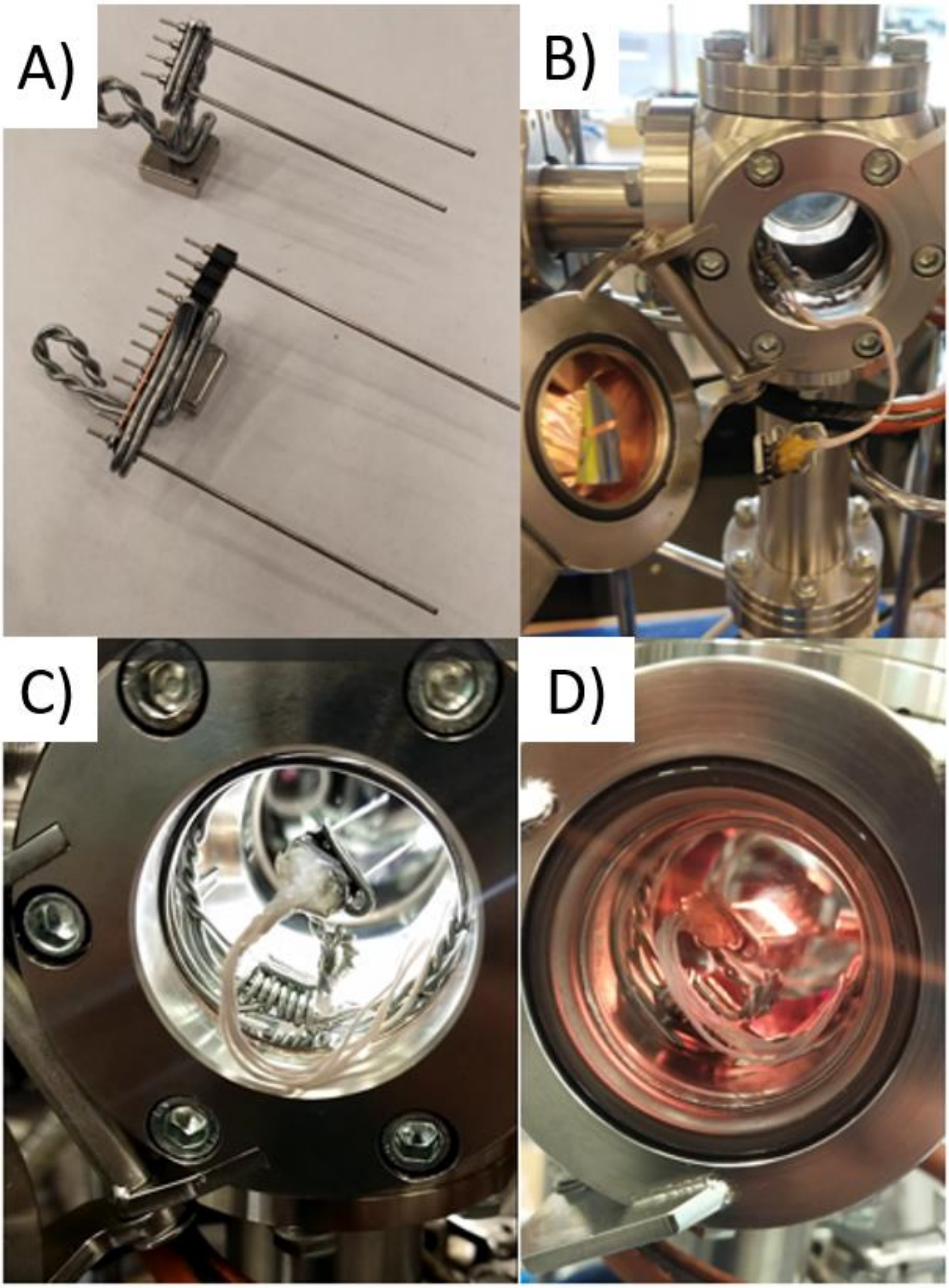

Figure 19: A) Photos of different width holders for low pressure Joule heating, B) picture of the processing chamber, C) sample connector placed in the magnetic holder of the chamber, D) sample in place glowing at temperature > 600°C.

Pressure-regulated high purity (99.9%) ethylene (C_2H_4) was fed to a mass flow controller (Alicat, USA) to a nozzle inside of the chamber (Figure 18, feed port) at a rate of 0.1-1 SCCM. The feed port is also used to supply Sn Aerosol for coating of the SWCNT FSF.

The vacuum chamber requires a special ceramic hermetic power feed to supply power to the sample and achieve the raise of temperature taking advantage of the Joule heating. For this purpose, the holders are dimensioned as necessary allowing the treatment of different membrane sizes.

A magnetic holder and DIL socket wired with PTFE-coated deoxidized copper vacuum wire was fabricated to hold the sample in place during the treatment improving the throughput of the reactor (Figure 19 B,C,D).

The vacuum system used in [82], was improved, it now comprises a turbomolecular station with membrane pump backing, an airlock operated with a scroll pump, a cold nitrogen trap to avoid vapor impurities from reaching the vanes of the turbomolecular pump, and a nitrogen venting system to avoid contamination by water vapor, allowing to reach pressures down to 3.94×10^{-8} atm in ~3 min from atmosphere.

A Kelvin RXR (ZAO Euromix, Russia) pyrometer working in the range of 1.0 to 1.6 µm and with a temperature detection range of 400 up to 2300°C was placed over the top borosilicate glass window to measure the temperature of the SWCNT FSF as shown in Figure 18.

2.5 Ethylene Welding

The flow of ethylene passed through the SWCNT membrane while heated, as shown in Figure 20. The membrane was heated in a single step by direct current (DC) with a power source Electro Automatics 3200-04C (Germany).

The temperature of the membrane was controlled with a pyrometer (Euromix RXR 2300, Russia) in the temperature range from 700 to 1700 °C on the basis of spectral response from 1.0 to 1.6 µm. A detailed description of the calibration procedure for the pyrometer is described elsewhere [82].

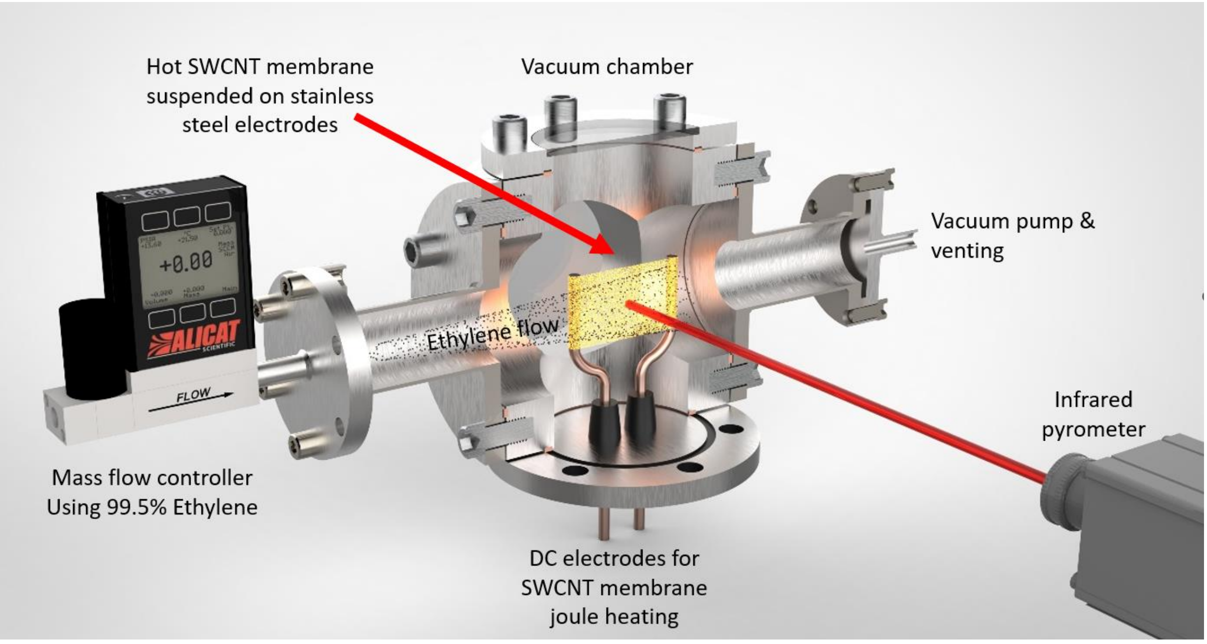

Figure 20: A scheme for SWCNT free-standing membrane on stainless steel rod holder inside of the low-pressure ethylene welding chamber.

The optimum treatment temperature was explored experimentally by comparative evaluation of the UV-vis-NIR spectra of various membranes treated at different temperatures during the same amount of time, and vice versa aiming to find the minimum increase of absorbance.

A “time (duration) of treatment” vs “transmittance decrease” relation was established. Krasnikov *et al.* [127] investigated the ethylene pyrolysis on a carbon surface in the range of 650-750°C showing the high temperature sensitivity of this process and a higher rate than that for volume pyrolysis of C_2H_4.

Since the membrane structure is composed of a random network of multi-chiral SWCNTs, the single-point pyrometer indication cannot be assumed to be the temperature of the bulk of the film.

According to [16], the bulk of the membrane possesses hot spots, thus a power *vs.* temperature calculation by Romanov *et al.* [82] suggests that there is a power constant to estimate the hot spot temperature of a randomly oriented network.

Due to the difficulty of measuring and understanding the Schottky barrier overheat and possible destruction; the optimum process temperature found is around 1100°C at which reproducibility (measured by absorbance increase) within 5% was obtained.

2.6 Doping of the SWCNT films

The doping of the samples to improve the electrical conductance of the films was performed by following the guidelines of [128] using a 30 mmol ethanol solution of $HAuCl_4$ (Figure 21) by drop casting with a 7 μl dose. After doping, the samples were dried at ambient conditions until the isopropyl alcohol had completely evaporated. After drying of the solvent, the sheet resistance of the samples on a quartz substrate was measured twice a month for 6 months after the doping procedure to understand the stability of the electric conductance of the resulting material.

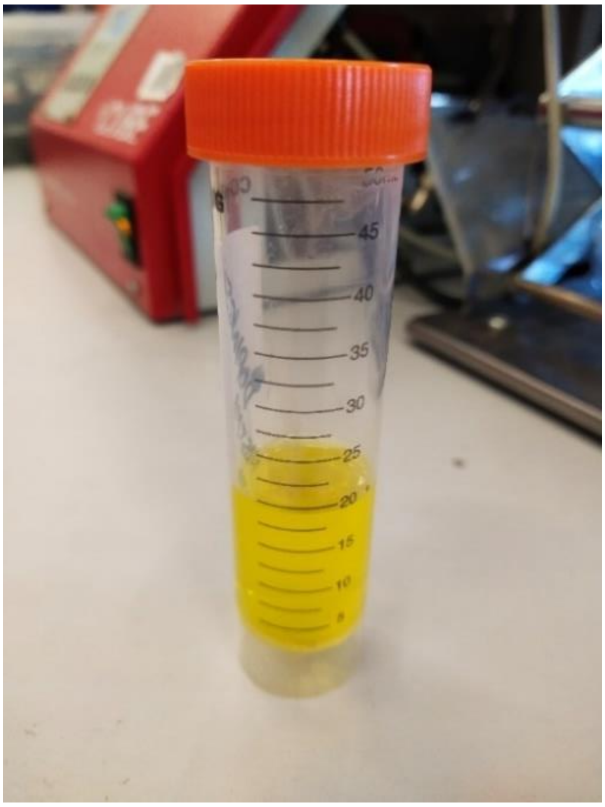

Figure 21: Photo of a vial with $HAuCl_4$ / C_2H_5OH *solution used for doping, with the guidelines provided in [128]*

The assessment of the doping procedure was performed by comparing the sheet resistance of pristine samples with those of doped samples. Spectroscopy characterization was deemed unnecessary since the transmittance affectation by doping is negligible *[128]*.

2.7 Production of model Sn and NaCl aerosols

Two model aerosols were produced for this research. The first aerosol model was produced through the pulsed plasma (spark) discharge between two high purity (99.95%) Sn electrodes with high purity nitrogen flow (Figure 22). Data of the vapor pressures for InSn from [129] was used to assess the temperature required to evaporate InSn from the SWCNT FSM surface (Figure 22).

The size distribution of the plasma discharge was tuned to effectively replicate the average size distribution produced by commercial EUV light sources. This aerosol was deposited on the surface of the SWCNT membrane to study the possible effects of Joule heating (Figure 20) regarding the nanotube morphology during and after pellicle renewal.

After successful determination of the interaction between surface deposited tin particles the membranes were tested in a EUV light source, which produces the same size distribution and concentration of aerosol particles with the aim of investigate *in-operando* regime.

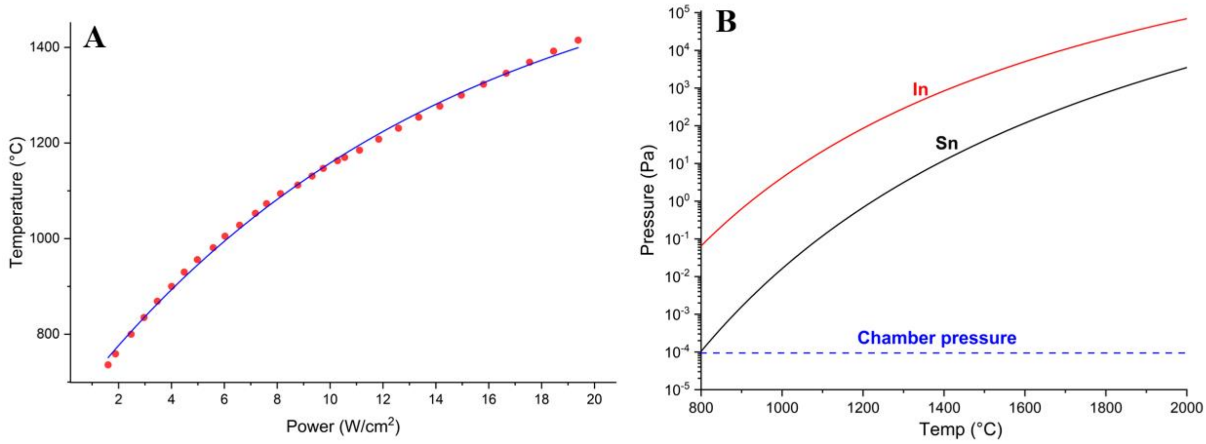

Figure 22: A) Power vs temperature estimation for an SWCNT membrane at low pressures, B) theoretical approximation of the vapor pressure for In and Sn relative to the chamber pressure to understand the temperature required for evaporation of the particles from the surface of the SWCNT FSFs. Data from A) [82], B) [129]

Aerosol Spectrometry was performed by using Differential Mobility Analyzer (DMA-CPC, TSI inc. USA), with measurement capabilities from 1 to 60 nm (Figure 23) and from 6 to 300 nm, depending on the DMA type used for the measurements.

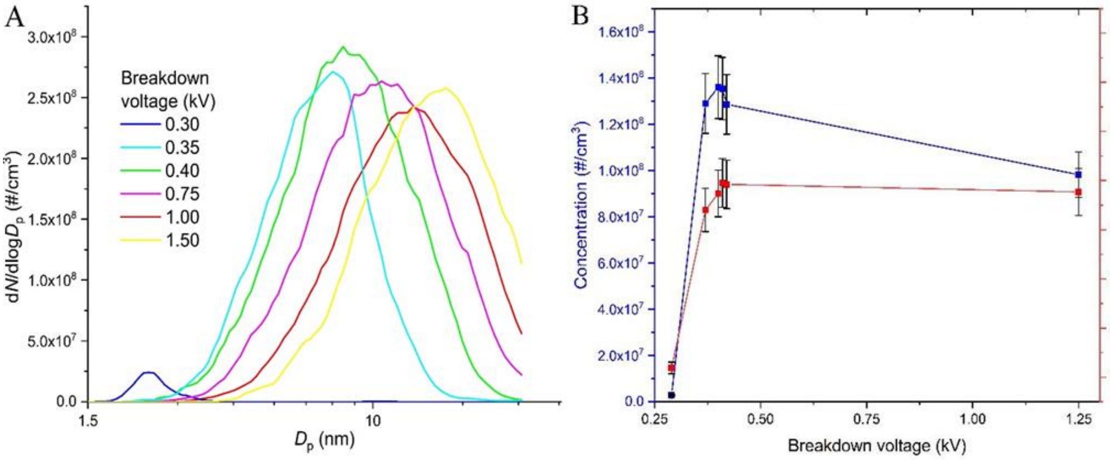

Figure 23: A) DMA particle size distributions of Sn aerosol produced by the spark discharge generator at different breakdown voltages. B) total concentration and geometric mean diameter of aerosol particles produced at different breakdown voltages. Reproduced from Publication I [7].

The second model aerosol was produced by an impactor nozzle (TSI Inc. USA) from a solution of NaCl in distilled water with a concentration of 0.1 mg/ml.

The nozzle was operated with a flow of 3.5 SLPM (standard liters per minute) and a pressure of 3 atm.

The flow was passed through a diffusion dryer containing 22 μm average pore size vacuum and heat dried molecular sieves.

The size distribution was analyzed by an Aerosol Optical Spectrometer (OOO Aerosol Devices, Novosibirsk, Russia) with a size measurement capability from $3x10^{-2}$ up to

$1x10^4$ μm and a concentration measurement capability up to $2x10^5$ particles/cm^3. Data acquisition and processing were performed using proprietary software (Figure 24).

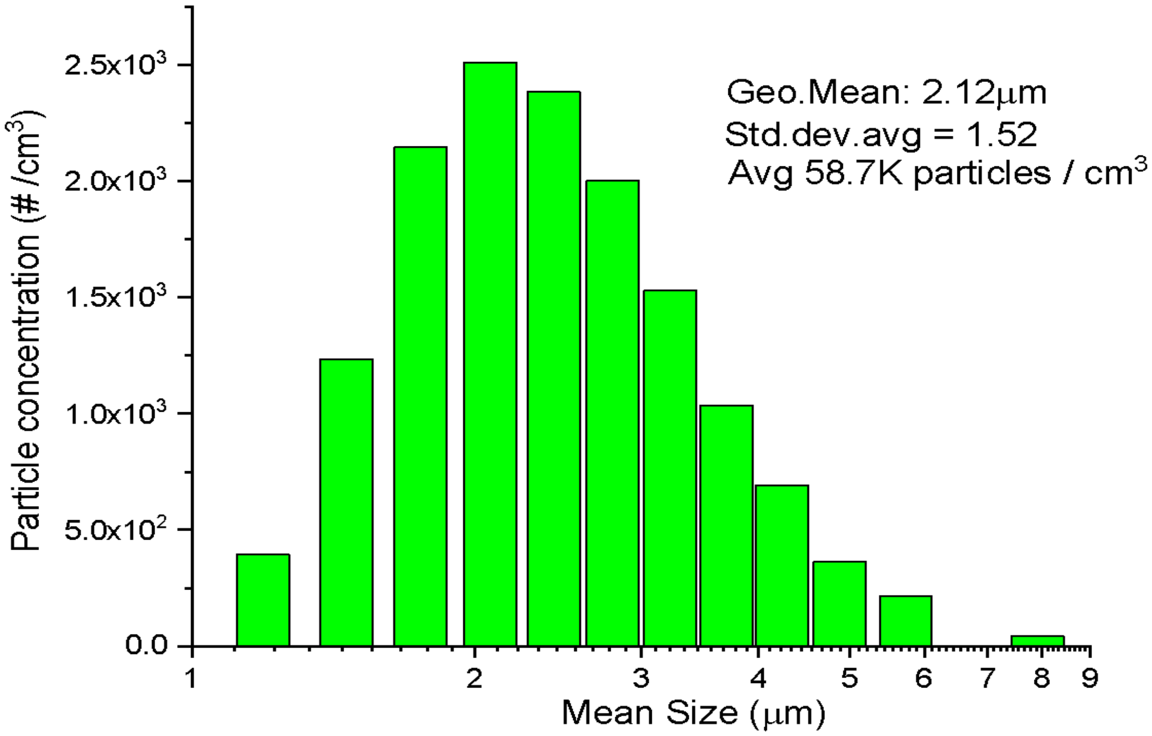

Figure 24: Size distribution of the model NaCl aerosol produced for evaluation of the SWCNT filter performance.

2.8 Quality factor evaluation of filters

Quality factor of an aerosol filter is defined by [130] the filtration efficiency and pressure drop caused by the flow through the filter.

Since high efficiency filters were fabricated, different standards for their evaluation were created.

The criteria that dictate the quality (or Q_F factor) of a gas filter relates to the pressure drop *vs.* the removal efficiency of 100 nm diameter particles, and it is defined by the equation:

$$Quality\ factor = \frac{-\ln(1-\eta)}{\Delta P}$$

where ΔP is the pressure drop across the filter, and η is a removal efficiency; a protocol for evaluation of the filter quality is described in [130]. The system built for this purpose is shown in Figure 25.

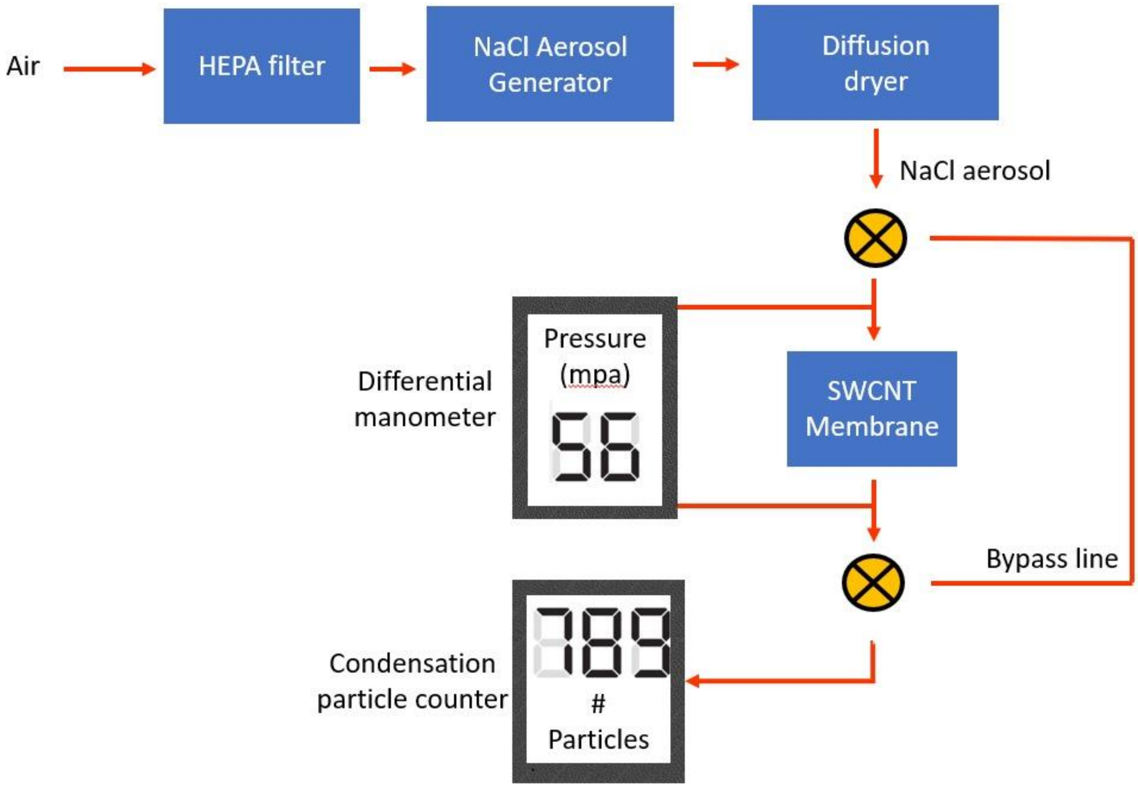

Figure 25: Scheme of a system built for the filter quality evaluation.

2.9 Optical methods for SWCNT characterization

The optical absorbance characterization of SWCNT FSFs is the routine method to understand and tune the thickness of films. Spectroscopic characterization of the free-standing membranes was done with 1 nm resolution from 174 to 2500 nm. It covers the full spectra from UV *via* visible to near infrared range.

In principle, the diameter of the nanotubes presents in the sample can be assessed by this method alone. Since it is non-destructive and fast, the absorbance data can be directly correlated with the properties of the SWCNTs and films.

The transitions between the Van Hove singularities [131] within SWCNT band structure cause the strong absorption peaks defined as the specific transition energies for certain tube chiralities. The strongest absorption points in the UV range correspond to the π electrons' collective resonance (plasmon peak).

The absorbance at 550 nm is used as the standard thickness / absorbance of the specimens. The equivalent sheet resistance (measured for FSFs with light transmittance of T = 90% at 550 nm) R_{90} assessment is performed by combining spectroscopic transmittance measurement and sheet resistance of the film.

To achieve a metric stating the balance between transmittance and sheet resistance for SWCNT FSF, a metric named R_{90} was established by [128].

It can be applied to any conductive transparent material. The optical transmittance for assessment of equivalent sheet resistance of T = 90% at a wavelength of 550 nm. Defined as: $R_{90} = 1/[K \log(10/9)]$ with the quality factor of $K = 1/(R_S \times A)$, where A is an absorbance measured at 550 nm and R_S denotes the sheet resistance ($\Omega\ sq^{-1}$) [132].

A special holder was built to accommodate freestanding samples to allow measurements from around 200 nm, the typical spectra can be observed in Figure 26. The optical absorbance spectroscopy (Figure 26) was measured using a high-performance UV-vis-NIR spectrometer (Perkin Elmer Lambda 1050).

The π plasmon on SWCNT corresponds to a peak of strong UV absorption in the wavelength around 284 nm, thus a collective excitation of π-electrons. The Van Hove singularities of the transitions in metallic (M_{11}) and semiconducting (S_{11}, S_{22}) correspond to the density of states of different species of SWCNTs present in the analyzed samples, where the ratio is approximately 33% metallic and 67% semiconducting.

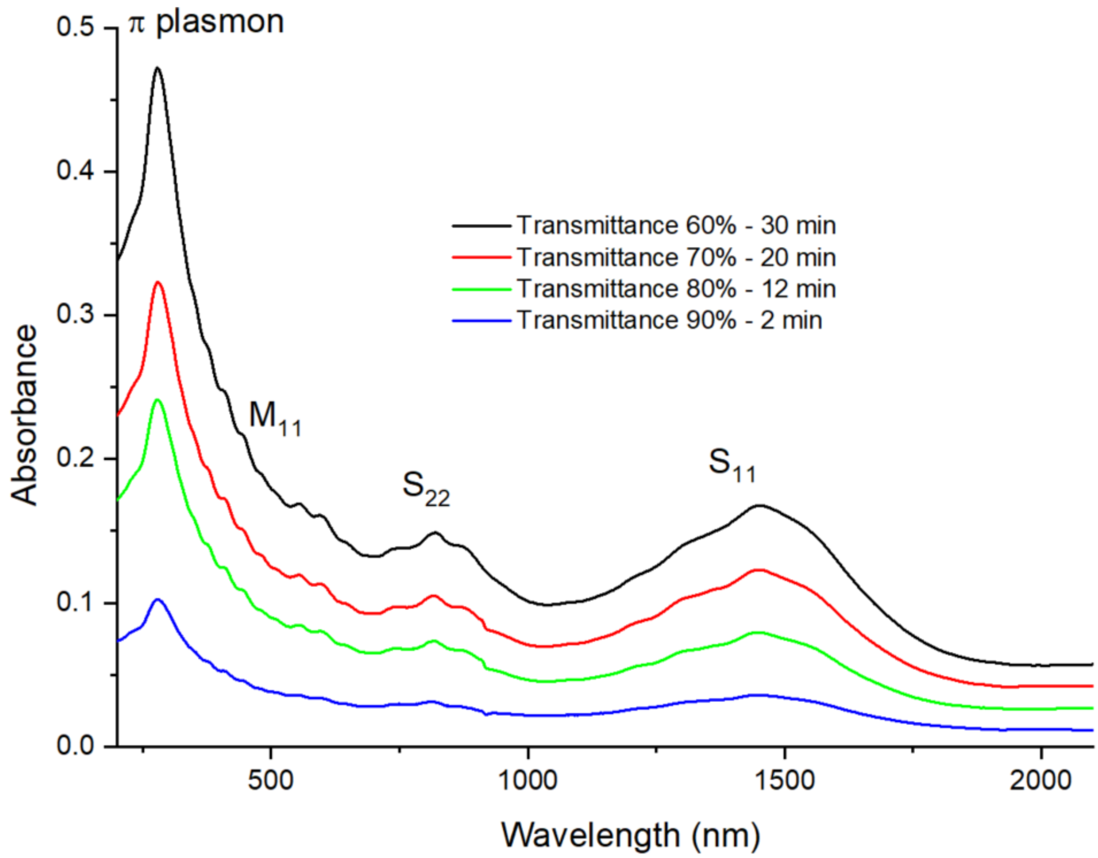

Figure 26: Typical UV-vis-NIR spectra of SWCNT FSFs with different transmittances.

Raman spectrometric characterization (Figure 27) was using a Thermoscientific DXRxi Raman Imaging microscope with a laser excitation wavelength of 532 nm. Raman spectra were normalized to G mode intensity.

Spectra obtained (Figure 27) was acquired and processed by computerized methods. The phonon spectra from Stokes resonance provides information about the in-plane vibration modes of the nanotubes, also considered as a graphitic material.

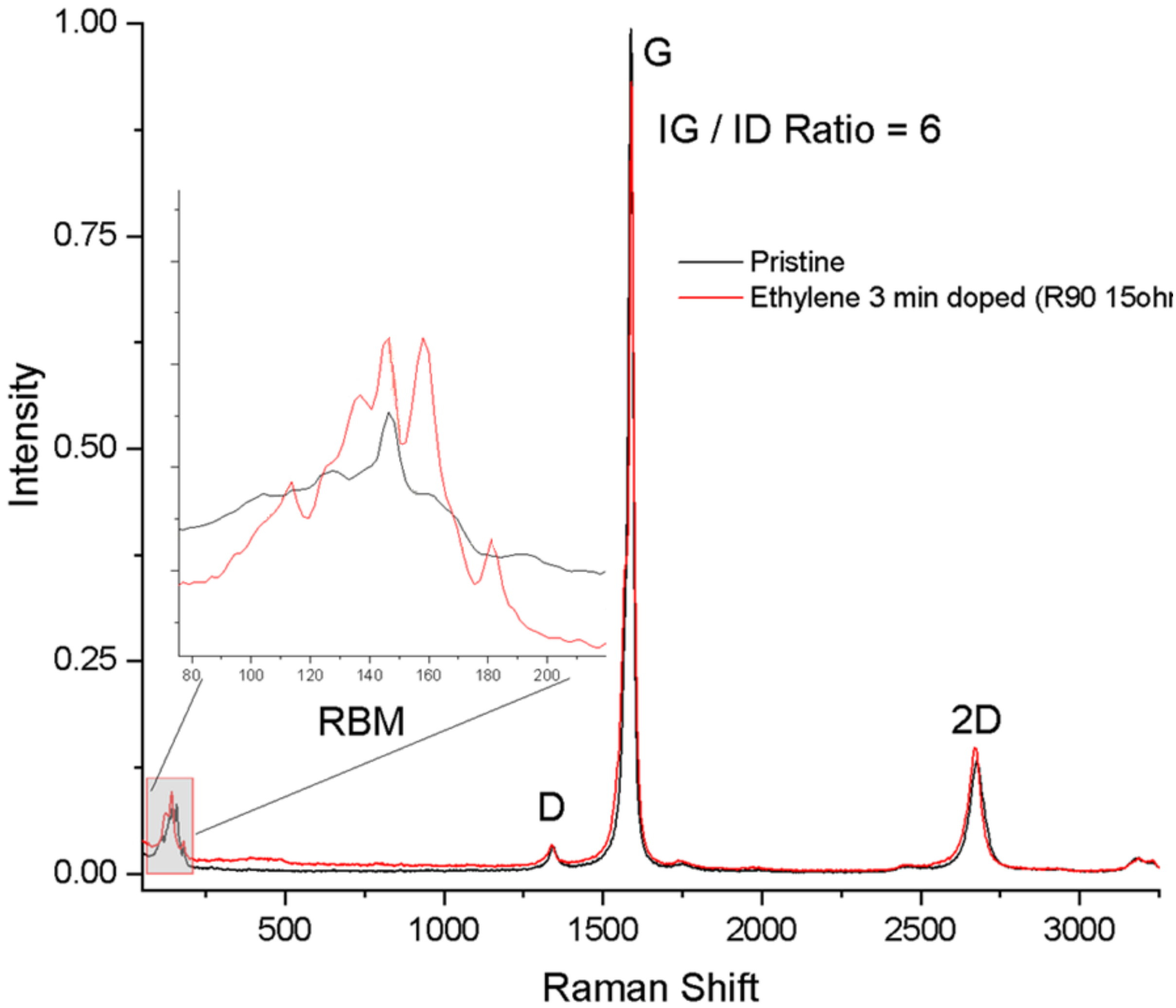

Figure 27: Raman spectra of doped vs pristine SWCNT sample. Inset containing enlarged RBM, confirming the presence, and lack of transformation of single walled CNTs.

The I_G/I_D ratio corresponds as the ratio of the maximum intensity of the defect (D) band against the graphitic (G) band. Thus, the peak of "defects" is a Raman mode oscillation of imperfect graphene-like structure.

The G band corresponds to fully populated sp^2 graphene structure. It is an indicator of the crystalline quality of the nanotubes present in the sample. The plasmonic RBM (RBM), plotted in the inset of Figure 26 are Raman resonant modes (RBM) [132], unique to nanomaterials, allows to understand the diameter of the nanotubes present in the sample [133] as well as the presence of SWCNTs.

Timmermans *et al.* studied the transmittance of FSFs [134] in The application of SWCNT FSF for EUV was also studied in [126]. The experimental investigation about the SWCNT FSF transmittance towards renewable FSFs using 13.5 nm EUV (EUV) light, required the design of a ceramic holder able to withstand the harsh conditions present inside an EUV light source.

This work was made in collaboration with V. Gubarev, Dr. M. Krivokorytov, Dr. V. Medvedev from Institute of Spectroscopy of the Russian Academy of Science (Troitsk, Moscow, Russia). In Figure 28, the graphical abstract of publication II [7] shows a SWCNT FSF held between two conductive rods, fed with a DC power, being Joule heated, and bombarded by droplets of Sn / In/Sn that are being evaporated whilst transmitting EUV light across its surface.

A fiber laser excited InSn plasma light source TEUS-S100 manufactured by EdgeWave, was used to produce EUV radiation. The ceramic holder with the SWCNT membrane was placed in the trajectory of the EUV beam where a EUV photodetector was placed.

A second EUV photodetector was used as a reference to understand the loss of light transmittance capability of the SWCNT film. By directly comparing the signal obtained from each photodetector, and comparing it with a previous optical power measurement, the optic EUV transmittance of the FSF was measured.

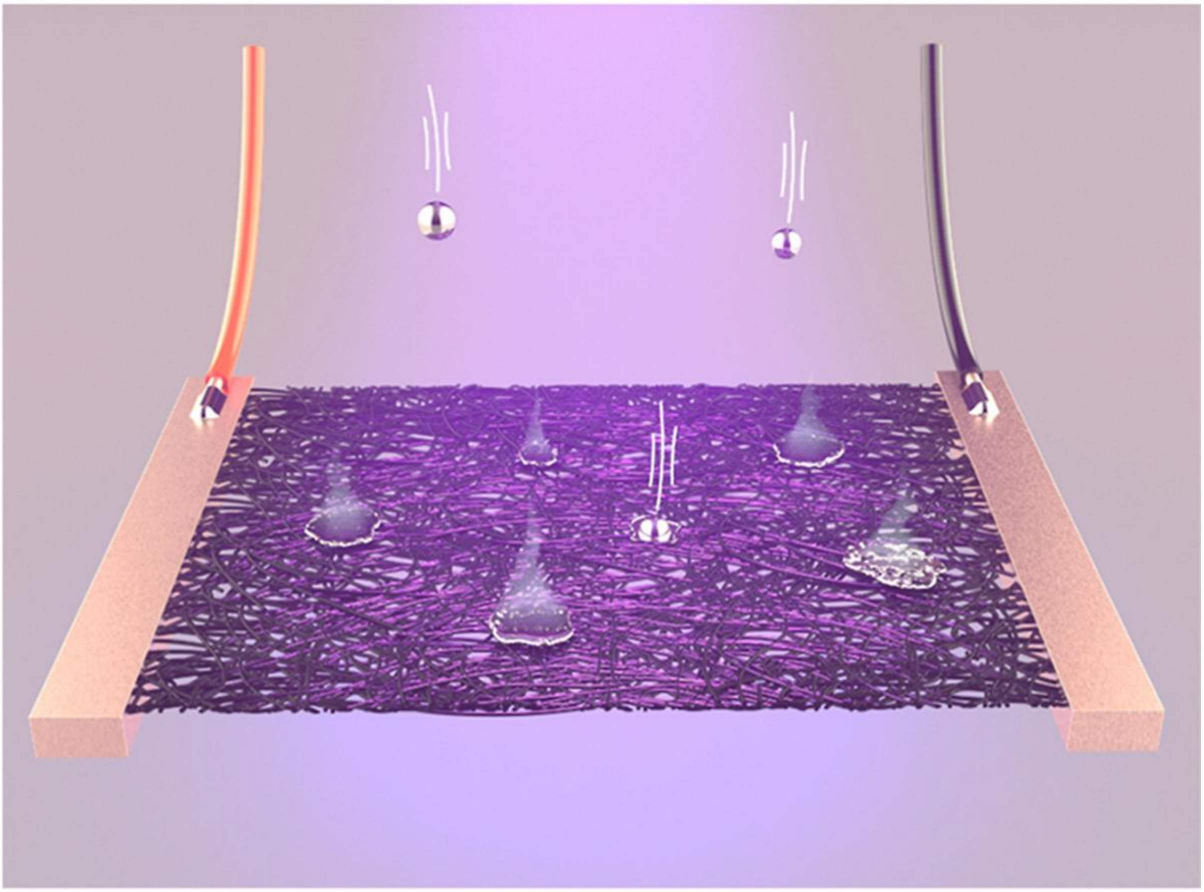

Figure 28: A Joule heated freestanding SWCNT membrane being bombarded by InSn particles and simultaneously self-cleaning (renewing) by evaporation of In and Sn [7].

2.10 Plasma Penetration through SWCNT membranes

SWCNT membrane samples with the thicknesses of 40 and 90 nm were fabricated to study the In-Sn plasma penetration. The SWCNT FSFs were characterized by UV-vis-NIR spectroscopy, the measurement results can be seen in Figure 29.

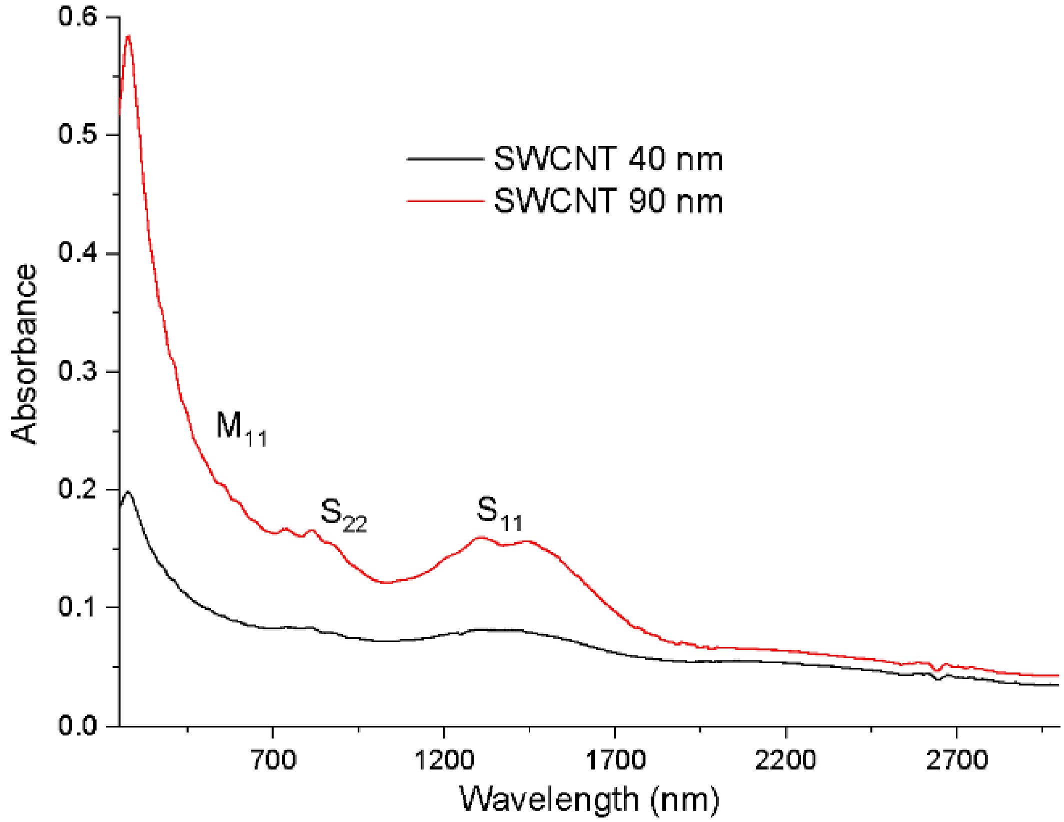

Figure 29: Optical spectra of ca. 40- and 90-nm-thick SWCNT membranes. The transitions between Van Hove singularities (S_{11}, S_{22}, M_{11}) in SWNCTs are denoted [135].

A high-brightness EUV LPP source TEUS-M generated plasma particles using EdgeWave Nd: YVO_4 laser with a pulse energy of 4 mJ (duration of 1.5 ns and repetition rate of 25 kHz). The laser beam was focused into a spot with a diameter of 60 µm at a $1/e^2$ level on a liquid target placed in a crucible. The target material was an alloy of Sn and In taken in mass proportion m_{Sn}/m_{In} = 52/48. The interaction of the laser beam with the liquid target produced plasma (ions and atoms) and aerosol microparticles. In order to suppress spattering of microparticles, the crucible was rotated at a frequency of 300 Hz, ensuring a tangential microparticle velocity = 190 m/s. The pressure of residual gases inside the setup during the operation was less than 0.01 Pa. Time-of-flight (TOF) measurements (Figure 30) of ions with a Faraday cup were used to characterize the charge energy spectrum of plasma. A cup-receiver and an electron-suppressor lid were made of stainless steel. To suppress primary electrons from the plasma, a negative bias (-20 V) was applied to the cup walls. The secondary electron emission was blocked by using a weak magnetic field at the entrance aperture.

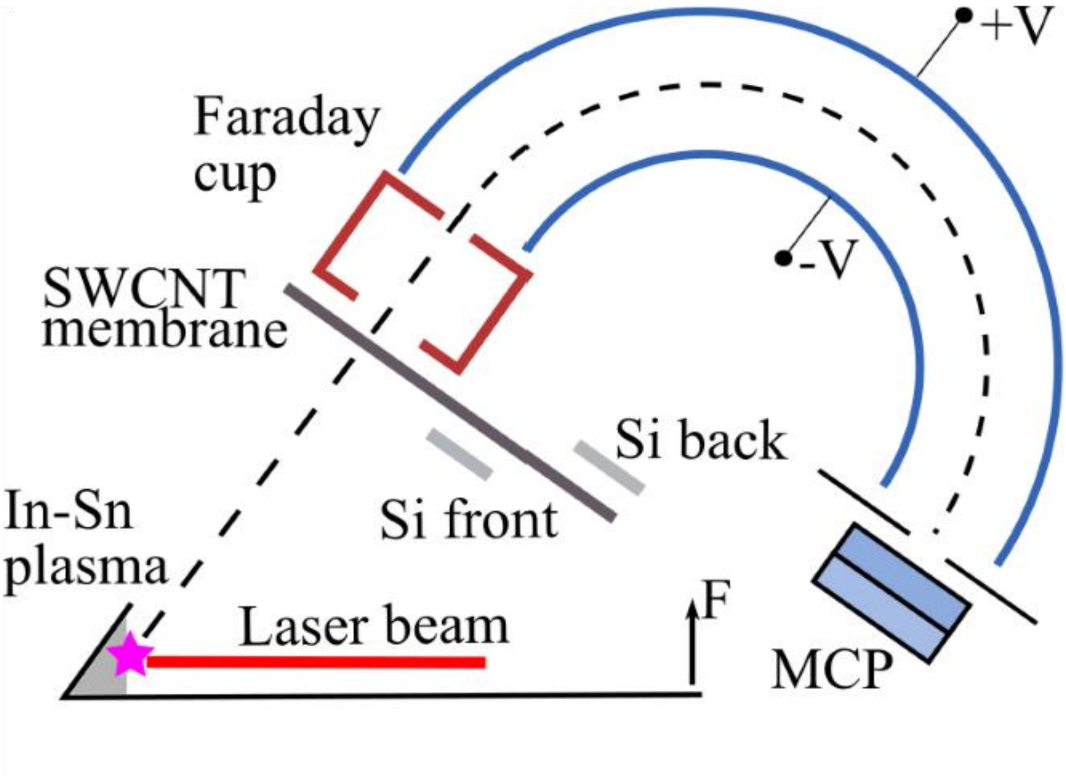

Figure 30: Schematic of the setup for the measurement of Plasma Penetration [135].

The distance from the plasma source to the entrance aperture of the Faraday cup was l_{FC} = 380 mm, and the diameter was d_{FC} = 6 mm. The electrostatic ion energy analyzer with a resolution dE/E = 0.06 was utilized to determine the plasma composition (ionization rates).

A 180° spherical condenser was employed as an ion analyzer. The radii of the outer and inner electrodes along the analyzer axis in the horizontal and vertical focusing planes were R_1 = 4.5 cm and R_2 = 3.5 cm and r_1 = 5 cm and r_2 = 4 cm, respectively. To increase the sensitivity of ion registration, use was made of an ion-current detector with two microchannel plates (MCPs) in V-stack (Chevron) assembly. The distance from the plasma source to the entrance aperture of MCPs was l_{EA} = 729 mm, and the diameter of the entrance aperture was d_{EA} = 2 mm. SEM images of Si witness samples after plasma radiation during 1 million laser pulses are shown in Figure 31 [135].

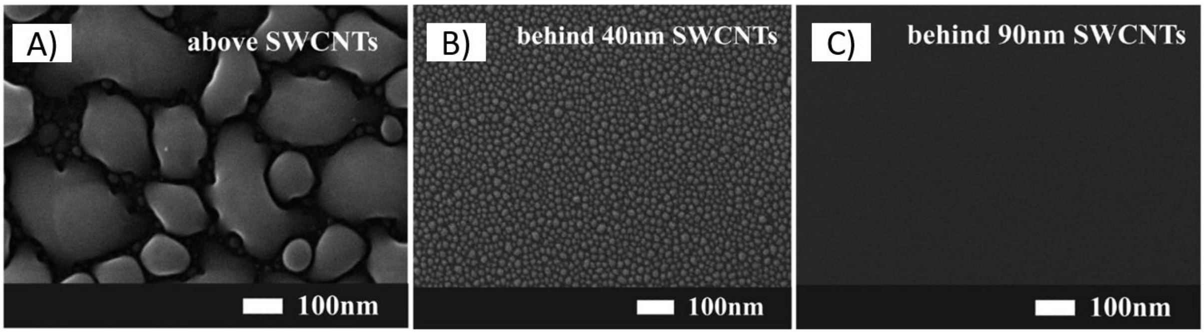

Figure 31: SEM images of Si wafer (after plasma radiation for 10^6 laser pulses) placed: A) above SWCNTs; B) behind 40 nm SWCNTs; C) behind 90 nm SWCNT membrane [135].

The SEM used in this work were a Thermo Scientific Quattro S, Teneo and a Versa 3D, all three functioning at 30 KV gun acceleration.

Samples were transferred directly to the surface of SEM supports and required no preparation.

The TEM instruments used were: a Thermo Scientific FEI Titan and a Tecnai G2 F30 both operating at 200kV acceleration. 95% transmittance samples were deposited on clamshell grids with no additional preparation.

EDX systems for all electron microscopes were Bruker and Metek (Germany).

2.11 Electrical Characterization

Sheet resistance of the samples was assessed with a four-probe station (Jandel RM3000, U.K.), which uses four equidistant spring-loaded electrodes to determine the resistance. Two acts as a current source (10 nA – 100 mA), and the other two are used to measure the voltage. This approach allows mitigating the measurement error associated with the sample-electrode resistance.

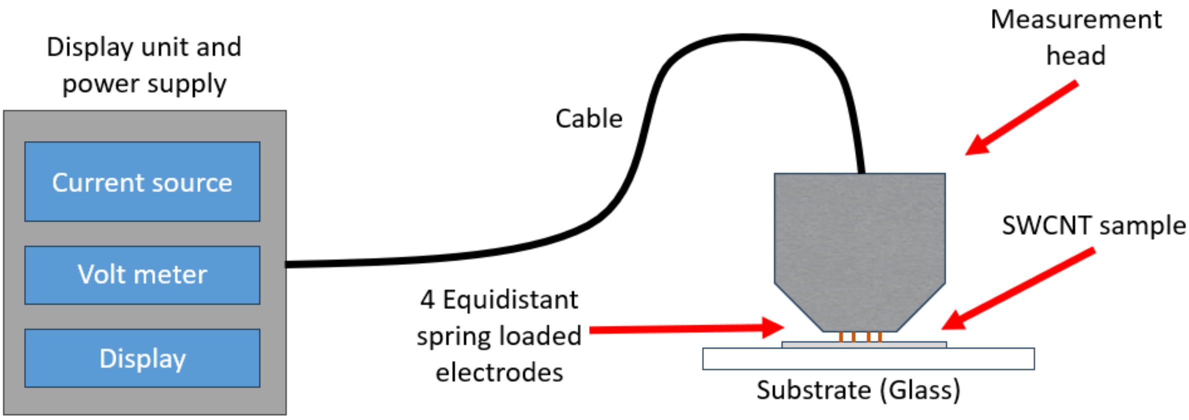

Figure 32: Scheme of the four-probe measurement device used for the SWCNT-film characterization.

According to the equipment manufacturer datasheet: "accuracy is better than 0.1% against resistors for 100 nA and greater". Each sample had five measurements taken in different places, respecting a minimum area of 5 mm^2, the average of 5 measurements was used as final value.

2.12 Ultimate tensile strength measurement

A device was built for the purpose of measuring the ultimate tensile strength; it is a linearly pushed round tip attached to a load cell, where the element pushing the needle is a free-standing SWCNT film, being displaced at constant velocity by a computer-controlled actuator (Figure 33).

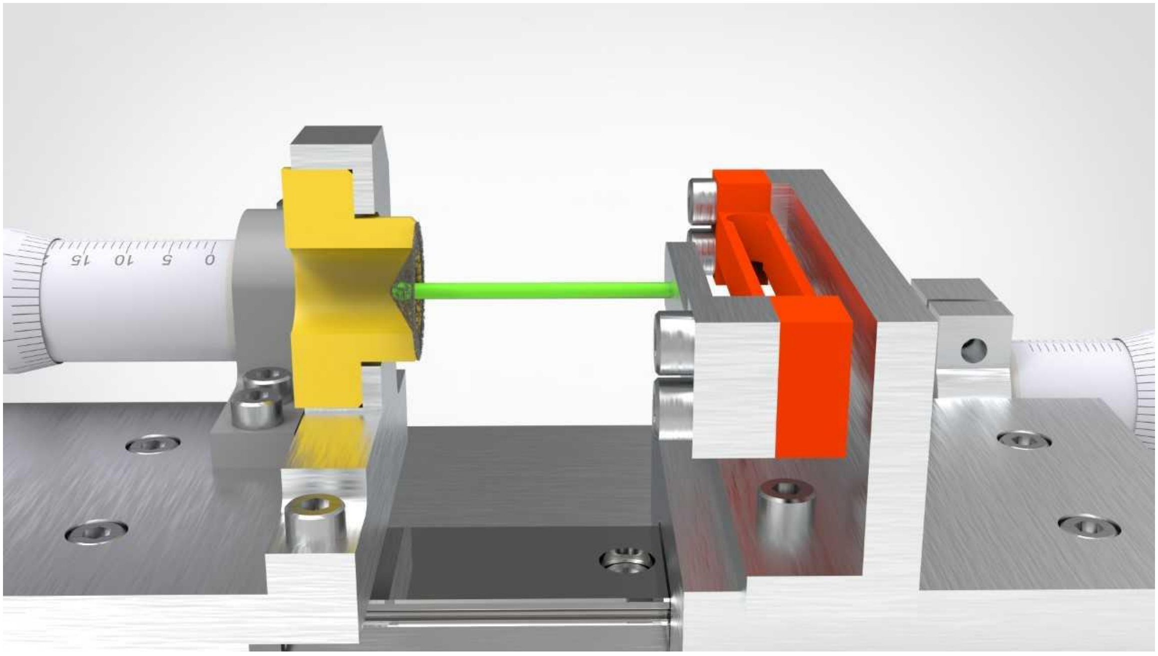

Figure 33: Scheme of the ultimate tensile strength measurement device, sample placement and deformation. Yellow: Sample holder, Grey: SWCNT membrane, green: penetrating needle, Red: load cell.

The device can be operated horizontally or vertically, allowing to calibrate the measurements with a known weight. The raw value of the measurement can be converted to any unit of interest. Since the geometry of the system is known, the guidelines used in [5] were applied. The pithagorean trigonometry model proposed by the authors allows a simple way to calculate the UTS directly from the maximum force excerpted by the film over the needle attached to the load cell. The membranes used for this research also show viscoelastic behavior as previously assessed by others [5].

Since the thickness of the freestanding membrane can be tuned by varying the collection time, a calibration sample set was characterized by means of UV-vis-NIR spectroscopy and later on the ultimate force device to establish a baseline for comparison against ethylene welded samples. This comparison is used to optimize treatment times towards maximization of the UTS for longer-lasting particulate filters.

Ultimate tensile strength tests were performed by a self-made device (Figure 33), containing a needle held by a load cell, a moving stage with an electronically actuated micrometric screw, and a fixed stage. The SWCNT membrane sample transferred onto a circular aluminum disk was perforated at continuous speed by the force measurement rod, which is a 2 mm in diameter steel sphere attached to a stainless-steel hollow tube. Pressure data was recorded by means of computer data acquisition.

The linear actuator has 1/32 step mode motor control and noise mitigation was implemented by signal averaging. A computer was used to record the data from the load cell and displacement. Lateral sample alignment was kept centered at the same position for different measurements to ensure that perforation happened in the center of the sample.

The calculation for the ultimate tensile strength was done by taking the cross section of the maximum stress area of the film in the area surrounding the tip of the force measurement rod. Pithagorean geometry was used to estimate the contact angle change related to the distance, and film thickness was considered to be constant during the measurement until the sample breakage.

The ultimate tensile strength of the films is multiparametric: the average length of the nanotubes being used is proportional to the maximum force and maximum stretching of the film if slippage (not welded nanotubes) is present on the films. At the same time, the thickness of the specimens is also directly proportional to the maximum force that the film can resist before breakage.

To understand and directly compare the force resistance of different film thicknesses and directly correlate the results of the ethylene welding process, a set of different pristine samples was measured to create a baseline to directly compare the mechanical resistance of the ethylene-welded films of the same original thickness.

To ensure uniformity on the thickness of every sample, the measurement of the optical transmittance of three random collection times, the collection time for the desired transmittance was calculated by linear extrapolation to achieve the desired light transmittance for the experimental specimens. The samples to be studied by SEM were collected to around 80% transmittance meanwhile for TEM the specimens were of 95% transmittance.

Chapter 3: Results and discussion

3.1 Tin aerosol evaporation from SWCNT membrane

A model Sn aerosol production unit (section 2.7; Figure 23) was developed to deposit tin aerosol particles on a SWCNT FSF (EUV renewable pellicle). The Sn aerosol coated SWCNT FSFs were studied by means of TEM (FEI Tecnai G20, FEI Titan, United States of America) and SEM microscopy (FEI Teneo, Versa 3D, Helios, United States of America).

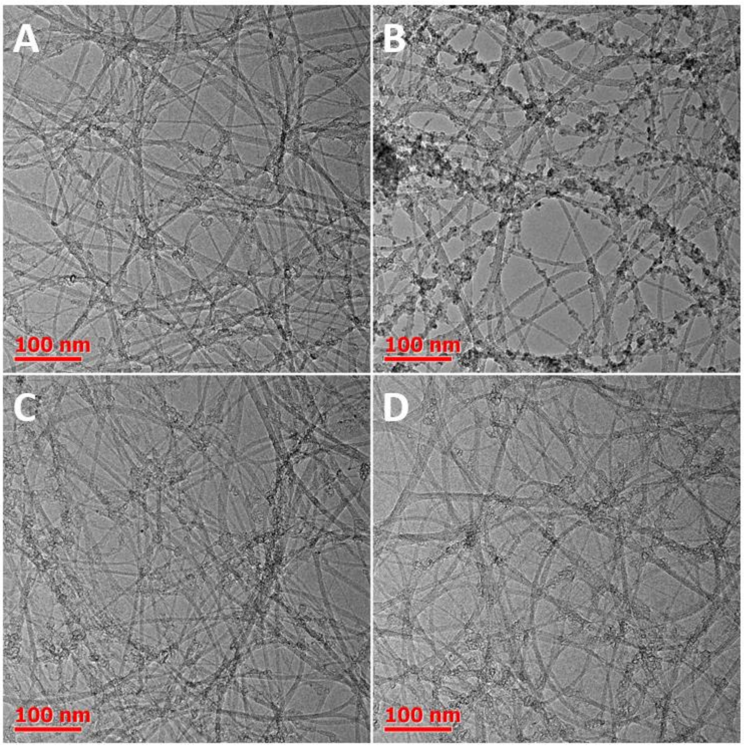

Figure 34: TEM images of SWCNT FSF coated with Sn aerosol. A) Pristine SWCNT, B) SWCNT with Sn aerosol deposited for 4 h, and regenerated at 750°C during 5 s, C) SWCNT with Sn aerosol deposited for 4 h, and regenerated at 1000°C during 30 s, D) SWCNT FSF with Sn aerosol deposited for 4 h, and regenerated at 1400°C for 3 min. Reproduced from [7].

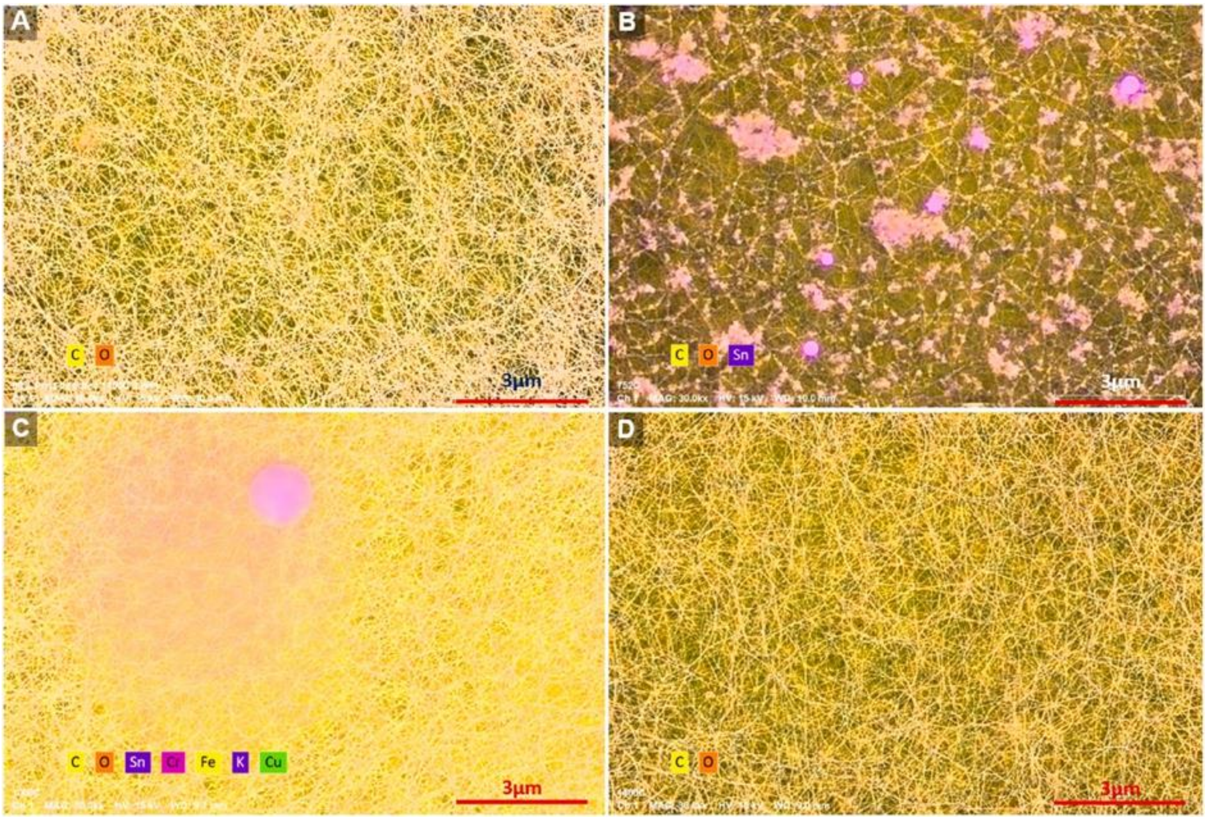

Figure 35: SEM EDS maps of SWCNT FSFs coated with Sn aerosol. A) Pristine SWCNTs, B) SWCNTs with Sn aerosol deposited for 4 h, and regenerated at 750°C for 5 s, C) SWCNTs with Sn aerosol deposited for 4 h, and regenerated at 1000°C for 30 s, D) SWCNTs with Sn aerosol deposited for 4 h, and regenerated at 1400°C for 3 min. Reproduced from [7]

After confirming the deposition of Sn aerosol by TEM (Figure 34) and SEM map (Figure 35) microscopy, the low-pressure Joule heating chamber (section 2.4) where the SWCNT FSFs were heated to a different temperature for a certain time. Figures 34 and 35 depict TEM and SEM map images of SWCNT FSFs different renewal stages, for assessment of the complete elimination of Sn aerosol.

After the Joule heating at low pressure, the SEM images and EDX map showed that the complete elimination of Sn particles happened after 3 minutes of heating at a temperature of 1400°C. The post renewal (after low pressure Joule heating treatment) SWCNT FSF morphology of the membrane used to trap Sn particles shows no significative changes compared to the exhibit A in the Figures 33 and 34, which corresponds to a pristine SWCNT FSF. A single sample was coating cycled and renewed 10 times, the results of UV-vis-NIR spectra measurements are shown in Figure 36. It was observed that after 10 cycles, meaningless transmittance changes occurred to the membrane, and no doping of the structure was observed during this analysis. The UV-Vis-NIR spectra of multiple renewal single sample reflects the same original features of the pristine SWCNT FSF.

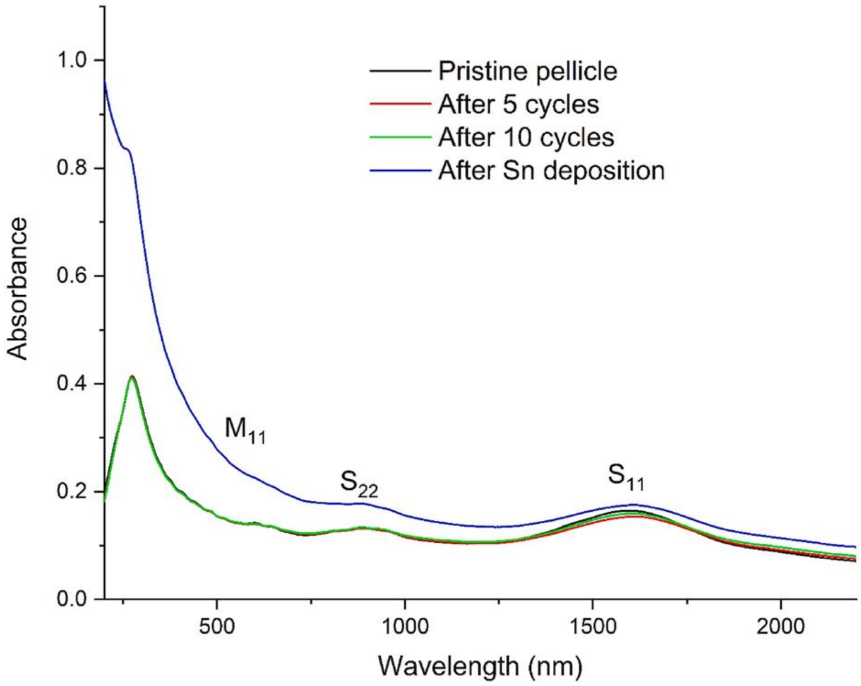

Figure 36: UV-vis-NIR spectra of pristine SWCNT FSFs (black), with tin deposited during 24 h and regeneration (for 3 min at 1400 °C). Optical transitions between van Hove singularities for semiconducting (S_{11}, S_{22}) and metallic SWCNTs (M_{11}) are denoted to show that the process preserves SWCNT band structure and provides no doping. Reproduced from [7].

In order to understand the damage to the bulk of the SWCNT FSF, a Raman spectroscopy analysis was made. The acquired spectra can be seen in Figure 37, they were normalized to G peak for assessment of the defect quantification.

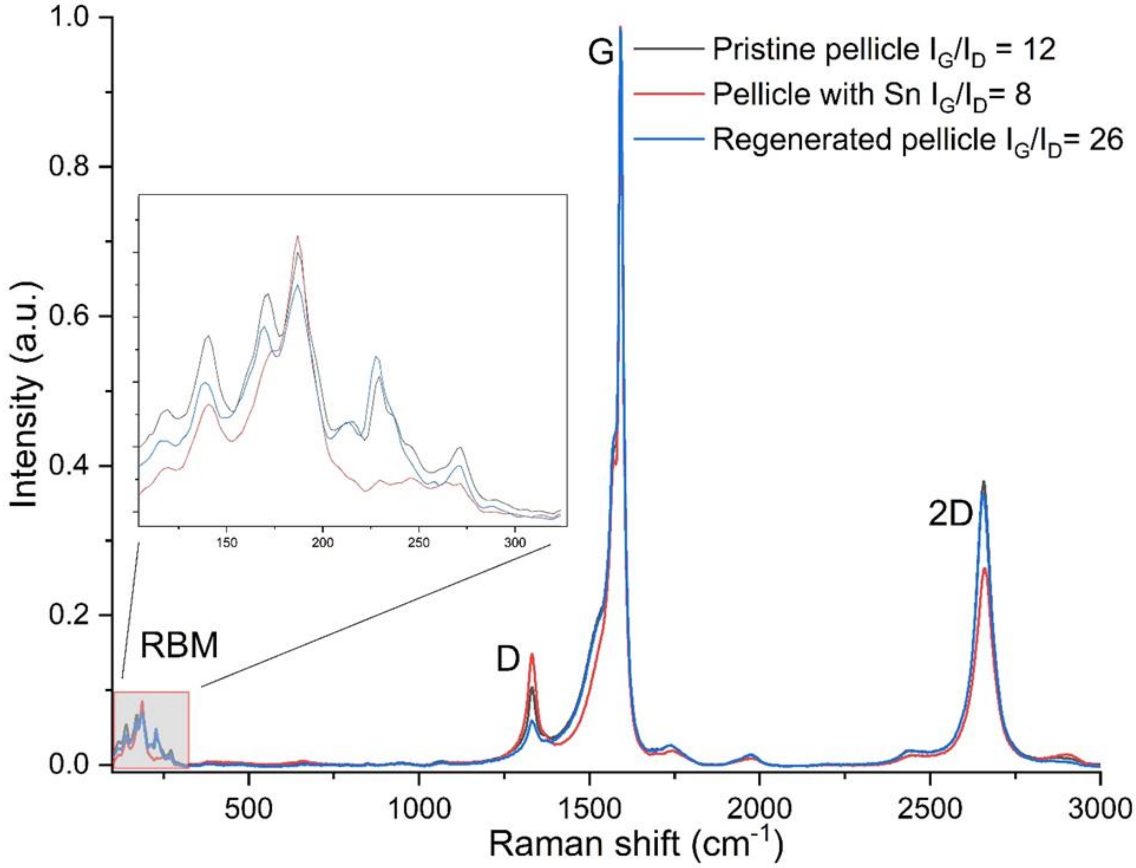

Figure 37: Raman spectra of SWCNT-based membranes (pellicles): pristine (black), after Sn deposition (red) and after regeneration at 1400 °C, 3×10 -1 Pa for 3 minutes (blue). Reproduced from [7].

It was observed that the calculated I_g/I_d ratio reflected a minor change of the value for the regenerated pellicle compared to the Pristine pellicle. The heating of the SWCNT FSF, while coated with Sn aerosol, does not cause any harm to the structure of the nanotubes and opens the possibility of applying the same process for other similar species like Pb, Co, In, Sb, *etc.* This study shows the potential of renewal of the SWCNT FSF developed beyond 10 cycles for Extreme UV applications. This result was published in [7].

3.2 *In operando* tin aerosol evaporation and EUV transmittance

In operando experiments were performed in collaboration with Institute of Spectroscopy (Troitsk, Moscow, Russia). The experiment scheme is in the Figure 38, During the first 10 minutes, the annealing of the membrane inside the EUV light source chamber was performed with a DC input power of 10 W/cm^2 (c.a. 1150 °C), it was applied while the EUV transmittance was constant 0.74. Then, In/Sn deposition (Figure 39; blue curve) was started and the transmittance of the EUV membrane dramatically dropped from 0.74 to 0.48.

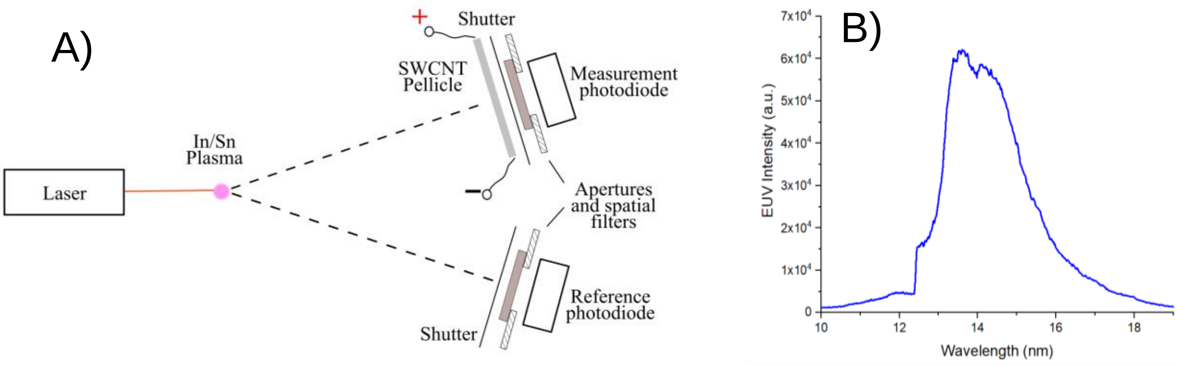

Figure 38: A) - Illustration of the experimental setup for the EUV transmission measurement of a free-standing SWCNT pellicle in situ during In/Sn deposition and regeneration; B) – EUV spectrum of the light source used for the measurements. Reproduced from [7]

After that moment, the deposition with In/Sn species was stopped and DC power was supplied with 1 W/cm^2 power (Figure 39, red curve; ~600 °C) that had negligible effect on the EUV transmittance of the SWCNT membrane.

With an increase of input power up to 5 W/cm^2 (Figure 39, red curve; ~900 °C), the transmittance coefficient increased from 0.50 to 0.58. Increasing the input power to 10 W/cm^2 (Figure 39, magenta curve; ~1100 °C) continued In-Sn evaporation without any rate variation on the transmittance increase gradient.

Finally, the EUV transmittance returned to its initial value of 0.74 confirming the applicability of the method with industrial EUV source. Thus, the obtained results verify our method to recover the free-standing SWCNT membranes with a threshold effect on the input power of 5-10 W/cm^2.

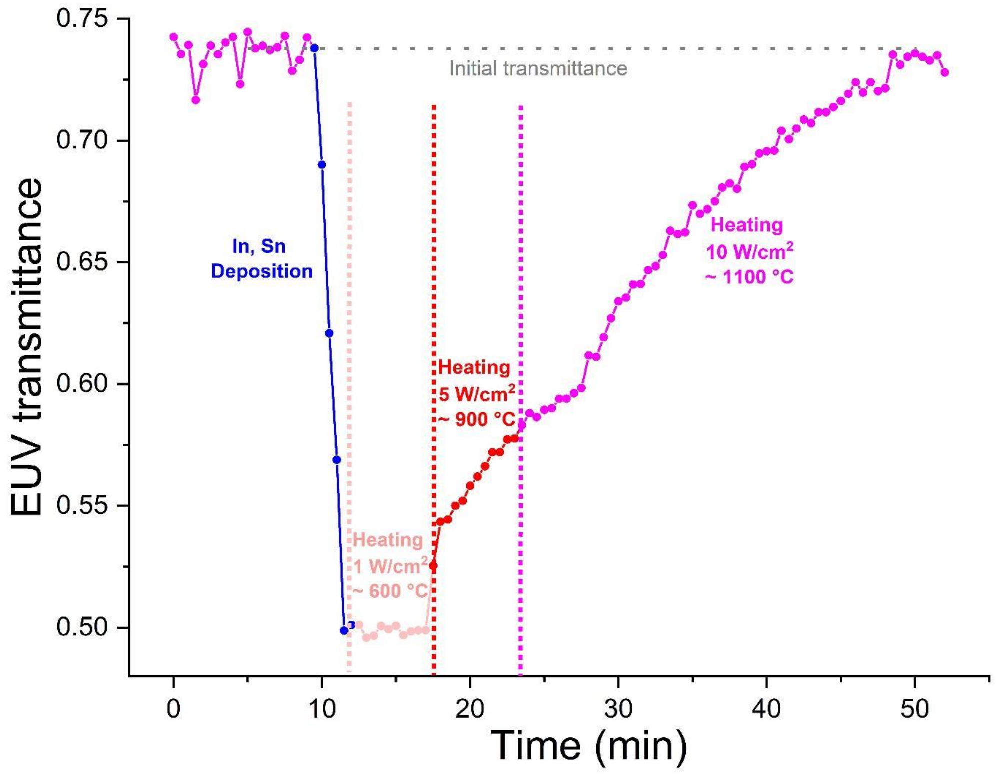

Figure 39: Evolution of EUV transmission of a free-standing SWCNT pellicle during In/Sn deposition and regeneration. Reproduced from [7].

Multiple renewal cycles were tested to investigate the endurance of the pellicle. The UV-vis-NIR spectroscopic measurements of the sample renewed 10 times can be observed in Figure 36, while the Raman measurement of a single cycle sample is shown in Figure 37.

No membrane detachment or breakage was observed; thus, the membrane retains its original features and from the SEM analysis it is possible to conclude that the damage due to In-Sn interaction is negligible.

This fact tells that the membrane can have a very long life, being renewed *in situ*, eliminating the need for removal out of the lithograph for cleaning, potentially decreasing downtime due to In-Sn particle contamination.

This proves the successful development of the first (to the best of our knowledge) EUV renewable (potentially *in situ*) pellicle for semiconductor production applications. This result is to be published.

3.3 Joule heating-induced welding via ethylene pyrolysis

In order to tune the mechanical properties and Schottky barriers between the nanotubes, the FSFs were treated at low pressure and high temperature in the presence of 99.5% ethylene flow and studied by means of scanning and transmission electron microscopies.

Figure 40 A shows the SEM micrography of a pristine membrane together with of a FSF treated during 5 min at 850°C with an ethylene flow of 0.5 SCCM (Standard cubic centimeters per minute). Figure 40 A shows filament like elements stacked randomly with well-defined borders and no visible interlinking. Figure 40 B shows a structure coating the filamentary nanotubes, forming a coating of carbon around the tube-tube junctions and also around the tubes which constitutes the welding after 5 minutes of treatment.

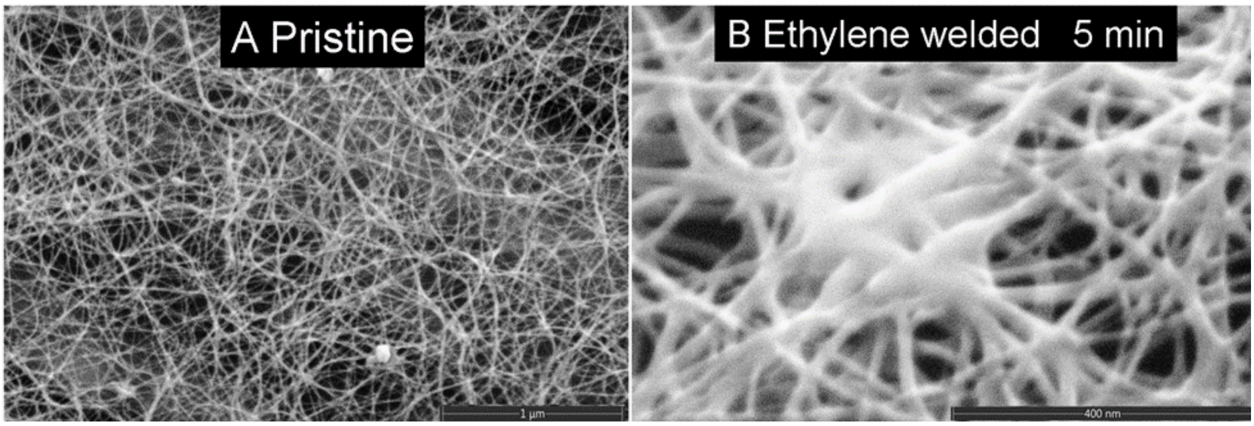

Figure 40: SEM images of pristine film vs ethylene welded during 5 min at 850°C. A) pristine membrane. B) 5-minute ethylene welding treatment, showing detail of carbon lamella formation and the presence of a closed structure wrapping the nanotubes and their bundles.

Figure 41 shows TEM Images of bundles of pristine (Figure 41A) SWCNTs with clearly visible borders on the overlaps without common bonding structures between the nanotubes. Figure 41B shows a micrography of a FSF treated during 5 min at 850°C, with an ethylene flow of 0.5 SCCM. One can see partial carbon lamella formation, thickening the original diameter of the CNTs, wrapping them in amorphous like carbon.

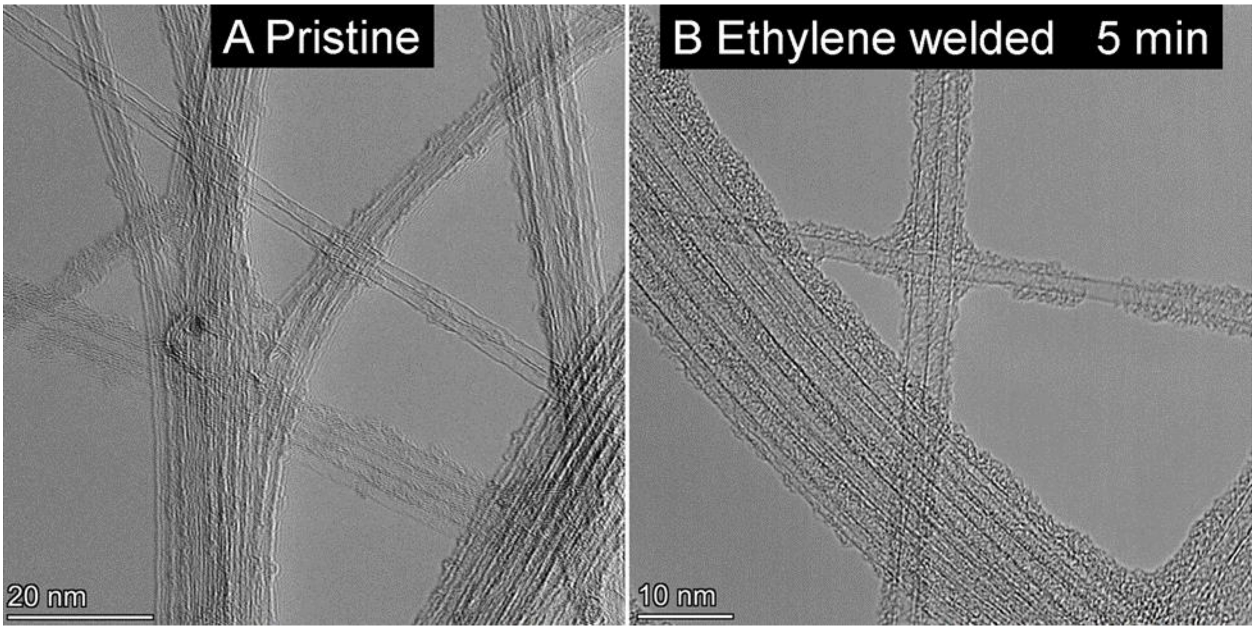

Figure 41: TEM images of A) pristine film, B) film after 5-minute ethylene treatment, showing partial carbon lamella formation and the presence of lateral amorphous deposits.

Figure 41 show TEM micrographs of SWCNT films: A) pristine, B) treated during 10 min at 1100°C, with an ethylene flow of 0.5 SCCM, One can observe partial coating formation at junctions on the Figures 42 B, C, D, and 44B (STEM regime) thickening the original diameter of the CNTs, wrapping them in amorphous like carbon.

The tube-tube contact zones have the higher amount of deposited material compared to the length of the bundles. This point to the highest temperature points to be the Schottky barriers formed between tubes, where occurs a faster ethylene decomposition rate, resulting in a higher volume of amorphous carbon coating these areas of the SWCNT FSF.

The complete coating formation was observed after 30 min of treatment (Figure 42 D), while during extended treatment times, the nanotube structure was buried in amorphous carbon where the nanotubes can be seen within the resulting material.

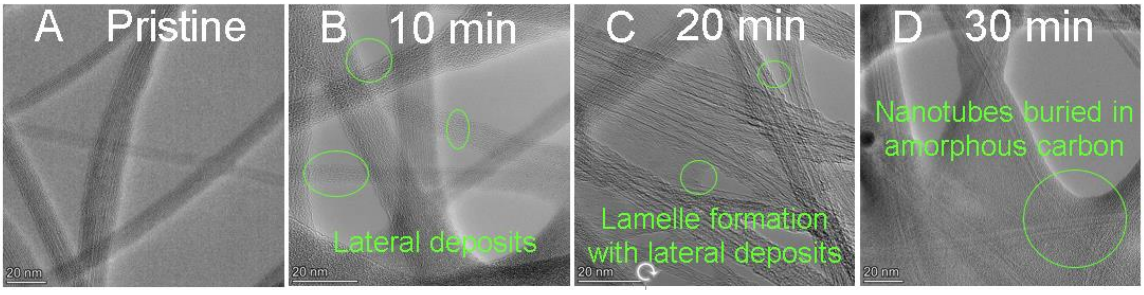

Figure 42: TEM Images showing the carbon lamella formation of different ethylene welding treatment times. A) pristine SWCNT membrane. B) Lateral deposits and junction coating. C) Partial carbon lamella formation. D) Nanotubes completely coated in carbon.

The non-uniform welding of bundles was investigated by means of SEM microscopy. It was observed that partial carbon lamella formation occurred after 5 minutes of treatment (Figure 41 B), without a defined border for the “weld”. Said borders can be seen after 10 minutes of treatment (Figure 42 B), suggesting a structure with a thickness comparable to the diameter of the pristine SWCNTs in the study (Figures 41A, 42A, 43A, 44A).

This fact also suggests that the bundles are the hottest parts of the film at low temperatures, and once they become coated, the images suggest that this once-hot spot, becomes cold, and the current flow changes towards a neighboring bundle, that will become coated due to its higher temperature compared to the previously coated bundle where the ethylene pyrolysis threshold is no longer.

Further research is required to establish any relationship between the flowrate, temperature and the structure of the carbon being deposited on the membrane by the ethylene pyrolysis process.

3.4 Doping of the welded films

Both treated and pristine membranes were transferred to fused silica quartz substrates of 9x12 mm^2 on which bilateral simultaneous doping by $HAuCl_4$ was performed by applying a single drop of a 30 mmol ethanol solution of $HAuCl_4$ following the guidelines from [128].

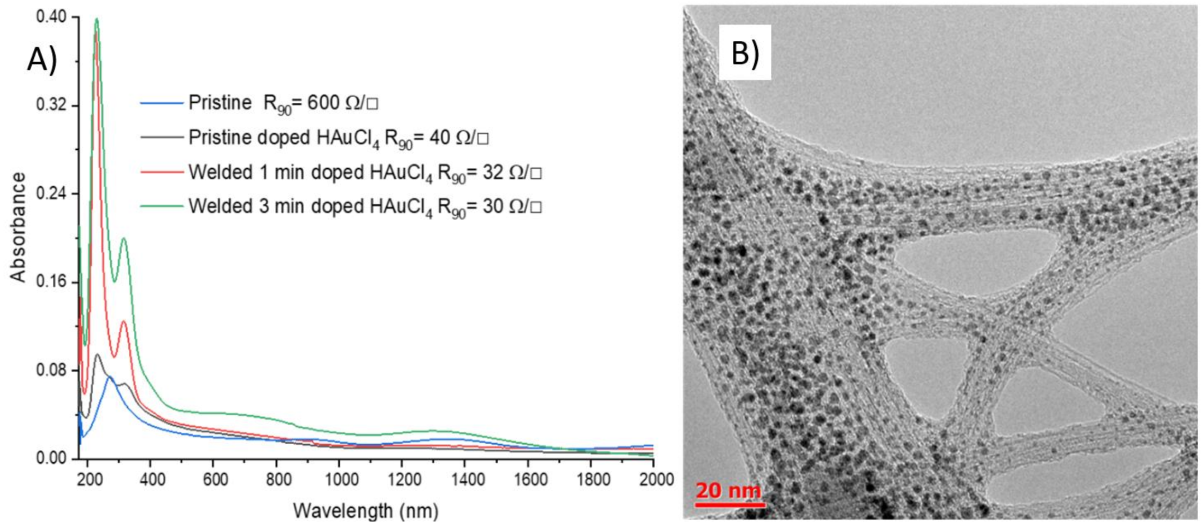

Figure 43: A) UV-vis-NIR spectra of bilaterally doped samples B) HRTEM image of SWCNT welded and doped with $HAuCl_4$.

The carbon coating formation (Figures 40B and 41B) provided additional volume to be doped by the cast drop method used (Figure 43), thus an improvement of the resulting R_{90} was observed while compared with similar pristine membranes (R_{90} = 2467 Ω/□) and after welding and doping (R_{90} =30 Ω/□).

Since the excess material changes the electronic dynamic of a randomly oriented nanotube network, there is a limit on which the process works positively. The electric resistivity becomes unacceptably high to be considered to be doped if the treatment times are longer than 30 minutes.

Thus, the treatment works best for the bilateral doping process between 10 up to 30 minutes. The goal of the chosen treatment is to keep the transmittance of the membranes lower or equal to 5% more of the original pristine membrane (transmittance of pristine = 95% to transmittance 90% welded ideally), thus the R_{90} value can be effectively minimized down to 90% compared to pristine desorbed samples for an originally 95% transmittance film (Table 1), higher transmittance FSFs were also studied.

The process of 10 sccm of ethylene with T= 1100 °C has a transmittance increase rate up to 20% per hour of treatment. The comparison of pristine and welded spectra was acquired and reflected a uniform increase of absorbance in the studied range from 174 to 2500 nm. Raman spectra (Figure 43 A) were measured to ensure the efficiency of the doping and the preservation of CNT structure on the membranes.

The results of the process behavior investigation are summarized in Table 1. The data from electrical characterization combined with UV-Vis-NIR spectroscopy, showed an improvement of R_{90} of 15 times for the welded samples, with respect to the pristine samples, proving that the welding treatment can improve the electric conductivity of doped FSFs.

Table 1 Equivalent sheet resistance R90 (Ω/□) and transmittance of the samples

SWCNT Film	**Transmittance@ 550 nm, %**	**R_{90}, Ω/□**
pristine	95	2467
pristine doped	94	57
welded 1 min and doped	93	32
welded 3 min and doped	93	30
welded 5 min and doped	92	34
welded 1 min	93	2272
welded 3 min	93	2204
welded 5 min	92	2100

3.5 Ultimate tensile strength improvement by ethylene welding

Since the mechanical integrity of pristine membranes depends on the Van der Waals interaction between the stack of nanotubes forming the membrane, the coating of the Schottky barriers formed by the tube-tube junctions by carbon, eliminates the slippage mechanism, converting effectively the random nanotube network in an aerogel [4] composed mostly by carbon but having also different allotropes.

This coating of tunable thickness enhances the mechanical stability of the membranes while minimally harming transparency. The extended time coating was investigated by SEM microscopy. Figures 40B and 41B show micrographs of a pristine and membrane after the treatment during 5 min at 1100°C with an ethylene flow of 0.5 SCCM. Figure 42C shows a continuous structure coating the previously randomly stacked nanotubes (carbon lamella, Figure 44 C and D), with the absence of well-defined borders and no visible zones of overlap. Figures 42D shows a thicker structure coating the filamentary nanotubes, forming a larger coating of carbon around the tube-tube junctions and also around the tubes which constitutes the welding, of bigger size than 5-minute treatment. Figure 44D also contains some degree of carbon lamella formation visible in the STEM regime.

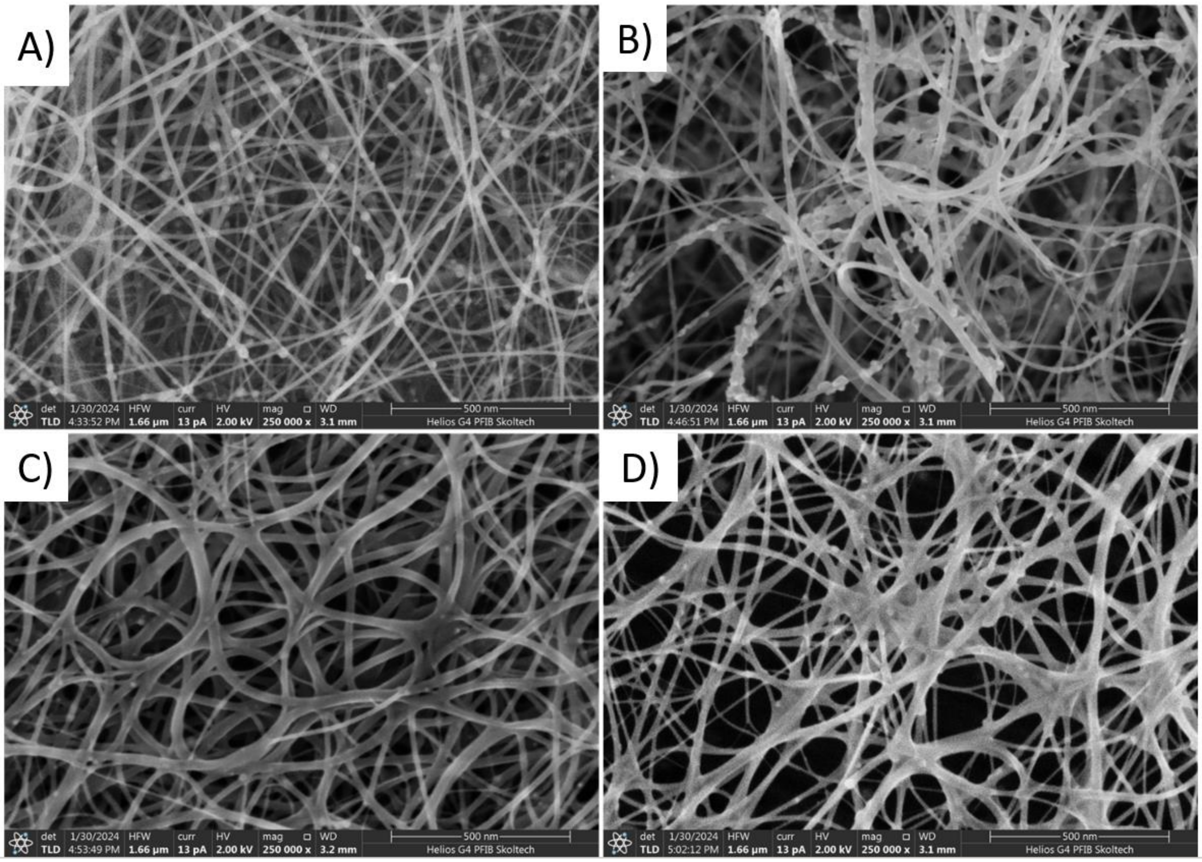

Figure 44: STEM images of different treatment times at 1100°C: A) Pristine membrane; B) 3 min treatment, showing carbon lamella formation and the presence of a closed structure around the bundles; C) 5 min treatment showing partial coating of a nanotube bundle; D) 10 min treatment showing full coating of nanotubes with formation of the coating.

Figure 45 shows a SWCNT FSF standing in a custom made 3d printed holder, made out of uncoated polylactic acid polymer, for performing standard tensile strength tests on a SWCNT film to calibrate and confirm the measurements of the self-built device.

Figure 45: Picture of the holder used to confirm the results of the UTS measurement in a standard tensile strength elongation machine.

While the morphological changes are observable by electron microscopy, different applied analysis show that the original properties of the membrane, including the chemical composition have been kept. This part of the study focuses on the potential applications where mechanical stability / sturdiness of the film are preferred over electrical conductivity, or the maintenance of the elastic properties of the pristine membranes. Since the stretchability of the FSFs relies on the tube-tube slippage, it was expected that the elasticity was to be lost after the welding procedure.

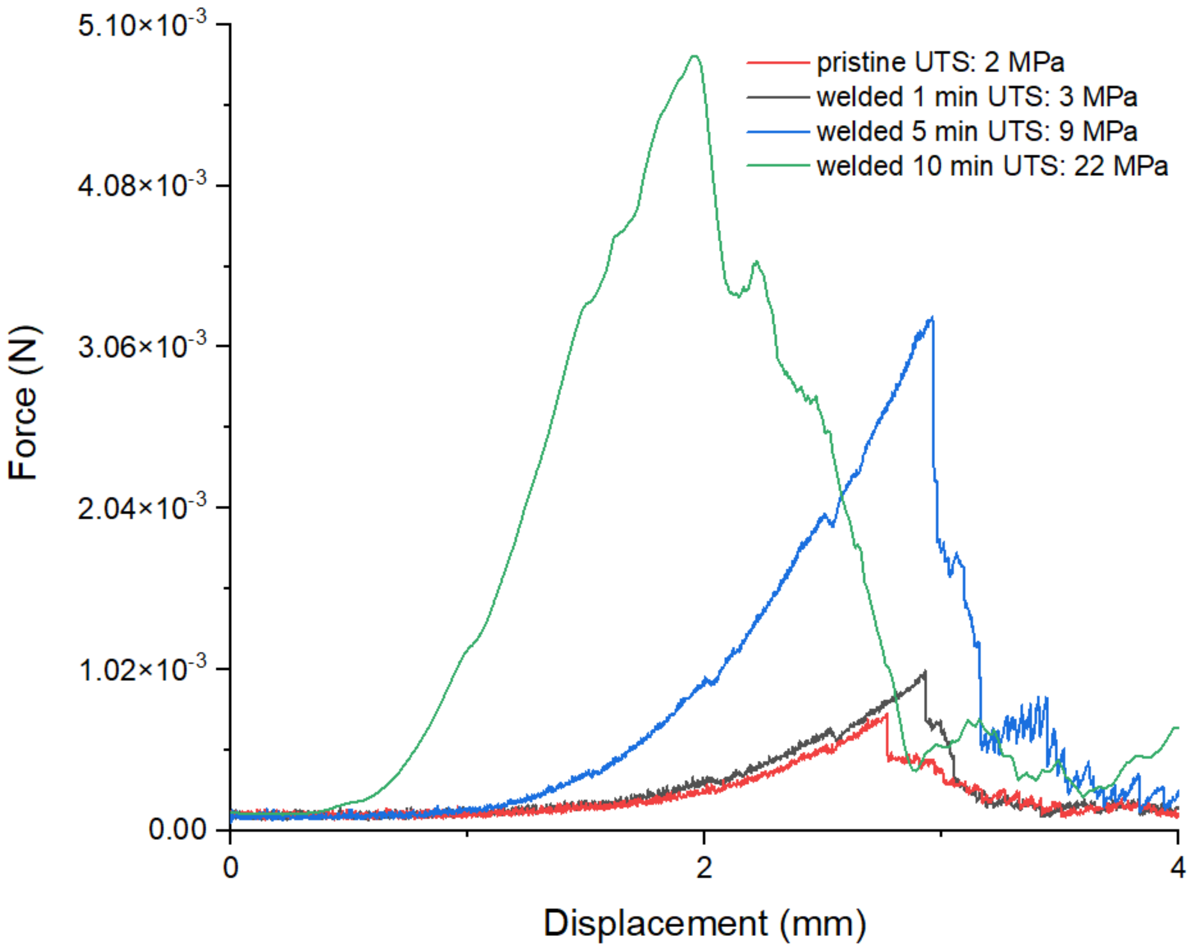

Figure 46: Measurement of the improvement of UTS for different SWCNT membrane ethylene welding times compared to a pristine sample.

Applications for traction, highly conductive and high tensile effort fibers and fabrics plus the welding of SWCNT fiber composed microstructures can be achieved by this method. Our method proved reliable and the maximum strength enhancement obtained ~400% the original UTS form the pristine sample (Figure 46). Measurements of the device were confirmed by a specially designed holder for a standard pull test machine with an ultra-high sensitivity load cell installed (Figure 44). The ultimate tensile strength data showed a standard deviation of 2.9 kPa, of the measured values between 22-27 kPa proving the quality of the calibration procedure.

The process worked successfully to mechanically reinforce the sample of SWCNT FSF in a cold low-pressure chamber with the advantage of a power input <12W instead for few kW furnace while also using much less amount of gas, requiring no purging or preheating, being around 30 times faster.

The measurements of this research stage reflect an improvement of mechanical stability of around 400% for the welded SWCNT FSF with respect to the pristine. This proves the application of the ethylene welding treatment for reinforcement of SWCNT FSFs and FSFs.

3.6 Evaluation of filtering performance of the welded membranes

The setup for filtration tests (Figure 24) was constructed using a recording differential manometer, a constant flow pump, a flowmeter, a HEPA filter, three three-way valves, a SWCNT membrane holder and a computer.

The pump has a soft start function to avoid sudden pressure surges that may prematurely break the filtering membrane. Once the desired flow is reached, the motor runs at constant voltage until the breakage of the membrane happens. The pristine FSFs were evaluated periodically with a CPC(TSI instruments Inc, USA, 3088) that detects particles in the nanometer size, allowing to understand the particle stopping capacity of the filter, shedding data on the continuous performance and degradation over time.

The quality factor measurement stated in section 2.8, results of the cycling of two test filter membranes one pristine and one welded during 10 minutes are shown in Figure 47. The black and red lines represent the repeated automated cycling of the pristine and welded membranes between air and HEPA filtered air demonstrating that the welding process does not harm the efficiency of the membranes for filtering purposes, potentially extending its lifetime thanks to the UTS improvement (Figure 46), which allows operation at higher pressures during a longer time.

The results of the SWCNT filter evaluation show no meaningful changes of efficiency between the welded and pristine samples. The absence of breakage of the tested membranes points to the potential life extension of CNT-based FSFs through the welding reinforcement treatment while maintaining the efficiency.

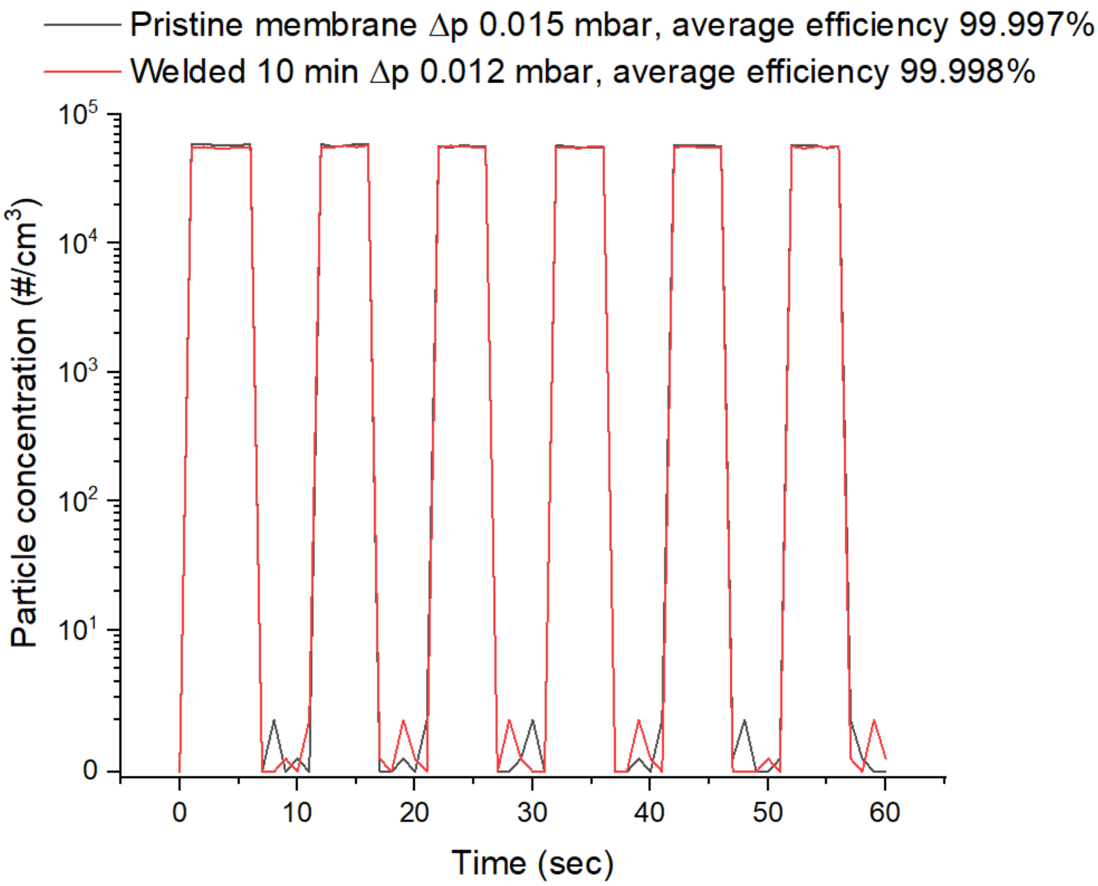

Figure 47: Average efficiency of the filters constructed with pristine and ethylene welded membranes.

Chapter 4: Conclusions and Outlook

4.1 Conclusions

In the present thesis, we synthesized SWCNTs, fabricated freestanding membranes with low outgassing holders allowing Joule heating, and developed methods for modification of the membranes to specific applications: EUV (EUV) pellicles, aerosol filters, and transparent electrodes. It resulted in two relevant technological needs for the advanced applications of SWCNT membranes, both scalable and industrially applicable, energetically efficient approaches to new applications and improving existent technology:

- The first patented invention is a technology (**Publication I)** comprising a SWCNT renewable membrane, which reduces the downtime of EUV lithographs. With both the model aerosol source and the industrial EUV light source, we proved the complete removal of contaminations trapped by nanotube membranes. Further annealing in a vacuum with resistive heating for 3 min at 1400 °C resulted in complete Sn absence on the pellicle surface. Only 20 W/cm^2 is needed for the complete renovation of the SWCNT-based pellicle while the membrane maintains its properties after ten cycles of aerosol exposure and cleaning. The membranes can be also altered by liquid densification (*i.e.*, an increase of density induced by the evaporation of a liquid), which makes the membrane stiffer and decreases the probability of penetration by an order of magnitude. Plasma does not affect the membranes significantly and the penetration reflects that the affectation of the material is negligible for this application (**Publication III)**.

- The welding of nanotube membranes by ethylene pyrolysis (**Publication II**) using resistive heating allowed to engineer the nanotube junctions within the membrane while further treatment induced the full coverage of original nanotubes with pyrolytic carbon. The method is energetically efficient as it requires 10 W/cm^2. Deposition of pyrolytic carbon resulted in an increased ultimate tensile strength (up to an order of magnitude) and lower equivalent sheet resistance (allows one the finest nanotube-based transparent electrodes; R_{90}, the sheet resistance of a film with a 90 % transmittance in the middle of the visible region, as low as 30 Ω/□).

The analysis of the materials after the exposition to different conditions, and under controlled conditions, demonstrates the successful development of technology for extreme UV renewable pellicles and the reinforcement of thin SWCNT membranes through ethylene DC Joule heating welding.

The proposed technology and techniques might not only be useful for EUV pellicle filters and protective membranes as well as transparent electrodes but also provide a fundamental basis for membrane treatment and processing. Transparent touch sensors are ubiquitous in consumer and industrial human interface screens. The evolution in methods to improve the electrical conductivity of SWCNT-based membranes paves the way to sustainably replace indium tin oxide-based technologies, including top electrodes for photoelectric generators and sensors. The Joule heating welding method and device built during this work pave the way towards simplified CVD methods for coating the membranes using gas precursors. Since the membranes maintain their flexibility, thin conductive heat-resistant substrates can be developed from the results obtained from this research for the construction of devices. The mechanical reinforcement of fibers and other carbon nanostructures can be achieved by Joule heating and hydrocarbon gas welding.

Future research can be developed by individual assessment of mechanical testing, to investigate tailoring of SWCNT welded structures.

The future of Microelectromechanical Systems (MEMS) technology hinges on the development of materials and fabrication techniques that enable smaller, more robust, and more functional devices. Current MEMS fabrication often faces limitations in material properties, particularly when miniaturization requires thinner and more flexible structures. The integration of plasticity-tuned welded single-walled carbon nanotube (SWCNT) membranes offers a compelling pathway to overcome these limitations and significantly enhance MEMS capabilities.

SWCNTs possess exceptional mechanical properties, including high strength, stiffness, and flexibility. However, harnessing these properties in MEMS applications requires precise control over the CNT network structure and its mechanical response. The concept of “plasticity-tuned welded SWCNT membranes” introduces a novel approach to achieve this control. By carefully tailoring the welding process – which connects individual SWCNTs to form a continuous membrane – the overall plasticity of the membrane can be precisely engineered. This tunability allows for the creation of membranes with tailored mechanical characteristics, ranging from highly elastic to highly plastic, depending on the specific application.

Several aspects of future MEMS technology can be improved through the use of these advanced membranes:

1. Enhanced Flexibility and Robustness: Plasticity-tuned welded SWCNT membranes offer superior flexibility compared to conventional MEMS materials like silicon. This allows for the creation of highly flexible, conformal MEMS devices that can adapt to complex geometries or integrate with curved surfaces. Furthermore, the inherent strength of the CNT network provides enhanced robustness against mechanical stress and fatigue, extending the lifespan of MEMS devices.

2. Improved Functionality: The tailored plasticity of the membrane opens exciting possibilities for creating MEMS devices with novel functionalities. For instance, a highly elastic membrane could be used to create micro-actuators or sensors with large deflections, while a more plastic membrane might be preferred for devices requiring high strain tolerance.

3. Reduced Manufacturing Costs: The scalability and relative simplicity of SWCNT membrane fabrication techniques offer potential cost advantages compared to traditional MEMS manufacturing processes. Large-area, high-quality membranes could be produced using roll-to-roll methods, enabling mass production and reducing the overall cost of MEMS devices.

4. Advanced Device Architectures: The unique properties of plasticity-tuned welded SWCNT membranes enable the development of novel device architectures. For example, integrating these membranes with other nanomaterials can create hybrid MEMS devices with enhanced functionality, such as integrated sensors and actuators on a single platform.

5. Integration with Other Nanomaterials: Welded SWCNT membranes provide a robust and flexible platform for integrating other nanomaterials, creating hybrid structures with enhanced functionality. For example, incorporating piezoelectric materials could enable energy harvesting capabilities.

However, challenges remain:

- **Precise Control of Welding:** Developing reliable and reproducible techniques for welding SWCNTs with precise control over the resulting plasticity is crucial.
- **Large-Scale Manufacturing:** Scaling up the fabrication process to meet industrial demands requires further research and development.
- **Integration with Existing MEMS Processes:** Seamless integration of SWCNT membranes with existing MEMS fabrication processes is essential for practical implementation.

By addressing these challenges, plasticity-tuned welded SWCNT membranes hold the potential to revolutionize MEMS technology, enabling the creation of smaller, more robust, more functional, and more cost-effective devices with a broad range of applications, including sensors, actuators, microfluidic devices, varactors [136,137] and lab-on-a-chip systems. This innovative approach promises to unlock new possibilities for miniaturization, improved performance, and expanded functionalities within the field of MEMS.

The semiconductor industry constantly seeks advancements in materials and manufacturing processes to create smaller, faster, and more energy-efficient chips. A critical component in extreme ultraviolet (EUV) lithography, the cornerstone of modern chip fabrication, is the pellicle – a thin, transparent membrane protecting the photomask from damage during the exposure process. Current pellicles, typically made of silicon nitride, suffer from limitations in mechanical robustness and chemical inertness, impacting throughput and lifespan.

However, a new generation of filters, based on high-mechanical-sturdiness, chemically inert thin films of carbon nanotubes (CNTs), offers a potential paradigm shift for filter and semiconductor industries, ushering in the era of the first renewable EUV pellicle.

Future research on CNT-based filters should focus on several key areas:

1. Controlled Synthesis and Assembly: Precise control over CNT growth and alignment is essential for creating high-quality films with uniform optical properties. Investigating innovative techniques such as directed self-assembly, template-assisted growth, and advanced chemical vapor deposition (CVD) methods is vital. Achieving consistent large-area films with minimal defects is critical for scalability in industrial applications.

2. Enhanced Mechanical Properties: The mechanical robustness of the CNT film is paramount for pellicle applications. Research efforts should focus on optimizing the CNT network structure, incorporating reinforcing agents, and exploring novel post-processing techniques to enhance tensile strength, flexibility, and resistance to deformation. The goal is a pellicle that can withstand the rigors of high-throughput EUV lithography without compromising transparency or quality.

3. Improved Chemical Inertness: Chemical inertness ensures the pellicle remains undamaged during the manufacturing process and resists contamination. Surface functionalization strategies that enhance chemical resistance without sacrificing optical transparency require further exploration. Understanding and mitigating interactions between the SWCNT film and various chemicals used in the semiconductor fabrication environment are key.

4. Optical Optimization: The pellicle must exhibit high transmittance in the EUV spectral range. Optimizing the SWCNT film's density, alignment, and thickness to maximize EUV transmission while minimizing absorption and scattering is crucial.

Advanced optical modeling and characterization techniques are necessary to achieve precise control over the optical properties.

5. Scalability and Cost-Effectiveness: The successful commercialization of CNT-based pellicles hinges on developing scalable and cost-effective manufacturing processes. Exploring high-throughput fabrication methods compatible with existing semiconductor manufacturing infrastructure is critical.

4.2 Outlook: prospective Applications and Impact

The successful development of high-performance SWCNT-based filters extends beyond EUV pellicles. Their exceptional mechanical strength, chemical inertness, and tunable optical properties make them suitable for various applications, including:

High-performance filtration: In various industries, including water purification and air filtration, CNT filters offer superior filtration efficiency and durability compared to traditional materials.

Protective coatings: CNT films can serve as robust and transparent protective layers for delicate optical components.

Biosensors and medical devices: Their biocompatibility and electrical properties open possibilities for advanced biosensing and medical device applications.

The creation of a renewable EUV pellicle from CNTs is a game-changer for the semiconductor industry. Eliminating the need for frequent pellicle replacements would significantly improve throughput and reduce manufacturing costs, enabling the production of more advanced and efficient semiconductor chips.

Moreover, the inherent sustainability of CNT-based materials aligns with the growing need for environmentally friendly manufacturing practices within the electronics industry. By addressing the remaining challenges through focused research, the remarkable potential of CNT-based filters can be fully realized, transforming both the filter and semiconductor industries.

References

[1] L.V. Radushkevich, V.M. Lukyanovich, On the structure of carbon formed during the thermal decomposition of carbon monoxide on an iron contact, Journal of Physical Chemistry 26 (1952) 88–95.

[2] S. Iijima, Helical microtubules of graphitic carbon, Nature 1991 354:6348 354 (1991) 56–58. https://doi.org/10.1038/354056a0.

[3] O. Gohardani, M.C. Elola, C. Elizetxea, Potential and prospective implementation of carbon nanotubes on next generation aircraft and space vehicles: A review of current and expected applications in aerospace sciences, Progress in Aerospace Sciences 70 (2014) 42–68. https://doi.org/10.1016/J.PAEROSCI.2014.05.002.

[4] J. Alemán, A. V. Chadwick, J. He, M. Hess, K. Horie, R.G. Jones, P. Kratochvíl, I. Meisel, I. Mita, G. Moad, S. Penczek, R.F.T. Stepto, Definitions of terms relating to the structure and processing of sols, gels, networks, and inorganic-organic hybrid materials (IUPAC recommendations 2007), Pure and Applied Chemistry 79 (2007) 1801–1829. https://doi.org/10.1351/PAC200779101801/MACHINEREADABLECITATION/RIS.

[5] A.G. Nasibulin, A. Kaskela, K. Mustonen, A.S. Anisimov, V. Ruiz, S. Kivistö, S. Rackauskas, M.Y. Timmermans, M. Pudas, B. Aitchison, M. Kauppinen, D.P. Brown, O.G. Okhotnikov, E.I. Kauppinen, Multifunctional Free-Standing Single-Walled Carbon Nanotube Films, ACS Nano 5 (2011) 3214–3221. https://doi.org/10.1021/nn200338r.

[6] S.A. Romanov, A.E. Aliev, B. V. Fine, A.S. Anisimov, A.G. Nasibulin, Highly efficient thermophones based on freestanding single-walled carbon nanotube films, Nanoscale Horiz 4 (2019) 1158–1163. https://doi.org/10.1039/c9nh00164f.

[7] J.A. Ramirez B., D. V. Krasnikov, V. V. Gubarev, I. V. Novikov, V.A. Kondrashov, A. V. Starkov, M.S. Krivokorytov, V. V. Medvedev, Y.G. Gladush, A.G. Nasibulin, Renewable single-walled carbon nanotube membranes for extreme ultraviolet pellicle applications, Carbon N Y 198 (2022) 364–370. https://doi.org/10.1016/j.carbon.2022.07.014.

[8] M. Rani, M. Sehrawat, R. Rani, B. Gahtori, B.P. Singh, Tailoring the physical characteristics of buckypaper via controlling the surfactant concentration, Surfaces and Interfaces 37 (2023) 102713. https://doi.org/10.1016/J.SURFIN.2023.102713.

[9] A. Kausar, H. Ilyas, M. Siddiq, Current Research Status and Application of Polymer/Carbon Nanofiller Buckypaper: A Review, Polymer - Plastics Technology and Engineering 56 (2017) 1780–1800. https://doi.org/10.1080/03602559.2017.1289407.

[10] V. Ya Iakovlev, Advanced synthesis of single-walled carbon nanotube films by aerosol CVD method for electro-optical applications A" Aalto University Advanced synthesis of single-walled carbon nanotube films by aerosol CVD method for electro-optical applications A" Aalto University Advanced synthesis of single-walled carbon nanotube films by aerosol CVD method for electro-optical applications A" Aalto University, (n.d.). www.aalto.fiwww.aalto.fiwww.aalto.fi (accessed December 5, 2023).

[11] S.E. Thompson, S. Parthasarathy, Moore's law: the future of Si microelectronics, Materials Today 9 (2006) 20–25. https://doi.org/10.1016/S1369-7021(06)71539-5.

[12] R.A. Lawson, A.P.G. Robinson, Overview of materials and processes for lithography, in: Frontiers of Nanoscience, Elsevier Ltd, 2016: pp. 1–90. https://doi.org/10.1016/B978-0-08-100354-1.00001-6.

[13] S.J. Yook, H. Fissan, C. Asbach, J. Hyeun Kim, J. Wang, P.Y. Yan, D.Y.H. Pui, Evaluation of protection schemes for extreme ultraviolet lithography (EUVL) masks against top-down aerosol flow, J Aerosol Sci 38 (2007) 211–227. https://doi.org/10.1016/j.jaerosci.2006.11.010.

[14] Y.T. Liu, T.T. Yao, W.S. Zhang, G.P. Wu, Laser welding of carbon nanotube networks on carbon fibers from ultrasonic-directed assembly, Mater Lett 236 (2019) 244–247. https://doi.org/10.1016/j.matlet.2018.09.161.

[15] S. Jiang, P.X. Hou, M.L. Chen, B.W. Wang, D.M. Sun, D.M. Tang, Q. Jin, Q.X. Guo, D.D. Zhang, J.H. Du, K.P. Tai, J. Tan, E.I. Kauppinen, C. Liu, H.M. Cheng, Ultrahigh-performance transparent conductive films of carbon-welded isolated single-wall carbon nanotubes, Sci Adv 4 (2018). https://doi.org/10.1126/sciadv.aap9264.

[16] Y. Yao, K.K. Fu, S. Zhu, J. Dai, Y. Wang, G. Pastel, Y. Chen, T. Li, C. Wang, T. Li, L. Hu, Carbon Welding by Ultrafast Joule Heating, Nano Lett 16 (2016) 7282–7289. https://doi.org/10.1021/ACS.NANOLETT.6B03888/SUPPL_FILE/NL6B03888_SI_001.PDF.

[17] Y. Yao, F. Jiang, C. Yang, K.K. Fu, J. Hayden, C.F. Lin, H. Xie, M. Jiao, C. Yang, Y. Wang, S. He, F. Xu, E. Hitz, T. Gao, J. Dai, W. Luo, G. Rubloff, C. Wang, L. Hu, Epitaxial Welding of Carbon Nanotube Networks for Aqueous Battery Current Collectors, ACS Nano 12 (2018) 5266–5273. https://doi.org/10.1021/acsnano.7b08584.

[18] C.B. Sweeney, B.A. Lackey, M.J. Pospisil, T.C. Achee, V.K. Hicks, A.G. Moran, B.R. Teipel, M.A. Saed, M.J. Green, Welding of 3D-printed carbon nanotube–polymer composites by locally induced microwave heating, Sci Adv 3 (2017). https://doi.org/10.1126/sciadv.1700262.

[19] XIII. On the atomic weight of graphite, Philos Trans R Soc Lond 149 (1859) 249–259. https://doi.org/10.1098/RSTL.1859.0013.

[20] A. Aqel, K.M.M.A. El-Nour, R.A.A. Ammar, A. Al-Warthan, Carbon nanotubes, science and technology part (I) structure, synthesis and characterization, Arabian Journal of Chemistry 5 (2012) 1–23. https://doi.org/10.1016/J.ARABJC.2010.08.022.

[21] A. Oberlin, M. Endo, T. Koyama, Filamentous growth of carbon through benzene decomposition, J Cryst Growth 32 (1976) 335–349. https://doi.org/10.1016/0022-0248(76)90115-9.

[22] M. Monthioux, V.L. Kuznetsov, Who should be given the credit for the discovery of carbon nanotubes? Carbon N Y 44 (2006) 1621–1623. https://doi.org/10.1016/J.CARBON.2006.03.019.

[23] L. Brillouin, Les électrons libres dans les métaux et le role des réflexions de Bragg, Journal de Physique et Le Radium 1 (1930) 377–400. https://doi.org/10.1051/JPHYSRAD:01930001011037700.

[24] N. Hamada, S.I. Sawada, A. Oshiyama, New one-dimensional conductors: Graphitic microtubules, Phys Rev Lett 68 (1992) 1579. https://doi.org/10.1103/PhysRevLett.68.1579.

[25] A.K. Geim, K.S. Novoselov, The rise of graphene, Nature Materials 2007 6:3 6 (2007) 183–191. https://doi.org/10.1038/nmat1849.

[26] K.S. Novoselov, A.K. Geim, S. V. Morozov, D. Jiang, Y. Zhang, S. V. Dubonos, I. V. Grigorieva, A.A. Firsov, Electric field in atomically thin carbon films, Science (1979) 306 (2004) 666. https://doi.org/10.1126/science.1102896.

[27] C. Singh, W. Song, Carbon nanotube structure, synthesis, and applications, The Toxicology of Carbon Nanotubes 9781107008373 (2012) 1–37. https://doi.org/10.1017/CBO9780511919893.001.

[28] W. Hoenlein, F. Kreupl, G.S. Duesberg, A.P. Graham, M. Liebau, R. Seidel, E. Unger, Carbon nanotubes for microelectronics: status and future prospects, Materials Science and Engineering: C 23 (2003) 663–669. https://doi.org/10.1016/J.MSEC.2003.09.153.

[29] H. Navas, M. Picher, A. Andrieux-Ledier, F. Fossard, T. Michel, A. Kozawa, T. Maruyama, E. Anglaret, A. Loiseau, V. Jourdain, Unveiling the Evolutions of Nanotube Diameter Distribution during the Growth of Single-Walled Carbon Nanotubes, ACS Nano 11 (2017) 3081–3088. https://doi.org/10.1021/ACSNANO.7B00077/SUPPL_FILE/NN7B00077_SI_001.PDF.

[30] H.W. Kroto, J.R. Heath, S.C. O'Brien, R.F. Curl, R.E. Smalley, C60: Buckminsterfullerene, Nature 1985 318:6042 318 (1985) 162–163. https://doi.org/10.1038/318162a0.

[31] S. Rathinavel, K. Priyadharshini, D. Panda, A review on carbon nanotube: An overview of synthesis, properties, functionalization, characterization, and the application, Materials Science and Engineering: B 268 (2021) 115095. https://doi.org/10.1016/J.MSEB.2021.115095.

[32] N. Arora, N.N. Sharma, Arc discharge synthesis of carbon nanotubes: Comprehensive review, Diam Relat Mater 50 (2014) 135–150. https://doi.org/10.1016/J.DIAMOND.2014.10.001.

[33] Y.C. Choi, Y.M. Shin, Y.H. Lee, B.S. Lee, G.S. Park, W.B. Choi, N.S. Lee, J.M. Kim, Controlling the diameter, growth rate, and density of vertically aligned carbon nanotubes synthesized by microwave plasma-enhanced chemical vapor deposition, Appl Phys Lett 76 (2000) 2367–2369. https://doi.org/10.1063/1.126348.

[34] J.H. Yen, I.C. Leu, C.C. Lin, M.H. Hon, Synthesis of well-aligned carbon nanotubes by inductively coupled plasma chemical vapor deposition, Applied Physics A 2004 80:2 80 (2005) 415–421. https://doi.org/10.1007/S00339-004-2545-X.

[35] S.D. Dutta, K.T. Lim, D.K. Patel, Carbon nanotube-based nanohybrids for agricultural and biological applications, Multifunctional Hybrid Nanomaterials for Sustainable Agri-Food and Ecosystems (2020) 505–535. https://doi.org/10.1016/B978-0-12-821354-4.00021-2.

[36] H. Chu, W. Han, F. Ren, L. Xiang, Y. Wei, C. Zhang, Flame Synthesis of Carbon Nanotubes on Different Substrates in Methane Diffusion Flames, ES Energy & Environment (2018). https://doi.org/10.30919/ESEE8C165.

[37] C.J. Lee, S.C. Lyu, H.W. Kim, C.Y. Park, C.W. Yang, Large-scale production of aligned carbon nanotubes by the vapor phase growth method, Chem Phys Lett 359 (2002) 109–114. https://doi.org/10.1016/S0009-2614(02)00648-6.

[38] A.G. Nasibulin, A. Moisala, H. Jiang, E.I. Kauppinen, Carbon nanotube synthesis from alcohols by a novel aerosol method, Journal of Nanoparticle Research 8 (2006) 465–475. https://doi.org/10.1007/S11051-005-9027-8/METRICS.

[39] A. Moisala, A.G. Nasibulin, D.P. Brown, H. Jiang, L. Khriachtchev, E.I. Kauppinen, Single-walled carbon nanotube synthesis using ferrocene and iron pentacarbonyl in a laminar flow reactor, Chem Eng Sci 61 (2006) 4393–4402. https://doi.org/10.1016/J.CES.2006.02.020.

[40] D. V. Krasnikov, B.Y. Zabelich, V.Y. Iakovlev, A.P. Tsapenko, S.A. Romanov, A.A. Alekseeva, A.K. Grebenko, A.G. Nasibulin, A spark discharge generator for scalable aerosol CVD synthesis of single-walled carbon nanotubes with tailored characteristics, Chemical Engineering Journal 372 (2019) 462–470. https://doi.org/10.1016/j.cej.2019.04.173.

[41] A.G. Nasibulin, A. Moisala, D.P. Brown, H. Jiang, E.I. Kauppinen, A novel aerosol method for single walled carbon nanotube synthesis, Chem Phys Lett 402 (2005) 227–232. https://doi.org/10.1016/j.cplett.2004.12.040.

[42] D. V. Krasnikov, E.M. Khabushev, A. Gaev, A.R. Bogdanova, V.Y. Iakovlev, A. Lantsberg, T. Kallio, A.G. Nasibulin, Machine learning methods for aerosol synthesis of single-walled carbon nanotubes, Carbon N Y 202 (2023) 76–82. https://doi.org/10.1016/j.carbon.2022.10.044.

[43] V.Y. Iakovlev, D. V. Krasnikov, E.M. Khabushev, J. V. Kolodiazhnaia, A.G. Nasibulin, Artificial neural network for predictive synthesis of single-walled carbon nanotubes by aerosol CVD method, Carbon N Y 153 (2019) 100–103. https://doi.org/10.1016/J.CARBON.2019.07.013.

[44] I. V. Novikov, D. V. Krasnikov, V.S. Shestakova, I.P. Rogov, V.A. Dmitrieva, A.E. Goldt, T. Kallio, A.G. Nasibulin, Boosting CO-based synthesis of single-walled carbon nanotubes with hydrogen, Chemical Engineering Journal 476 (2023). https://doi.org/10.1016/j.cej.2023.146527.

[45] A.R. Bogdanova, D. V. Krasnikov, E.M. Khabushev, J.A. Ramirez, Y. Matyushkin, A.G. Nasibulin, Role of Hydrogen in Carbon Nanotube Synthesis, SSRN Electronic Journal (2022). https://doi.org/10.2139/SSRN.4305756.

[46] S.L. Pirard, S. Douven, J.P. Pirard, Large-scale industrial manufacturing of carbon nanotubes in a continuous inclined mobile-bed rotating reactor via the catalytic chemical vapor deposition process, Front Chem Sci Eng 11 (2017) 280–289. https://doi.org/10.1007/S11705-017-1635-1/METRICS.

[47] Y. Wang, F. Wei, G. Luo, H. Yu, A. Gu, The large-scale production of carbon nanotubes in a nano-agglomerate fluidized-bed reactor, Chem Phys Lett 364 (2002) 568–572. https://doi.org/10.1016/S0009-2614(02)01384-2.

[48] Q. Zhang, W. Zhou, X. Xia, K. Li, N. Zhang, Y. Wang, Z. Xiao, Q. Fan, E.I. Kauppinen, S. Xie, Transparent and Freestanding Single-Walled Carbon Nanotube Films Synthesized Directly and Continuously via a Blown Aerosol Technique, Advanced Materials 32 (2020) 1–8. https://doi.org/10.1002/adma.202004277.

[49] S. Morais, Advances and Applications of Carbon Nanotubes, Nanomaterials 13 (2023). https://doi.org/10.3390/NANO13192674.

[50] H.L. Guo, Q.X. Zhang, Y.P. Liu, D.K. Zhao, Properties and Defence Applications of Carbon Nanotubes, J Phys Conf Ser 2478 (2023) 042010. https://doi.org/10.1088/1742-6596/2478/4/042010.

[51] T. Fukuyama, N. Mukai, G. Togawa, Dynamic behaviours of a flame as plasma in a strong electric field, Sci Rep 9 (2019) 1–8. https://doi.org/10.1038/s41598-019-50537-x.

[52] A. Venkataraman, E.V. Amadi, Y. Chen, C. Papadopoulos, Carbon Nanotube Assembly and Integration for Applications, Nanoscale Research Letters 2019 14:1 14 (2019) 1–47. https://doi.org/10.1186/S11671-019-3046-3.

[53] K. Koziol, J. Vilatela, A. Moisala, M. Motta, P. Cunniff, M. Sennett, A. Windle, High-performance carbon nanotube fiber, Science (1979) 318 (2007) 1892–1895. https://doi.org/10.1126/SCIENCE.1147635.

[54] E. Oh, H. Cho, J. Kim, J.E. Kim, Y. Yi, J. Choi, H. Lee, Y.H. Im, K.H. Lee, W.J. Lee, Super-Strong Carbon Nanotube Fibers Achieved by Engineering Gas Flow and Postsynthesis Treatment, ACS Appl Mater Interfaces 12 (2020) 13107–13115. https://doi.org/10.1021/ACSAMI.9B19861.

[55] S.H. Lee, J. Park, S.Y. Moon, S.Y. Lee, S.M. Kim, Strong and Highly Conductive Carbon Nanotube Fibers as Conducting Wires for Wearable Electronics, ACS Appl Nano Mater 4 (2021) 3833–3842. https://doi.org/10.1021/ACSANM.1C00248/SUPPL_FILE/AN1C00248_SI_001.PDF.

[56] A. Takakura, K. Beppu, T. Nishihara, A. Fukui, T. Kozeki, T. Namazu, Y. Miyauchi, K. Itami, Strength of carbon nanotubes depends on their chemical structures, Nat Commun 10 (2019). https://doi.org/10.1038/S41467-019-10959-7.

[57] S.Y. Moon, B.R. Kim, C.W. Park, S.H. Lee, S.M. Kim, High-crystallinity single-walled carbon nanotube aerogel growth: Understanding the real-time catalytic decomposition reaction through floating catalyst chemical vapor deposition, Chemical Engineering Journal Advances 10 (2022) 100261. https://doi.org/10.1016/J.CEJA.2022.100261.

[58] V.L. Kuznetsov, V.I. Suslyaev, I.O. Dorofeev, M.A. Kazakova, S.I. Moseenkov, T.E. Smirnova, D. V. Krasnikov, Investigation of electromagnetic properties of MWCNT aerogels produced via catalytic ethylene decomposition, Phys Status Solidi B Basic Res 252 (2015) 2519–2523. https://doi.org/10.1002/pssb.201552254.

[59] W. Wan, R. Zhang, W. Li, H. Liu, Y. Lin, L. Li, Y. Zhou, Graphene–carbon nanotube aerogel as an ultra-light, compressible and recyclable highly efficient absorbent for oil and dyes, Environ Sci Nano 3 (2016) 107–113. https://doi.org/10.1039/C5EN00125K.

[60] H. LIPSON, A.R. STOKES, A New Structure of Carbon, Nature 1942 149:3777 149 (1942) 328–328. https://doi.org/10.1038/149328a0.

[61] A.N. Popova, Crystallographic analysis of graphite by X-Ray diffraction, Coke and Chemistry 60 (2017) 361–365. https://doi.org/10.3103/S1068364X17090058.

[62] Z.Q. Li, C.J. Lu, Z.P. Xia, Y. Zhou, Z. Luo, X-ray diffraction patterns of graphite and turbostratic carbon, Carbon N Y 45 (2007) 1686–1695. https://doi.org/10.1016/J.CARBON.2007.03.038.

[63] R. Das, S. Hamid, Md. Ali, S. Ramakrishna, W. Yongzhi, Carbon Nanotubes Characterization by X-ray Powder Diffraction – A Review, Curr Nanosci 11 (2014) 23–35. https://doi.org/10.2174/1573413710666140818210043.

[64] Vladar, Andras, Strategies for scanning electron microscopy sample preparation and characterization of multiwall carbon nanotube polymer composites, (n.d.). https://doi.org/10.6028/NIST.SP.1200-17.

[65] R. Herrera-Basurto, Á.I. López-Lorente, M. Valcárcel, Scanning electron microscopy of carbon nanotubes dispersed in ionic liquid: Solvent influence study, Microchemical Journal 122 (2015) 137–143. https://doi.org/10.1016/J.MICROC.2015.04.012.

[66] M. Ishii, K. Nakashima, I. Tajima, M. Yamamoto, Investigation of hydrogen plasma etched si surfaces, Jpn J Appl Phys 31 (1992) 4422–4427. https://doi.org/10.1143/JJAP.31.4422.

[67] H.A. Butt, S. V. Lomov, I.S. Akhatov, S.G. Abaimov, Self-diagnostic carbon nanocomposites manufactured from industrial epoxy masterbatches, Compos Struct 259 (2021) 113244. https://doi.org/10.1016/J.COMPSTRUCT.2020.113244.

[68] J.S. Bulmer, A. Kaniyoor, J.A. Elliott, A Meta-Analysis of Conductive and Strong Carbon Nanotube Materials, Advanced Materials 33 (2021). https://doi.org/10.1002/adma.202008432.

[69] I. V. Novikov, D. V. Krasnikov, A.M. Vorobei, Y.I. Zuev, H.A. Butt, F.S. Fedorov, S.A. Gusev, A.A. Safonov, E. V. Shulga, S.D. Konev, I. V. Sergeichev, S.S. Zhukov, T. Kallio, B.P. Gorshunov, O.O. Parenago, A.G. Nasibulin, Multifunctional Elastic Nanocomposites with Extremely Low Concentrations of Single-Walled Carbon Nanotubes, ACS Appl Mater Interfaces 14 (2022) 18866–18876. https://doi.org/10.1021/acsami.2c01086.

[70] A. Jorio, R. Saito, Raman spectroscopy for carbon nanotube applications, J Appl Phys 129 (2021). https://doi.org/10.1063/5.0030809.

[71] A.C. Ferrari, D.M. Basko, Raman spectroscopy as a versatile tool for studying the properties of graphene, (2013).

[72] L.M. Malard, M.A. Pimenta, G. Dresselhaus, M.S. Dresselhaus, Raman spectroscopy in graphene, Phys Rep 473 (2009) 51–87. https://doi.org/10.1016/J.PHYSREP.2009.02.003.

[73] Tuball, Tuball articles carbon-nanotube-powder, (2022). https://tuball.com/articles/carbon-nanotube-powder (accessed November 22, 2024).

[74] Q.P. Leigh Ann Larkin, Advisor: Dean Pamela Norris, University of Virginia, V. Charlottesville, A Forest of Carbon Nanotubes | National Nanotechnology Initiative, (n.d.). https://www.nano.gov/node/1797 (accessed July 4, 2024).

[75] K.W. Guo, H.-Y. Tam, K.W. Guo, H.-Y. Tam, TEM Morphology of Carbon Nanotubes (CNTs) and its Effect on the Life of Micropunch, The Transmission Electron Microscope - Theory and Applications (2015). https://doi.org/10.5772/60713.

[76] X. Huang, R. Farra, R. Schlögl, M.G. Willinger, Growth and Termination Dynamics of Multiwalled Carbon Nanotubes at Near Ambient Pressure: An in-Situ Transmission Electron Microscopy Study, Nano Lett 19 (2019) 5380–5387. https://doi.org/10.1021/ACS.NANOLETT.9B01888/SUPPL_FILE/NL9B01888_SI_007.AVI.

[77] A.G. Ryabenko, T. V. Dorofeeva, G.I. Zvereva, UV–VIS–NIR spectroscopy study of sensitivity of single-wall carbon nanotubes to chemical processing and Van-der-Waals SWNT/SWNT interaction. Verification of the SWNT content measurements by absorption spectroscopy, Carbon N Y 42 (2004) 1523–1535. https://doi.org/10.1016/J.CARBON.2004.02.005.

[78] A.I. Zhbanov, E.G. Pogorelov, Y.C. Chang, Van der Waals interaction between two crossed carbon nanotubes, ACS Nano 4 (2010) 5937–5945. https://doi.org/10.1021/NN100731U/ASSET/IMAGES/MEDIUM/NN-2010-00731U_0008.GIF.

[79] J. Njuguna, O.A. Vanli, R. Liang, A Review of Spectral Methods for Dispersion Characterization of Carbon Nanotubes in Aqueous Suspensions, Journal of Spectroscopy 2015 (2015). https://doi.org/10.1155/2015/463156.

[80] G.A. Rance, D.H. Marsh, R.J. Nicholas, A.N. Khlobystov, UV-vis absorption spectroscopy of carbon nanotubes: Relationship between the π-electron plasmon and nanotube diameter, Chem Phys Lett 493 (2010) 19–23. https://doi.org/10.1016/J.CPLETT.2010.05.012.

[81] H.A. Butt, I. V. Novikov, D. V. Krasnikov, A. V. Sulimov, A.K. Pal, S.A. Evlashin, A.M. Vorobei, Y.I. Zuev, D. Ostrizhiniy, D. Dzhurinskiy, Y.A. Popov, O.O. Parenago, A.G. Nasibulin, Binder-free, pre-consolidated single-walled carbon

nanotubes for manufacturing thermoset nanocomposites, Carbon N Y 202 (2023) 450–463. https://doi.org/10.1016/J.CARBON.2022.10.088.

[82] S.A. Romanov, A.A. Alekseeva, E.M. Khabushev, D. V. Krasnikov, A.G. Nasibulin, Rapid, efficient, and non-destructive purification of single-walled carbon nanotube films from metallic impurities by Joule heating, Carbon N Y 168 (2020) 193–200. https://doi.org/10.1016/j.carbon.2020.06.068.

[83] H. Lee, J. Park, H. Cho, J. Lee, K.H. Lee, Investigation of shear-induced rearrangement of carbon nanotube bundles using Taylor–Couette flow, RSC Adv 11 (2021) 38152–38160. https://doi.org/10.1039/D1RA07354K.

[84] Y. Liu, S. Zhang, J. Guo, W. Qiu, G. Zhou, Q. Li, Debundling and reorganization of CNT networks under high temperature treatment, Carbon N Y 222 (2024) 119004. https://doi.org/10.1016/J.CARBON.2024.119004.

[85] R. Dubey, D. Dutta, A. Sarkar, P. Chattopadhyay, Functionalized carbon nanotubes: synthesis, properties and applications in water purification, drug delivery, and material and biomedical sciences, Nanoscale Adv 3 (2021) 5722–5744. https://doi.org/10.1039/D1NA00293G.

[86] B. Singh, S. Lohan, P.S. Sandhu, A. Jain, S.K. Mehta, Functionalized carbon nanotubes and their promising applications in therapeutics and diagnostics, Nanobiomaterials in Medical Imaging: Applications of Nanobiomaterials (2016) 455–478. https://doi.org/10.1016/B978-0-323-41736-5.00015-7.

[87] E.M. Alosime, A review on surface functionalization of carbon nanotubes: methods and applications, Discover Nano 18 (2023) 1–11. https://doi.org/10.1186/S11671-023-03789-6/FIGURES/7.

[88] S. Tyagi, S. Negi, Side wall functionalization of carbon nanotube using MOPAC software, AIP Conf Proc 2752 (2023). https://doi.org/10.1063/5.0136283/2893512.

[89] A. Hirsch, O. Vostrowsky, Functionalization of Carbon Nanotubes, Top Curr Chem 245 (2005) 193–237. https://doi.org/10.1007/B98169.

[90] D. Mitin, A. Vorobyev, A. Pavlov, Y. Berdnikov, A. Mozharov, V. Mikhailovskii, J.A.B. Ramirez, D. V. Krasnikov, D.S. Kopylova, D.A. Kirilenko, M. Vinnichenko, R. Polozkov, A.G. Nasibulin, I. Mukhin, Tuning the Optical Properties and Conductivity of Bundles in Networks of Single-Walled Carbon Nanotubes, Journal of Physical Chemistry Letters 13 (2022) 8775–8782. https://doi.org/10.1021/ACS.JPCLETT.2C01931/SUPPL_FILE/JZ2C01931_SI_001.PDF.

[91] S.A. Romanov, A.E. Aliev, B. V Fine, A.S. Anisimov, A.G. Nasibulin, Highly efficient thermophones based on freestanding single-walled carbon nanotube films †, Nanoscale Horiz 4 (2019) 1158. https://doi.org/10.1039/c9nh00164f.

[92] S. Huang, Y. Liu, Y. Zhao, Z. Ren, C.F. Guo, Flexible Electronics: Stretchable Electrodes and Their Future, Adv Funct Mater 29 (2019) 1805924. https://doi.org/10.1002/adfm.201805924.

[93] D.S. Hecht, L. Hu, G. Irvin, Emerging Transparent Electrodes Based on Thin Films of Carbon Nanotubes, Graphene, and Metallic Nanostructures, Advanced Materials 23 (2011) 1482–1513. https://doi.org/10.1002/adma.201003188.

[94] D.K. Han, C.A. Li, S.H. Song, K. Cho, J.S. Choi, S.E. Son, G.H. Seong, Electroanalytical biosensor based on GOx/FCA/PEG-modified SWCNT

electrode for determination of glucose, J Anal Sci Technol 14 (2023). https://doi.org/10.1186/S40543-023-00371-8.

[95] N. Behabtu, C.C. Young, D.E. Tsentalovich, O. Kleinerman, X. Wang, A.W.K. Ma, E.A. Bengio, R.F. Ter Waarbeek, J.J. De Jong, R.E. Hoogerwerf, S.B. Fairchild, J.B. Ferguson, B. Maruyama, J. Kono, Y. Talmon, Y. Cohen, M.J. Otto, M. Pasquali, Strong, light, multifunctional fibers of carbon nanotubes with ultrahigh conductivity, Science (1979) 339 (2013) 182–186. https://doi.org/10.1126/SCIENCE.1228061.

[96] S. Lakard, I.A. Pavel, B. Lakard, Electrochemical Biosensing of Dopamine Neurotransmitter: A Review, Biosensors (Basel) 11 (2021). https://doi.org/10.3390/BIOS11060179.

[97] L. Xiao, Z. Chen, C. Feng, L. Liu, Z.Q. Bai, Y. Wang, L. Qian, Y. Zhang, Q. Li, K. Jiang, S. Fan, Flexible, stretchable, transparent carbon nanotube thin film loudspeakers, Nano Lett 8 (2008) 4539–4545. https://doi.org/10.1021/NL802750Z/SUPPL_FILE/NL802750Z_SI_005.AVI.

[98] K. Adu, R. Rajagopalan, C. Kaschalk, C. Randall, CNT flexible membranes for energy storage and conversion systems, MRS Commun 9 (2019) 670–674. https://doi.org/10.1557/MRC.2019.45.

[99] R. Dettmer, Prophet of the integrated circuit, Electronics and Power 30 (1984) 279. https://doi.org/10.1049/EP.1984.0159.

[100] J.S. Kilby, Miniaturized Electronic Circuits (U. S. Patent No. 3,138, 743), IEEE Solid-State Circuits Newsletter 12 (2009) 44–54. https://doi.org/10.1109/N-SSC.2007.4785580.

[101] L. Berlin, The man behind the microchip : Robert Noyce and the invention of Silicon Valley, (2008) 402.

[102] Yayi. Wei, R.L. Brainard, Society of Photo-Optical Instrumentation Engineers., Advanced processes for 193-nm immersion lithography, (2009) 315.

[103] H. Mizoguchi, T. Saitou, T. Yamazaki, Development Status of High-Power EUV Light Source Development for Exposure in Semiconductor Mass Production, 2017.

[104] G.E. Moore, Cramming more components onto integrated circuits, Proceedings of the IEEE 86 (1998) 82–85. https://doi.org/10.1109/JPROC.1998.658762.

[105] B. Turkot, S.L. Carson, A. Lio, T. Liang, M. Phillips, B. McCool, E. Stenehjem, T. Crimmins, G. Zhang, S. Sivakumar, EUV progress toward HVM readiness, Extreme Ultraviolet (EUV) Lithography VII 9776 (2016) 977602. https://doi.org/10.1117/12.2225014.

[106] N. Fu, Y. Liu, X. Ma, Z. Chen, EUV Lithography: State-of-the-Art Review, Journal of Microelectronic Manufacturing 2 (2019) 1–6. https://doi.org/10.33079/jomm.19020202.

[107] S.N. Srivastava, K.C. Thompson, E.L. Antonsen, H. Qiu, J.B. Spencer, D. Papke, D.N. Ruzic, Lifetime measurements on collector optics from Xe and Sn extreme ultraviolet sources, J Appl Phys 102 (2007). https://doi.org/10.1063/1.2756525.

[108] D. Brouns, Development and performance of EUV pellicles, Advanced Optical Technologies 6 (2017) 221–227. https://doi.org/10.1515/aot-2017-0023.

[109] F. Scholze, C. Laubis, M. Krumrey, M.Y. Timmermans, I. Pollentier, E.E. Gallagher, EUV optical characterization of alternative membrane materials for

EUV pellicles , in: P.D. Buck, E.E. Gallagher (Eds.), Photomask Technology 2017, SPIE, 2017: pp. 182 – 189. https://doi.org/10.1117/12.2280553.

[110] D.L. Goldfarb, Fabrication of a full-size EUV pellicle based on silicon nitride, Photomask Technology 2015 9635 (2015) 96350A. https://doi.org/10.1117/12.2196901.

[111] Y.A. Shroff, M. Leeson, P.-Y. Yan, E. Gullikson, F. Salmassi, High transmission pellicles for extreme ultraviolet lithography reticle protection, Journal of Vacuum Science & Technology B, Nanotechnology and Microelectronics: Materials, Processing, Measurement, and Phenomena 28 (2010) C6E36-C6E41. https://doi.org/10.1116/1.3505126.

[112] R.P. Venkatesh, M.S. Kim, J.G. Park, Contamination Removal From UV and EUV Photomasks, Elsevier Inc., 2017. https://doi.org/10.1016/B978-0-323-43157-6.00005-7.

[113] D. Ruzic, W. Lytle, D. Andruczyk, Removal Of Organic Contaminants From Lithographic Materials EUV Mask Production and Cleaning, n.d.

[114] D. Ruzic, W. Lytle, EUV Mask Production and Cleaning Removal Of Organic, (2011).

[115] N. Böwering, C. Meier, In situ transformation and cleaning of tin-drop contamination on mirrors for extreme ultraviolet light , Journal of Vacuum Science & Technology B, Nanotechnology and Microelectronics: Materials, Processing, Measurement, and Phenomena 36 (2018) 021602. https://doi.org/10.1116/1.5016821.

[116] D.T. Elg, J.R. Sporre, G.A. Panici, S.N. Srivastava, D.N. Ruzic, In situ collector cleaning and extreme ultraviolet reflectivity restoration by hydrogen plasma for

extreme ultraviolet sources , Journal of Vacuum Science & Technology A: Vacuum, Surfaces, and Films 34 (2016) 021305. https://doi.org/10.1116/1.4942456.

[117] D.S. Kopylova, N.Y. Boldyrev, V.Y. Iakovlev, Y.G. Gladush, A.G. Nasibulin, A bolometer based on single-walled carbon nanotubes and hybrid materials, Quantum Elec (Woodbury) 46 (2016) 1163–1169. https://doi.org/10.1070/qel16146.

[118] H. Chen, Flexible and Stretchable Devices from Other Materials, in: Flexible and Stretchable Triboelectric Nanogenerator Devices, Wiley-VCH Verlag GmbH & Co. KGaA, Weinheim, Germany, 2019: pp. 183–202. https://doi.org/10.1002/9783527820153.ch11.

[119] Carbon nanotubes push the limit of flexible electronics | IBM Research Blog, (n.d.). https://www.ibm.com/blogs/research/2018/03/cnt-flex-electronics/ (accessed March 27, 2023).

[120] L. Nela, J. Tang, Q. Cao, G. Tulevski, S.J. Han, Large-Area High-Performance Flexible Pressure Sensor with Carbon Nanotube Active Matrix for Electronic Skin, Nano Lett 18 (2018) 2054–2059. https://doi.org/10.1021/acs.nanolett.8b00063.

[121] M. Han, Overview of Flexible and Stretchable Approaches, in: Flexible and Stretchable Triboelectric Nanogenerator Devices, Wiley-VCH Verlag GmbH & Co. KGaA, Weinheim, Germany, 2019: pp. 95–111. https://doi.org/10.1002/9783527820153.ch6.

[122] Z. Zhang, X. Sun, P. Yuan, S. Yokokawa, Y. Zheng, H. Jiang, L. Jin, A. Anisimov, E. Kauppinen, R. Xiang, S. Maruyama, S. Yamashita, S.Y. Set, SWCNT@BNNT

with 1D Van der Waals Heterostructure with a High Optical Damage Threshold for Laser Mode-Locking, Journal of Lightwave Technology 39 (2021) 5875–5883. https://doi.org/10.1109/JLT.2021.3092522.

[123] E.M. Khabushev, D. V. Krasnikov, O.T. Zaremba, A.P. Tsapenko, A.E. Goldt, A.G. Nasibulin, Machine Learning for Tailoring Optoelectronic Properties of Single-Walled Carbon Nanotube Films, Journal of Physical Chemistry Letters (2019) 6962–6966. https://doi.org/10.1021/acs.jpclett.9b02777.

[124] A. Kaskela, A.G. Nasibulin, M.Y. Timmermans, B. Aitchison, A. Papadimitratos, Y. Tian, Z. Zhu, H. Jiang, D.P. Brown, A. Zakhidov, E.I. Kauppinen, Aerosol-synthesized SWCNT networks with tunable conductivity and transparency by a dry transfer technique, Nano Lett 10 (2010) 4349–4355. https://doi.org/10.1021/NL101680S/SUPPL_FILE/NL101680S_SI_006.PDF.

[125] A. Kaskela, A.G. Nasibulin, M.Y. Timmermans, B. Aitchison, A. Papadimitratos, Y. Tian, Z. Zhu, H. Jiang, D.P. Brown, A. Zakhidov, E.I. Kauppinen, Aerosol-synthesized SWCNT networks with tunable conductivity and transparency by a dry transfer technique, Nano Lett 10 (2010) 4349–4355. https://doi.org/10.1021/nl101680s.

[126] V.M. Gubarev, V.Y. Yakovlev, M.G. Sertsu, O.F. Yakushev, V.M. Krivtsun, Y.G. Gladush, I.A. Ostanin, A. Sokolov, F. Schäfers, V. V. Medvedev, A.G. Nasibulin, Single-walled carbon nanotube membranes for optical applications in the extreme ultraviolet range, Carbon N Y 155 (2019) 734–739. https://doi.org/10.1016/j.carbon.2019.09.006.

[127] D. V. Krasnikov, V.L. Kuznetsov, A.I. Romanenko, A.N. Shmakov, Side reaction in catalytic CVD growth of carbon nanotubes: Surface pyrolysis of a hydrocarbon

precursor with the formation of lateral carbon deposits, Carbon N Y 139 (2018) 105–117. https://doi.org/10.1016/j.carbon.2018.06.033.

[128] A.E. Goldt, O.T. Zaremba, M.O. Bulavskiy, F.S. Fedorov, K. V. Larionov, A.P. Tsapenko, Z.I. Popov, P. Sorokin, A.S. Anisimov, H. Inani, J. Kotakoski, K. Mustonen, A.G. Nasibulin, Highly efficient bilateral doping of single-walled carbon nanotubes, J Mater Chem C Mater 9 (2021) 4514–4521. https://doi.org/10.1039/d0tc05996j.

[129] C. Yaws, The Yaws Handbook of Vapor Pressure, Elsevier, 2015. https://doi.org/10.1016/C2014-0-03590-3.

[130] W.C. Hinds, Aerosol Technology Properties, Behavior, and Measurement of Airborne Particles Second Edition, n.d.

[131] F. Wang, D. Yang, L. Li, Y. Liu, X. Wei, W. Zhou, H. Kataura, H. Liu, S. Xie, Electronic Type and Diameter Dependence of the Intersubband Plasmons of Single-Wall Carbon Nanotubes, Adv Funct Mater 32 (2022) 2107489. https://doi.org/10.1002/ADFM.202107489.

[132] I. V. Anoshkin, A.G. Nasibulin, Y. Tian, B. Liu, H. Jiang, E.I. Kauppinen, Hybrid carbon source for single-walled carbon nanotube synthesis by aerosol CVD method, Carbon N Y 78 (2014) 130–136. https://doi.org/10.1016/J.CARBON.2014.06.057.

[133] H. Kuzmany, W. Plank, M. Hulman, C. Kramberger, A. Grüneis, T. Pichler, H. Peterlik, H. Kataura, Y. Achiba, Determination of SWCNT diameters from the Raman response of the radial breathing mode, European Physical Journal B 22 (2001) 307–320. https://doi.org/10.1007/S100510170108/METRICS.

[134] M.Y. Timmermans, M. Mariano, I. Pollentier, O. Richard, C. Huyghebaert, E.E. Gallagher, Free-standing carbon nanotube films for extreme ultraviolet pellicle application, Https://Doi.Org/10.1117/1.JMM.17.4.043504 17 (2018) 043504. https://doi.org/10.1117/1.JMM.17.4.043504.

[135] V. Gubarev, M. Krivokorytov, J.A. Ramirez Benavides, V. Krivtsun, V. Ivanov, V. Medvedev, A. Pal, D. Krasnikov, A. Nasibulin, InSn plasma penetration through protective single-walled carbon nanotube-based membranes, Appl Phys Lett 121 (2022). https://doi.org/10.1063/5.0097517/2834365.

[136] P.A. Dróżdż, M. Haras, A. Przewłoka, A. Krajewska, M. Filipiak, M. Słowikowski, B. Stonio, K. Czerniak-Łosiewicz, Z. Mierczyk, T. Skotnicki, D. Lioubchenko, A graphene/h-BN MEMS varactor for sub-THz and THz applications, Nanoscale 15 (2023) 12530–12539. https://doi.org/10.1039/D2NR06863J.

[137] A.A. Generalov, I. V. Anoshkin, M. Erdmanis, D. V. Lioubtchenko, V. Ovchinnikov, A.G. Nasibulin, A. V. Räisänen, Carbon nanotube network varactor, Nanotechnology 26 (2015). https://doi.org/10.1088/0957-4484/26/4/045201.